THE APPLICATION OF THE ADDITIVITY PRINCIPLE TO RECRYSTALLIZATION

by

KENNETH HOWARD MAGEE

A THESIS SUBMITTED IN PARTIAL FULFILMENT OF
THE REQUIREMENTS FOR THE DEGREE OF
MASTER OF APPLIED SCIENCE

in

THE FACULTY OF GRADUATE STUDIES
Department of Metallurgical Engineering

We accept this thesis as conforming
to the required standard

THE UNIVERSITY OF BRITISH COLUMBIA

July 1986

In presenting this thesis in partial fulfilment of the requirements for an advanced degree at the The University of British Columbia, I agree that the Library shall make it freely available for reference and study. I further agree that permission for extensive copying of this thesis for scholarly purposes may be granted by the Head of my Department or by his or her representatives. It is understood that copying or publication of this thesis for financial gain shall not be allowed without my written permission.

Department of Metallurgical Engineering

The University of British Columbia
2075 Wesbrook Place
Vancouver, Canada
V6T 1W5

Date: July 1986

ABSTRACT

This research is part of an ongoing program at the University of British Columbia to mathematically model industrial annealing processes. To enable one to predict the final mechanical properties of a cold rolled steel sheet after being subjected to an industrial annealing cycle, the progress of recrystallization must be predicted with temperature increase during annealing. This is accomplished by applying the additivity principle to isothermal recrystallization kinetic data.

To determine whether additivity is applicable to recrystallization, isothermal recrystallization kinetic data for a low carbon, rimmed, cold rolled steel sheet, was determined over a temperature range of 440°C-560°C, using molten salt annealing and diamond pyramid microhardness evaluation methods. The data was characterized using the Avrami equation. Continuous heating recrystallization trials were carried out using resistance heated strip specimens. The progress of recrystallization was monitored using an x-ray procedure based on examining the increased $K\alpha$ doublet peak resolution of the {211} plane, experienced during the formation of recrystallized material. Diamond pyramid microhardness evaluation was also applied to the continuously heated specimens.

Applying the Additivity principle to the isothermal kinetic data resulted in computer predictions which displayed reasonably good agreement with the kinetics

obtained experimentally. The difference between the predicted and the experimental recrystallization behaviour was related to recovery effects. The degree of recovery, which is thermal history dependent, determines the amount of stored strain energy available for recrystallization. Once the recovery effect was eliminated by applying suitable heat treatments prior to the continuous heating cycle, the computer predictions displayed excellent correlation with the experimentally obtained continuous heating recrystallization kinetics.

The x-ray procedure used to monitor recrystallization was found to be effective. However, modifications to the procedure will be necessary to enable it's use for the insitu monitoring of specimens subjected to the high heating rates typical of continuous annealing conditions.

LIST OF TABLES

LIST OF FIGURES

LIST OF SYMBOLS

X	:Volume fraction of recrystallized material.
t	:time.
N	:Nucleation rate of recrystallized grains.
Q_N	:Activation energy for nucleation.
G	:Growth rate of recrystallized grains.
Q_G	:Activation energy for growth.
R	:Gas constant.
T	:Temperature.
ρ	:Dislocation density.
$\bar{b}$	:Burgers vector.
d	:Grain size.
e	:Plastic strain.
D	:Dimension of recrystallized grain.
τ	:Incubation period prior to recrystallization.
v	:Volume of the recrystallized grain.
$\bar{N}$	:Assumed number of pre-existing preferred nucleation sites prior to recrystallization.
N_τ	:The number of nucleation sites existing after time τ.
ν	:Nucleation frequency of each preferred nucleation site.
n	:Number of nuclei existing in unrecrystallized matrix.
n'	:Number of nuclei in both recrystallized and unrecrystallized matrix.

X_{ex} :Extended volume recrystallized.

δ :Thickness of a thin sheet, or diameter of a fine wire.

f :Shape factor of recrystallized grains.

b :Temperature dependent parameter in the Avrami equation.

k :Temperature dependent time exponent in the Avrami equation.

t_s :Start of recrystallization under continuous heating conditions.

t_{av} :Start of recrystallization under isothermal heating conditions.

d_o :Unstrained crystal lattice spacing.

θ :Incident angle of x-ray beam with the crystal surface.

λ :Wavelength of x-ray beam.

B :Fractional residual x-ray line broadening parameter.

I :X-ray beam intensity.

θ_B :Bragg angle.

DPH_0 :Hardness of the steel at the start of recrystallization.

DPH_{100} :Hardness of the steel at the completion of recrystallization.

DPH_t :Hardness of the steel at time t during the recrystallization cycle.

t_{est} :Estimated time at which recrystallization starts during isothermal annealing.

R_I :{211} x-ray peak ratio used for evaluating the degree of recrystallization.

P :P value used in hypothesis testing.

t_{99} :Time at which X=.99, for a given isothermal temperature. Based on the best fit Avrami parameters b and k.

t_{end} :Experimentally determined isothermal recrystallization completion time.

ACKNOWLEDGEMENTS

I would like to thank Dr. E.B. Hawbolt for his advice and guidance during the course of the project. I would also like to thank Professor R.G. Butters and Mr. B. Chau for their help given during the experimental part of this work. Thanks are also extended to Dana Magee for helping with the preparation of this thesis.

Table of Contents

1. INTRODUCTION

This study is part of an ongoing program at the University of British Columbia to develop mathematical models of industrial deformation, annealing and heat treatment processes. This research is aimed at developing a mathematical model to predict the structure and mechanical properties of cold rolled, steel sheet after being subjected to an industrial continuous or batch annealing cycle.

In order to accomplish this goal, the model must be able to predict the progress of recrystallization with increase in temperature during the continuous heat treatment cycle. Other factors affecting a steels' mechanical properties such as grain growth after recrystallization, as well as carbide precipitation and coarsening during cooling and overaging will also have to be incorporated into the final mathematical model.

The purpose of this research is to determine whether isothermal recrystallization kinetic data generated for a cold rolled, high deformability steel sheet can be used in conjunction with the additivity principle to predict recrystallization kinetics during a continuous heating cycle.

In addition, an attempt is made to develop an insitu procedure that monitors recrystallization in a steel specimen being subjected to a continuous heating cycle.

Similar approaches are currently being taken to predict the mechanical proporties of plain carbon steel rods during

controlled cooling processes. In this case austenite decomposition kinetics during continuous cooling is predicted, using isothermal transformation kinetics, and the resulting microstructural components are then used to determine final mechanical properties.[1,2]

2. LITERATURE REVIEW

2.1 MICROSTRUCTURAL ASPECTS OF ANNEALING

During the plastic deformation of a metal or alloy, energy will be stored in the material due to the introduction of dislocations and their associated strain energy. This stored energy provides the driving force for the two relaxation processes that occur during annealing of a cold worked metal, recovery and recrystallization.[3]

2.1.1 RECOVERY

Recovery can be defined as any modification to the properties of a cold worked metal that occurs during annealing prior to recrystallization. Generally, hardness and other mechanical properties change very little during recovery.[3] However, depending on the alloy, either an increase or decrease in these properties can be observed during the recovery period.

There is no incubation period observed during recovery, which generally proceeds in an exponential decay pattern with time, ie.,

$$Z=K_1\exp(-kt) \qquad ...(2.1)$$

where Z is the instantaneous value of some property of the material, t is time, and K_1 and k are constants.[3]

The stored energy of cold work serves a dual purpose during recovery. It combines with thermal energy to satisfy the activation energy requirements, and provides the driving

force for the various recovery processes. A wide variety of mechanisms may occur during recovery. The first defects to be annealed out are point defects, which have the lowest activation energy. As the annealing temperature increases, the energy input will be sufficient to overcome the activation energy requirements for dislocation movement. Finally at higher temperatures, large scale dislocation movements can occur, creating strain-free grains which may act as the nucleation centers for recrystallization.

The initial structure that exists after heavy deformation as occurs in cold rolled sheet steels (60-80 percent cold worked) consists of cells whose walls are tangled dislocation arrays of very high density, with some dislocations in the cell interiors. During the first stages of recovery, the interior dislocations tend to migrate towards the walls, and are also reduced in numbers due to a variety of annihilation processes. In addition, the cell walls become more clearly defined, with higher dislocation density, higher energy, and greater misorientation.[3]

Hu[4] examined the microstructural changes during annealing of a iron-silicon crystal that had been cold rolled 70 percent. He found that during the recovery stage of annealing the subgrain boundary size increased slightly. He suggested this to be due to subgrain coalescence which he described as the gradual moving of dislocations out of the subgrain boundary between two cells, to the boundaries surrounding them. A schematic representation of this process

is shown in Figure 2.1. Here boundary CH is being eliminated, and subgrain CDEFGH is being rotated into the same orientation as it's neighboring subgrain. For this to occur, atom diffusion must take place along the subgrain boundaries from the shaded to the unshaded areas. Finally, a geometrical rearrangement occurs to the boundaries originally connected to CH.

Another recovery process, called polygonization[5] is thought to occur when the applied deformation creates a structure with an excess of dislocations of one type. This theory states that during recovery, walls of dislocations form at right angles to the glide planes which had been active during the original bending, as shown in Figure 2.2. The driving force for polygonization is the reduction in strain energy in the material that occurs during conversion from a deformed to a polygonized structure. The polygonization reaction occurs at high temperatures.

Although there is some dispute as to the exact mechanism active during recovery of iron based alloys, experimental observations indicate that both subgrain coalescence and polygonization do occur.[8]

The recovery and recrystallization behaviour of rimmed and aluminum killed steels annealed in the temperature range of 427-871°C (800-1600°F) was examined by Goodenow.[6] He noted a correlation between the type of subgrain structure present, and the cold worked structure previously occupying the same area. Large subgrains with low angle grain

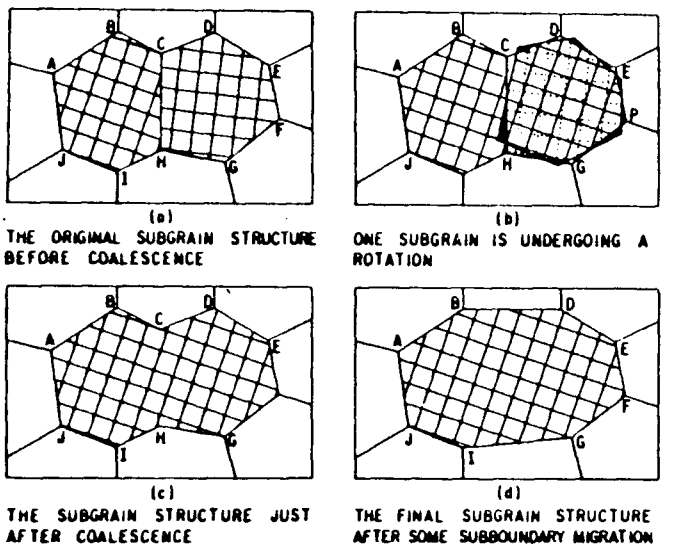

Fig. 2.1 Schematic representation of subgrain coalescence by subgrain rotation. (Ref.8)

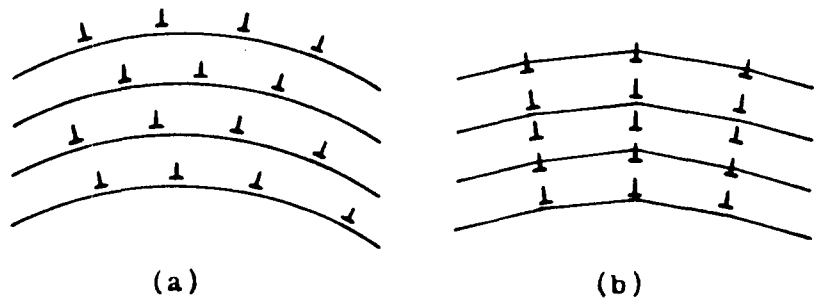

Fig. 2.2 Schematic representation of the polygonization process: (a) Random arrangement of edge dislocations, and (b) alignment of edge dislocations to form walls. (Ref.8)

boundaries existed in areas previously occupied by large cold worked grains. These grains exhibited little growth due to the low mobility of their boundaries. Other areas consisted of small subgrains which formed from small, elongated cold rolled grains. These subgrains were determined to be the nuclei responsible for subsequent nucleation.

The ease with which recovery processes are able to operate depend largely on metal purity. Pure metals having a high stacking fault energy, such as iron, usually experience a large amount of softening due to recovery during annealing. This is due to the relative ease with which dislocation motion can occur.

Impurity atoms generally reduce the dislocation mobility in iron by exerting attractive forces on dislocations, resulting in drag. The ease with which recovery can occur in alloy systems is greatly reduced due to impurity drag.

Pure iron is found to display much more softening during annealing than can be attributed to recrystallization alone, Figure 2.3.[12] This increase in softening can be attributed to recovery processes occuring at the same time as recrystallization. Carbon additions will decrease the ease with which the recovery processes are able to occur, as shown in Figure 2.3. Both manganese[14] and molybdenum[15] were found to display similar effects, Figures 2.4 and 2.5. The combined effect on softening of alloying additions in

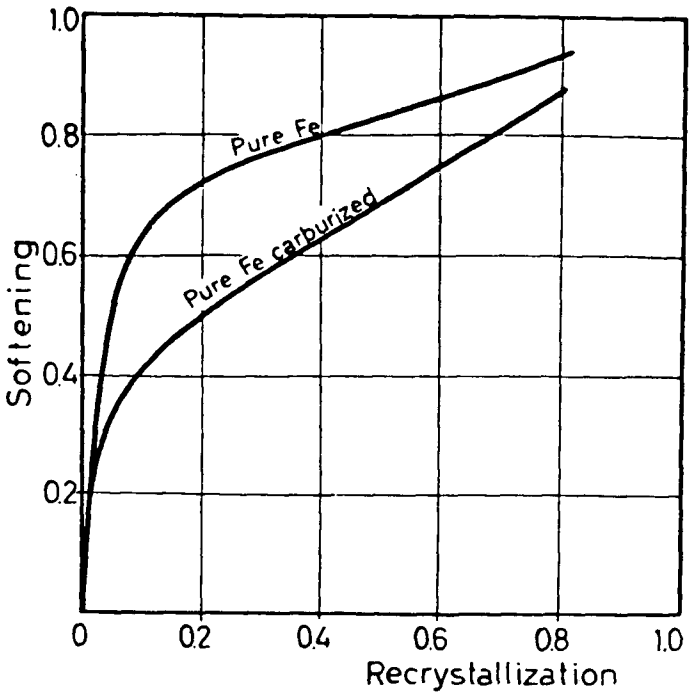

Fig. 2.3 Softening as a function of fraction recrystallized in pure iron and carburized iron. Annealing time=3h, temperature range=380-490°C.(Ref.12)

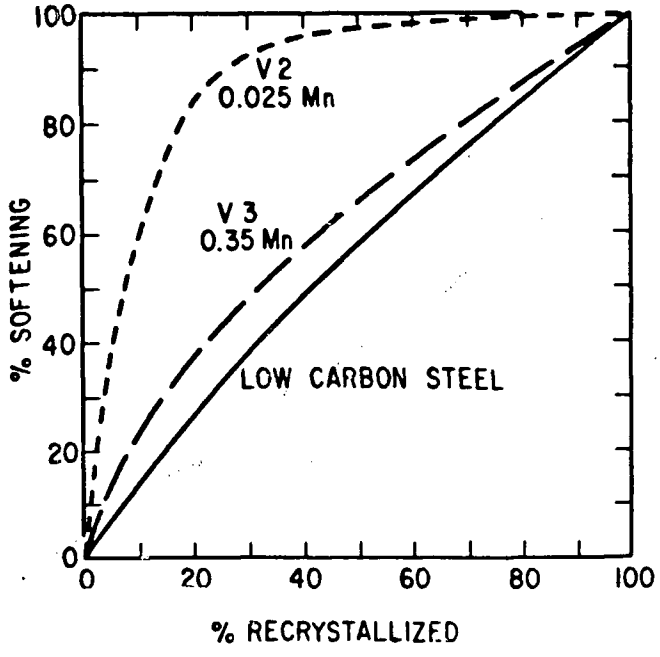

Fig 2.4 Softening of three iron alloys. Temperature range=480-650°C.(Ref.14)

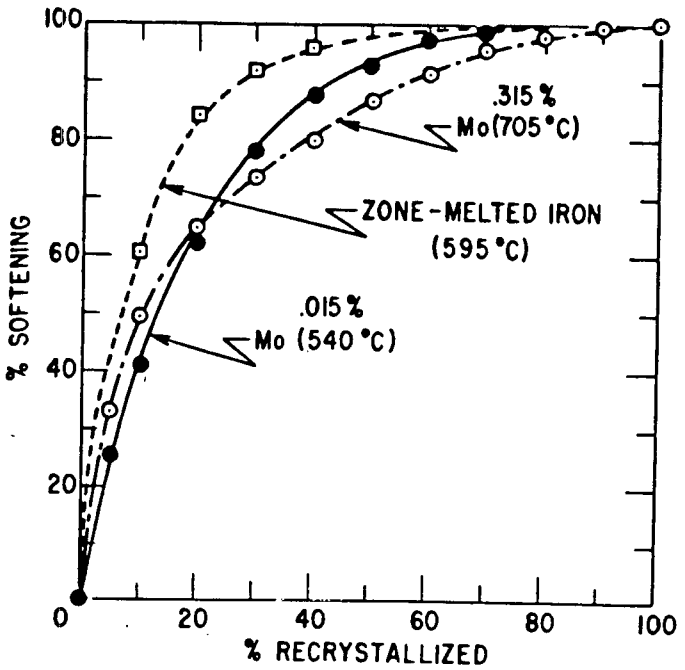

Fig. 2.5 The effect of molybdenum on the softening of iron. Temperature range=480-705°C.(Ref.15)

amounts typical of low carbon steel (0.52 Mn, 0.06 C, 0.005 Al) is shown in Figure 2.4. Therefore, since recovery is reduced, recrystallization is responsible for the majority of softening in low carbon steels. Recrystallization of low carbon steel can be quantified by studying the amount of softening with time during an annealing cycle.

2.1.2 PRIMARY RECRYSTALLIZATION

Primary recrystallization can be defined as the nucleation and growth of new strain free grains at the expense of the cold worked matrix. The growth is accomplished by the movement of high angle grain boundaries that exist between the cold worked matrix and the nuclei that form during recovery.[3,8]

It is common to characterize recrystallization data in terms of activation energies. Since recrystallization takes place by both nucleation and growth processes, both nucleation and growth activation energies are determined.

The nucleation rate is usually determined by plotting the number of recrystallized grains present versus time of annealing, the slope being the nucleation rate. The nucleation rate, N, is related to temperature by:

$$N=N_0\exp(-Q_N/RT) \qquad ...(2.2)$$

where Q_N is the activation energy for nucleation, T is the temperature in °K, R the gas constant, and N_0 a constant.

Similarily, the growth rate of a recrystallized grain is obtained experimentally by plotting the diameter of the

largest unimpinged grain against the annealing time, the slope being the growth rate, G. As before, G is related to temperature by:

$$G=G_0\exp(-Q_G/RT) \qquad ...(2.3)$$

where Q_G is the activation energy for growth, and G_0 is a constant.

If growth rate and nucleation rate data are obtained for a range of temperatures, the values of Q_G, Q_N, G_0 and N_0 can be determined by plotting the natural logarithm of G or N versus the inverse of temperature, the slope will equal $-Q_G/R$ or $-Q_N/R$, respectively.

There has been extensive research into the factors which affect recrystallization. Burke and Turnbull[7] formulated the following series of laws concerning many of these effects:

1. A minimum amount of deformation is needed to initiate recrystallization.
2. The smaller the amount of deformation, the higher is the temperature required to cause recrystallization.
3. Increasing the annealing time decreases the temperature necessary to cause recrystallization.
4. The recrystallized grain size depends chiefly upon the degree of deformation, and to a lesser extent on the annealing temperature, being smaller the greater the degree of deformation and the lower the annealing temperature.
5. The larger the original grain size, the greater is the

amount of cold deformation required to give an equivalent recrystallization temperature and time.

6. The amount of cold work required to give equivalent deformation hardening increases with increasing temperature of working.
7. Continued heating after recrystallization is complete causes the grain size to increase.

The extent of deformation affects recrystallization since the strain energy resulting from cold work provides the driving force for nucleation and growth processes. A minimum amount of strain energy is needed for nucleation and for the migration of high angle grain boundaries during growth.

The activation energies are affected by the amount of cold work, as shown in Figure 2.6. At low strains, Q_N is greater than Q_G, while at large strains, Q_N decreases towards Q_G resulting in easier nucleation and a resulting finer grained structure. Lowering the activation energies will result in higher N and G for a given temperature.

The initial grain size can contribute to variation in the dislocation density and distribution. The dislocation density is related to grain size by:

$$\rho = e/\alpha k \bar{B} d^n \qquad \ldots(2.4)$$

where ρ is the density, $\bar{B}$ the burgers vector, d the grain size, e the plastic strain, α,k and n are constants.[8] The effect of grainsize on dislocation density is shown in Figure 2.7. At higher strains, the dislocation density

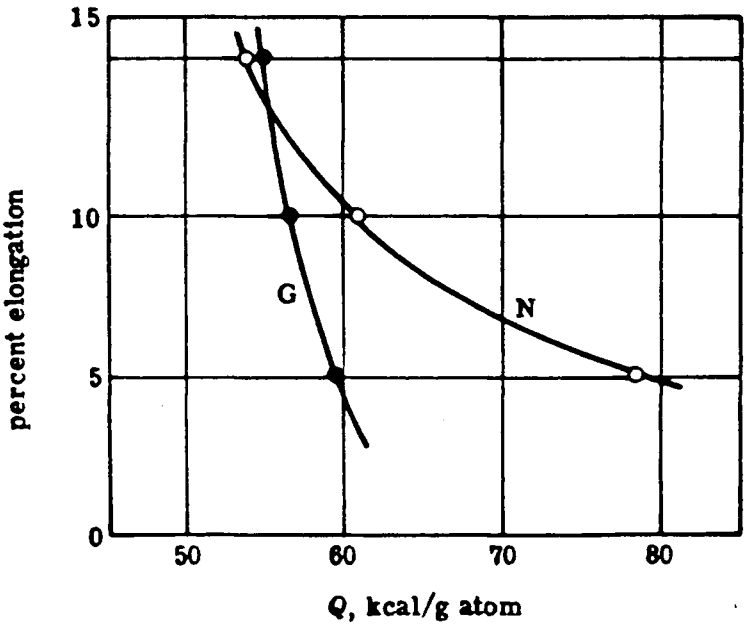

Fig. 2.6 Recrystallization data for aluminum, activation energies for nucleation (N) and for growth (G) as a function of prior deformation.(Ref.8)

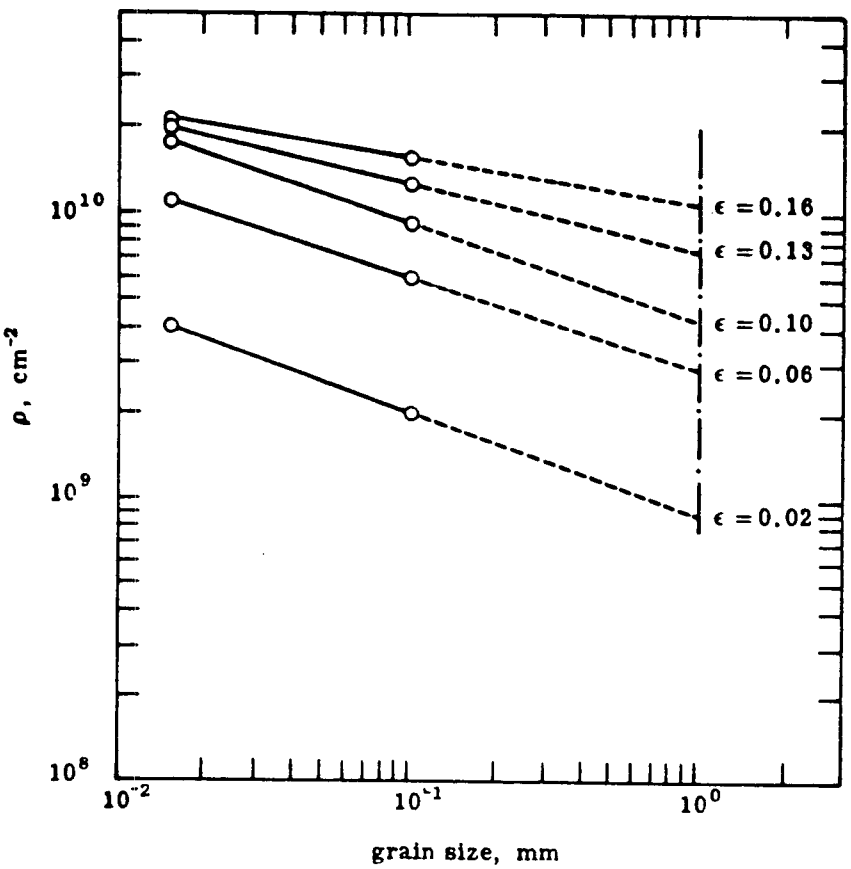

Fig. 2.7 Dislocation density versus grainsize in iron deformed by various amounts at room temperature.(Ref.8)

becomes less sensitive to grain size.

Dislocations generated by the application of strain will concentrate at grain boundaries. This results in preferential nucleation generally occuring at these sites since Q_N will be lower. Rosen, et. al.[9] as well as Goodenow[6] have varified metallographically that preferential nucleation does occur at grain boundaries.

Second phase particles can affect recrystallization by changing the number and distribution of dislocations in the metal matrix.[10] If the particles are harder than the matrix, cold work will plastically deform the matrix to a greater extent immediately adjacent to the particles. The main influence of hard second phase particles appears to be in the distribution of dislocations, rather than on the total number. This however depends upon the particle size. Gawne and Higgins[11] determined that a critical particle size of 0.74 μm is necessary in a 0.4 weight percent carbon steel for particle stimulated nucleation to occur. However, it was also noted that if the particle spacing is small, the critical particle size will decrease due to the formation of joint deformation zones.

The effect of both interstitial and substitutional alloying additions on recovery and recrystallization of steel has been investigated at length. Venturello et. al.[12] found that small amounts of carbon (up to 0.0086 weight percent) added to high purity iron slightly affected the recrystallization rate. They speculated that any reduction

in grain boundary mobility caused by interstitial carbon would be compensated for by the greater stored energy in the system due to less recovery, as explained previously.

It was also noted that at higher carbon levels nucleation increased due to the formation of iron carbide (Fe_3C) and the occurrence of particle stimulated nucleation.

Nitrogen was found to have a slightly more pronounced retarding effect on recrystallization as shown in Figure 2.8.[13]

Manganese[14] and molybdenum[15] were found to both slightly decrease the recrystallization kinetics.

The affect of killing practice on recrystallization of cold rolled steel has been the subject of many investigations.[16-18] Aluminum-killed steels were sometimes found to show a sluggish response during recrystallization. Unlike the sigmoidal shaped recrystallization curve exhibited by rimmed steels, Figure 2.9(a), steels killed with aluminum displayed an initial period of recrystallization, followed by a leveling off period of very slow kinetics, finishing off in rapid recrystallization, Figure 2.9(b).[16] The time necessary for complete recrystallization to occur is significantly longer for aluminum killed steels than for rimmed steels.

This type of sluggish response has been attributed to the precipitation of aluminum nitride (AlN) during recrystallization;[17] the precipitates cause grain boundary drag to occur, therely impeding the mobility of the high

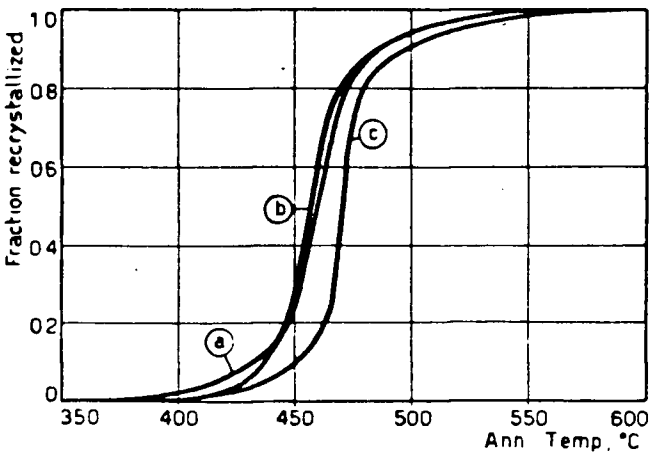

Fig. 2.8 Fraction recrystallized versus annealing temperature (isochronal anneals of 3 h). (a) Pure iron, (b) iron with carbon additions, (c) iron with nitrogen additions.(Ref.13)

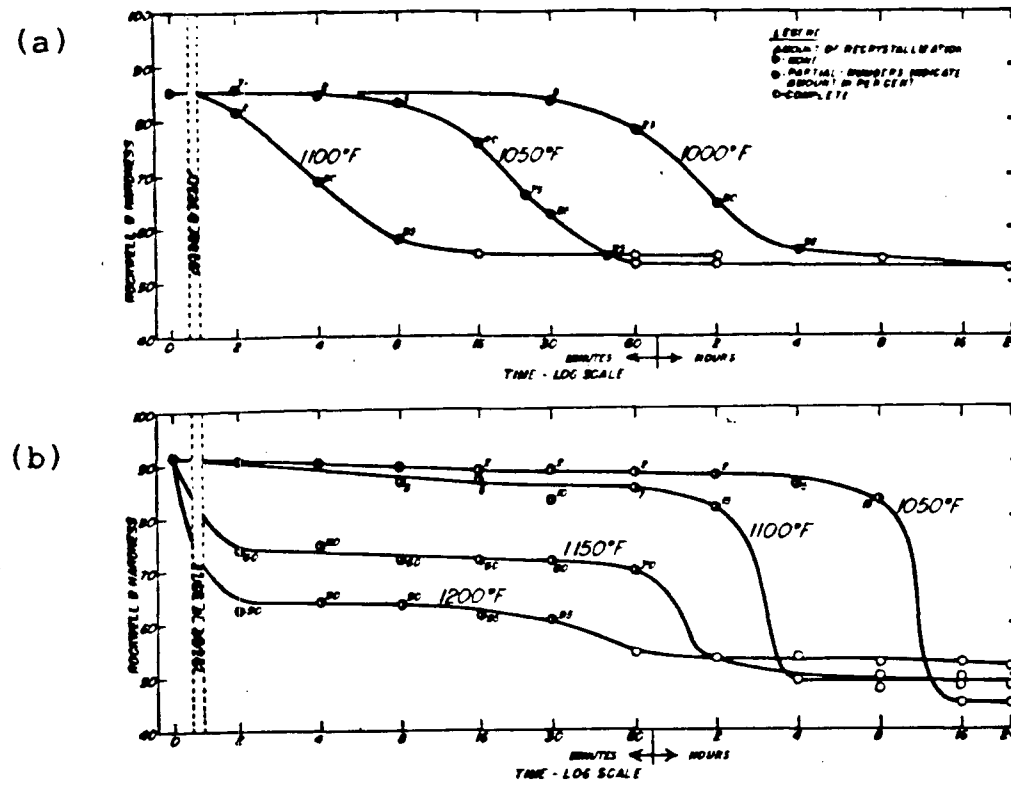

Fig. 2.9 Effect of temperature on the recrystallization kinetics of (a) rimmed and (b) aluminum-killed steels.(Ref.16)

angle grain boundaries. The exact size of the precipitate which is necessary to cause this effect is not known. However, it would appear that pre-precipitation clustering of the aluminum and nitrogen might be responsible for the sluggish kinetics.[18]

Any heat treatment which precipitates AlN prior to recrystallization can be used to prevent the delay during subsequent recrystallization.

2.2 ANALYTICAL MODELLING OF PRIMARY RECRYSTALLIZATION KINETICS

Typically, primary recrystallization follows a sigmoidal pattern with time, as shown in Figure 2.10. An incubation period during which the various recovery processes are active, is followed by an initially slow recrystallization rate, which then accelerates, and finally decelerates near completion of the reaction. Eventually, all of the cold worked structure will be consumed by recrystallized grains.

Burke and Turnbull[7] presented a formal theory describing recrystallization kinetics in terms of nucleation and growth.

If D describes the dimension of a grain experiencing growth isothermally into a cold worked matrix, it can be described by the relation:

$$D=G(t-\tau) \qquad \ldots(2.5)$$

where G is the linear growth rate, t is the time of the

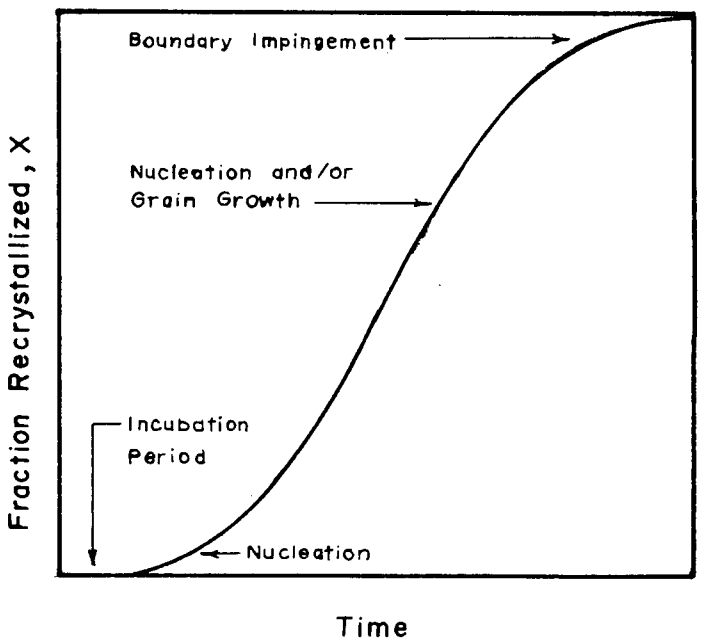

Fig. 2.10 Typical sigmoidal shaped recrystallization kinetic curve.

reaction, and τ is the length of the incubation period at the start of recrystallization.

Assuming the grain to be growing in three dimensions, the volume (v) of the grain at any particular time can be given by:

$$v=fG_xG_yG_z(t-\tau)^3 \qquad ...(2.6)$$

where G_x, G_y and G_z are the linear growth rates in the x, y and z directions, and f is a shape factor.

According to Johnson and Mehl,[19] and Avrami,[20] the number of nuclei, dn, originating in the unrecrystallized matrix during a time interval, $d\tau$, can be expressed by the relation:

$$dn=N(1-X)d\tau \qquad ...(2.7)$$

where N is the nucleation frequency per unit volume and X is the volume fraction recrystallized.

The number of nuclei originating during the same time interval in both the recrystallized and unrecrystallized structure, dn′, can be given by:

$$dn'=dn+NXd\tau=Nd\tau \qquad ...(2.8)$$

Therefore, $NXd\tau$ can be considered to be the number of "ghost" nuclei originating in the transformed material, if it had not already recrystallized. This extended volume transformed, which disregards grain impingement (ie. assumes the grains grow through one another), and includes the ghost nuclei is given by:

$$X_{ex}=\int_0^t v\,dn' \qquad ...(2.9)$$

Substituting equations (2.6) and (2.8) into (2.9) yields the relationship:

$$X_{ex}=fG_xG_yG_z\int_0^t(t-\tau)^3Nd\ \tau \qquad ...(2.10)$$

Avrami and Johnson-Mehl have written an equation relating the extended volume, X_{ex} and the actual volume recrystallized, X, as:

$$dX/dX_{ex}=1-X \qquad ...(2.11)$$

Substituting equation (2.11) into (2.10) we obtain:

$$\int_0^X dX/(1-X)=-\ln(1-X)\ =fG_xG_yG_z\int_0^t(t-\tau)^3Nd\tau \qquad ...(2.12)$$

Performing the necessary integration and making the assumption that growth rates are equal in all directions, we obtain the Johnson-Mehl[19] equation for three dimensional recrystallization:

$$X=1-\exp(-fG^3Nt^4/4) \qquad ...(2.13)$$

If growth occurs in a very thin sheet of thickness δ, so that growth in one direction is negligible, equation (2.6) can be modified to:

$$v=fG^2\delta(t-\tau)^2 \qquad ...(2.14)$$

The Johnson-Mehl[19] equation for two dimensional growth is:

$$X=1-\exp(-fG^2\delta Nt^3/3) \qquad ...(2.15)$$

Similarly, for recrystallization in a thin wire of diameter δ, growth will occur in one dimension only, with $G_x=G_y=0$. Equation (2.13) then becomes:

$$X=1-\exp(-fG\delta^2Nt^2/2) \qquad ...(2.16)$$

The Johnson-Mehl[19] equation assumes the nucleation rate N to be constant, and determined by experimentation.

Avrami[20] assumed there to be a number of pre-existing preferred nucleation sites in the matrix, $\bar{N}$, each having a certain nucleation frequency, ν. The number of nucleation sites existing after time τ is given by:

$$N_{\tau}=\bar{N}\exp(-\nu\tau) \qquad ...(2.17)$$

Therefore, the nucleation rate at time τ can be expressed by:

$$N=\bar{N}\nu\exp(-\nu\tau) \qquad ...(2.18)$$

Substituting equation (2.18) into (2.12), assuming growth in all directions to be equal to G, and performing the necessary integration, we obtain:

$$X=1-\exp(-fG^{3}\bar{N}t^{3}) \qquad ...(2.19)$$

for $\nu\tau$ approaching infinite. If $\nu\tau$ approaches zero, equation (2.19) becomes:

$$X=1-\exp(-fG^{3}\bar{N}\nu t^{4}/4) \qquad ...(2.20)$$

If N is assumed to be independent of time, equation (2.18) becomes:

$$N=\bar{N}\nu \qquad ...(2.21)$$

and equation (2.20) will be the same as that obtained by Johnson-Mehl[19] for three dimensional recrystallization, given in equation (2.13).

Avrami[20] proposed the general recrystallization equation to be:

$$X=1-\exp(-bt^{k}) \qquad ...(2.22)$$

with $3\leq k\leq 4$ for three dimensional recrystallization, $2\leq k\leq 3$ for two dimensional recrystallization, and $1\leq k\leq 2$ for one dimensional recrystallization.

2.3 ADDITIVITY

Due to the independent variation of nucleation and growth rates with temperature, the transformation rate of nonisothermal reactions are difficult to characterize. However, if the reaction rate at any instant in time can be shown to be a function only of the amount of transformed material already present, and of the temperature, the reaction is additive and can be mathematically described.

Christian[21] explained additivity by considering a simple non-isothermal reaction combining two isothermal treatments. If a transformation reaction partially occurs at temperature T_1, where the kinetic law is $X=f_1(t)$, for a time t_1, and then is transferred instantaneously to a slightly lower temperature T_2 (in the case of recrystallization), the reaction is additive if the reaction continues at t_2 as if the fraction transformed $f_1(t_1)$ had been transformed at T_2. Therefore, if t_2 is the time taken at T_2 to produce the same amount of volume transformed as $f_1(t_1)$, then $f_1(t_1)=f_2(t_2)$, and the whole reaction can be written:

$$\left.\begin{aligned} X &= f_1(t), (t<t_1) \\ &= f_2(t+t_2-t_1), (t>t_1) \end{aligned}\right\} \qquad \ldots(2.23)$$

The first equation in the above set refers to the fraction transformed at the initial temperature T_1, where the transformation depends only on the reaction kinetics and the time spent at T_1. The second equation gives the fraction transformed at T_2 with $f_1(t_1)$ already present. Both real and virtual time terms are contained in this expression. Since

t_1 has already been spent at T_1, the additional real time at T_2 must be $(t-t_1)$. The virtual time t_2, which is the time the component must be held at T_2 for the formation of $f_1(t_1)$, must be added in. For example, if a component is held at temperature T_1 for a time t_{a1}, the fraction transformed during this time interval will be X_a, Figure 2.11. The time necessary to cause the same amount of transformation at T_2 is given by t_{a2}. In the two stage example given above, the total time will be the sum of the time spent at both temperatures, or:

$$t=t_1+t_{a2}-t_2 \qquad ...(2.24)$$

This applies if the reaction is additive. Dividing by t_{a2} and rearranging, equation (2.24) becomes:

$$(t-t_1)/t_{a2}+(t_2/t_{a2})=1 \qquad ...(2.25)$$

When the difference between the two temperatures is small, the kinetics of the transformation at each temperature will approach each other. As the time increments spent at each temperature approach zero,

$$(t_1/t_{a1})=(t_2/t_{a2}) \qquad ...(2.26)$$

Substituting equation (2.26) into (2.25) we obtain:

$$(t-t_1)/t_{a2}+(t_1/t_{a1})=1 \qquad ...(2.27)$$

Therefore, the total time to reach a specified amount of transformation, X_a, under continuous heating or cooling is obtained by adding the isothermal time fractions at each temperature until the sum reaches unity. Therefore, additivity can be generalized by the equation:

$$\int_{t_s}^{t_{xa}} dt/t_a(T)=1 \qquad ...(2.28)$$

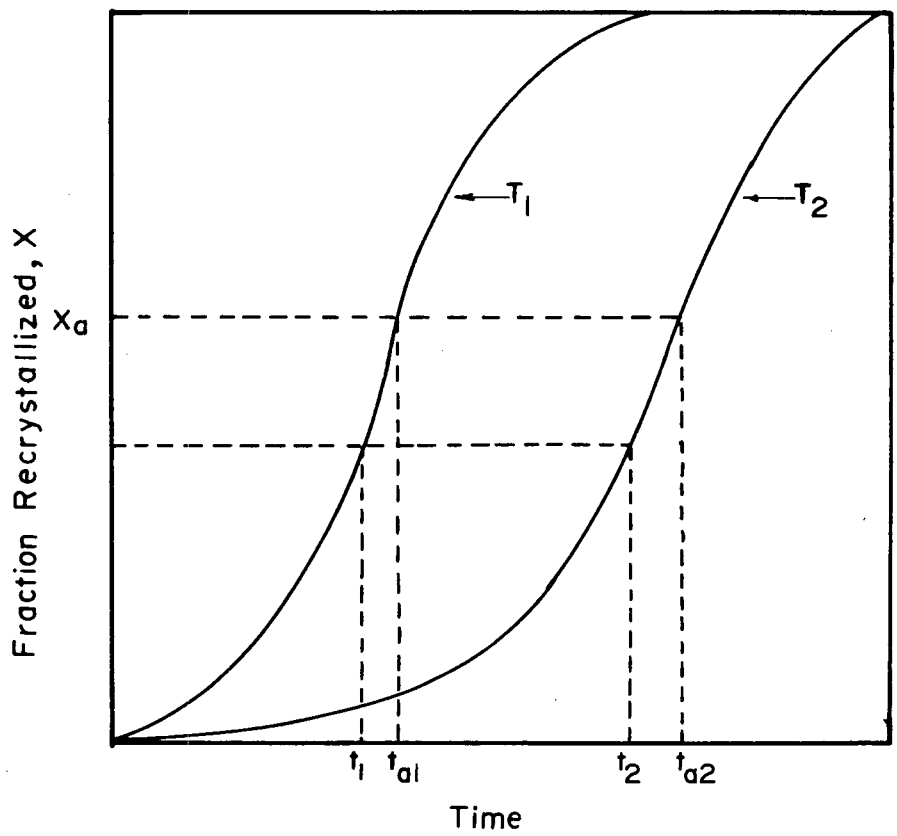

Fig. 2.11 Schematic representation of the principle of additivity.

where $t_a(T)$ is the time to transform X_a at temperature T, t_s is the time at which the transformation begins during continuous heating or cooling, and t_{xa} is the time at which X_a is formed under non-isothermal conditions.

Scheil[22] proposed a similar equation to determine the incubation period during a non-isothermal transformation event. Assuming the incubation period at any particular temperature to be represented by τ_i and the time spent at this temperature to be t_i, the fraction of the incubation period that is exhausted during t_i can be given by t_i/τ_i. * If the successive "fractional nucleation times" are summed up, the transformation will start once the sum equals one, or:

$$\sum_{i=1}^{n} t_i/\tau_i = 1 \qquad \ldots(2.29)$$

Therefore, the total nucleation time is given by:

$$\int_0^{t_s} dt/\tau(T) = 1 \qquad \ldots(2.30)$$

where t_s is the time at which the reaction starts, and $\tau(T)$ is the incubation period at temperature T.

Equations (2.28) and (2.30) differ in that they describe the transformation and incubation events respectively. In addition, the development of the Scheil equation is quite restrictive in that it only applies when the temperatures T_1 and T_2 are so close together that the kinetics approach one another.

Avrami[20] examined the possibility of applying the additivity principle and isothermal kinetic data to predict

---

* The Scheil equation assumes the incubation event to be a linear function with time.

austenite decomposition during continuous cooling. He believed that this approach would be valid providing that an isokinetic range of temperatures exist where the nucleation and growth rates remain constant with respect to each other. If this condition exists, then the reaction would be additive.

Cahn[23] suggested that the isokinetic condition is two restrictive, and that additivity could be satisfied if early site saturation occurs. In this case, nucleation is complete at the beginning of transformation, and the reaction is governed by the growth of the transformed material.

Kuban et. al.[2] suggested that "effective site saturation" would also satisfy the additivity requirement. This condition is based on the idea that the nuclei formed early in the reaction will dominate the volume fraction transformed, while nuclei formed later in the reaction contribute very little to the total volume transformed.

2.4 METHODS OF MONITORING RECRYSTALLIZATION

2.4.1 HARDNESS

Probably the most common method for measuring the progress of recrystallization is hardness. This is due to its ease of use, and its significance in industrial situations. However, depending on factors such as alloy content, softening does not always correspond with recrystalliztion on a one to one basis. If a metal

experiences recovery during recrystallization, hardness will give a false estimate of the amount of recrystallized structure actually present.[8]

Macrohardness is the means by which most recrystallization studies using hardness have been done.[12-15,24] However, the use of macrohardness is limited by the thickness of the cold rolled steel sheet being studied. For thinner material, microhardness indentations using lighter loads are necessary to ensure that the indentation is not affected by the specimen thickness. A specimen thickness of at least ten times the depth of penetration is recommended[36] for hardness testing.

In partially recrystallized metals, regions which are composed of recrystallized grains will be significantly softer than regions which have yet to recrystallize. Therefore, to obtain the correct distribution of indentations located in the recrystallized or unrecrystallized regions, a large number of readings must be taken to reduce statistical inaccuracies. This is particularly true in the case of microhardness evaluation methods, where each indentation is located in a very small area.

A microhardness population count technique has been applied to the study of copper recrystallization by Gordon.[37] This technique involves making a large number of indentations, (typically 200-400) in each specimen in a series of samples annealed for varying lengths of time, at a

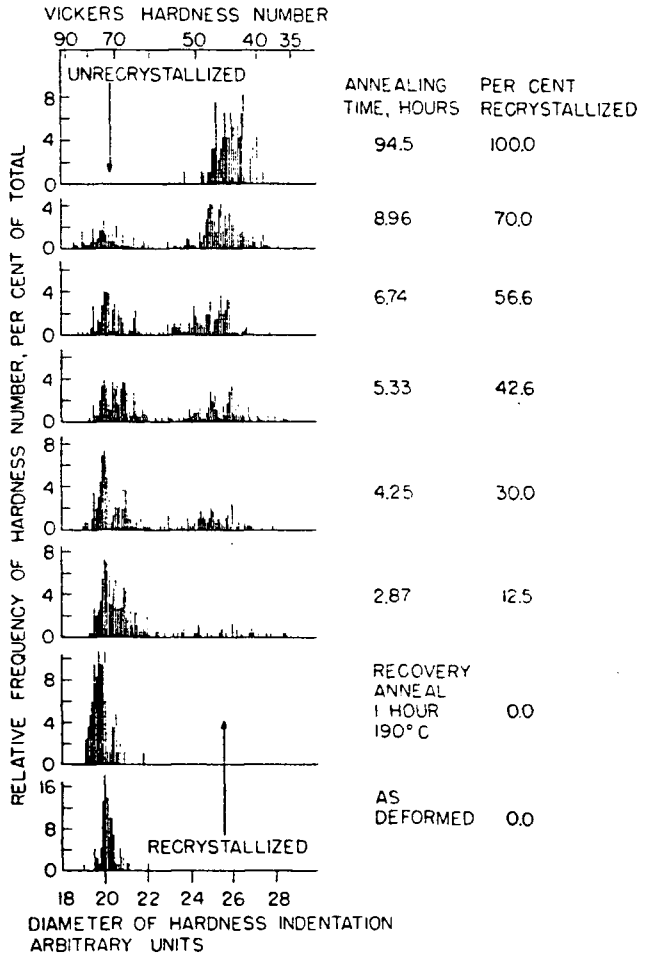

Fig. 2.12 Microhardness distribution charts.(Ref.37)

specified temperature. Microhardness distribution diagrams are determined for each specimen, as illustrated in Figure 2.12. In specimens which have not experienced any recrystallization, one population distribution at a hardness value typical of the cold worked structure is present, clustered around the softer hardness value. For partially recrystallized specimens, both values are present.

The percent recrystallized is determined by comparing the size of both populations to the total number of indentations made. Good correlation was found to exist between kinetic curves obtained by this method, and those obtained by calorimetric means.

2.4.2 X-RAY TECHNIQUES

When a metal is plastically deformed by rolling, the grains in the metal workpiece will experience a shape change, becoming elongated in the rolling direction. The grains interact during deformation, resulting in regions of compression, and other regions of tension.

The effect of varying strain on the lattice spacing and x-ray line position and shape is shown in Figure 2.13.[25] The position of the diffracted peak can be determined from Braggs law:

$$\lambda = 2d_0 \sin\theta \qquad \ldots(2.31)$$

where λ is the wavelength of the x-ray beam, θ is the incident angle the beam makes with the crystal surface, and d_0 is the unstrained lattice spacing.

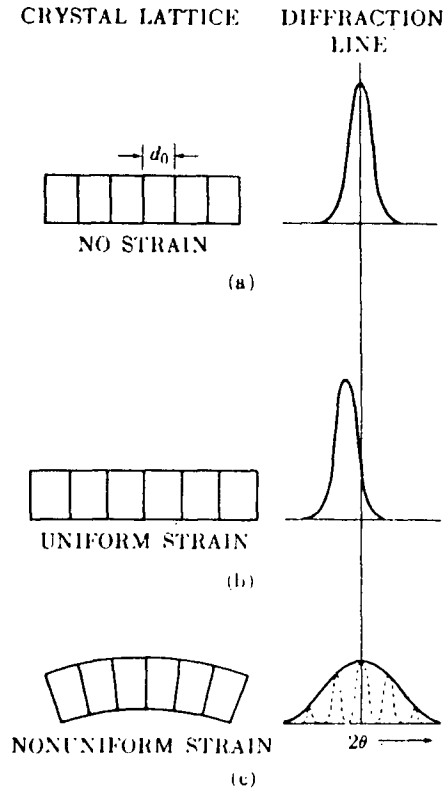

Fig. 2.13 Effect of lattice strain on Debye-line width and position.(Ref.25)

If the crystal is given a uniform tensile strain at right angles to the reflecting planes, the lattice spacing will increase by Δd, resulting in a shift in peak position.

If a non-uniform strain is given to the crystal, such as in bending, one side will be in tension with a lattice spacing $d_o + \Delta d$, while the other side will be in compression, spacing $d_o - \Delta d$. In between, a wide variety of spacings will exist between these two extremes. A plastically deformed crystal can then be assumed to be comprised of a number of small regions of varying plane spacings. The single large diffraction peak characteristic of spacing d_o will be replaced by a greater number of smaller peaks, represented in the figure by dotted curves. Combining these curves, a broadened diffraction line is produced, Figure 2.13(c).

To enable use of a single peak diffraction line as a means to determine the amount of cold work in a metal, standard peak widths, that of the annealed and fully cold worked specimens must be known. However, if the $K\alpha$ doublet peak of a cold worked metal is examined, the two peaks $K\alpha_1$ and $K\alpha_2$ will combine, at higher degrees of cold work, to produce one broad peak, Figure 2.14. When a cold worked metal is fully annealed, both peaks will be resolved. Therefore, a better estimation of the amount of strain introduced into a metal by cold work can be obtained by inspection of the $K\alpha$ doublet.

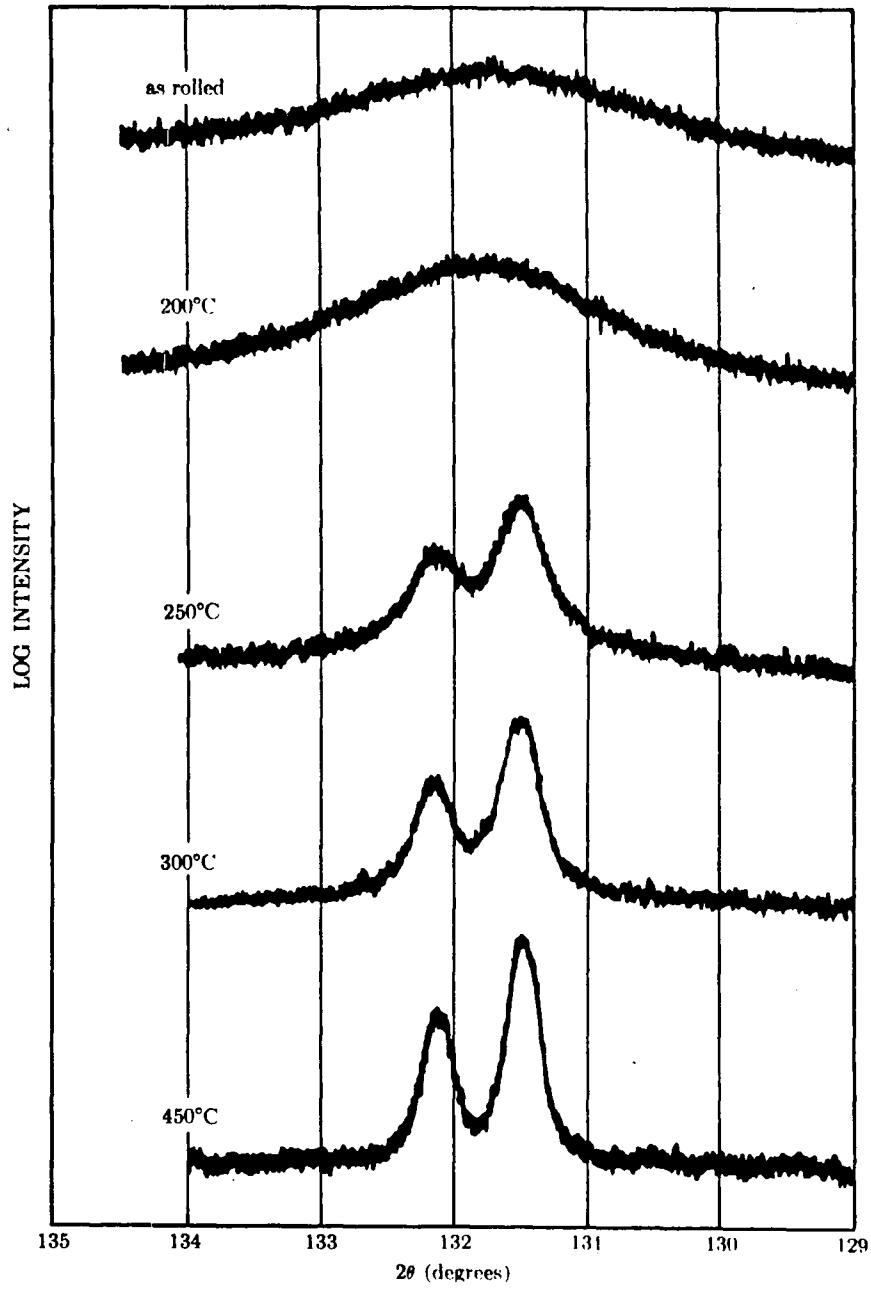

Fig. 2.14 Effect of strain on the {331} doublet peak resolution in 70-30 brass.(Ref.25)

Since recovery involves partial stress relief, on both a microscopic and macroscopic level, the broad x-ray peaks of a cold worked metal will partially sharpen during recovery. When recrystallization occurs, the Kα doublet peaks will become partially resolved, with sharper resolution occuring as recrystallization proceeds. Unfortunately, grain growth after recrystallization cannot be detected using x-ray diffractometry.

Grain growth can be detected using back reflection pinhole photographs. The sharply defined Debye lines associated with a fine grained, annealed metal will become spotty as the grain size increases, Figure 2.15.[25] The initial peak of the cold rolled metal is very broad and diffuse.

There has been some research done to characterize the degree of peak resolution on various x-ray diffraction peaks during annealing of cold worked steels. Hawbolt[26] and DiCello[27] both examined the effect of recovery and recrystallization on the {211} x-ray 1/2 peak width using Fe Kα and Cr Kβ radiation, respectively. Both researchers found that considerable resolution of the peak occurred during recovery and recrystallization. Figure 2.16[26] compares the x-ray results obtained by Hawbolt with the hardness results obtained on the same specimens. The hardness results display an inflection point at approximately 12s, at which point recrystallization starts, followed by a sigmoidal hardness drop with time characteristic of recrystallization. The 1/2

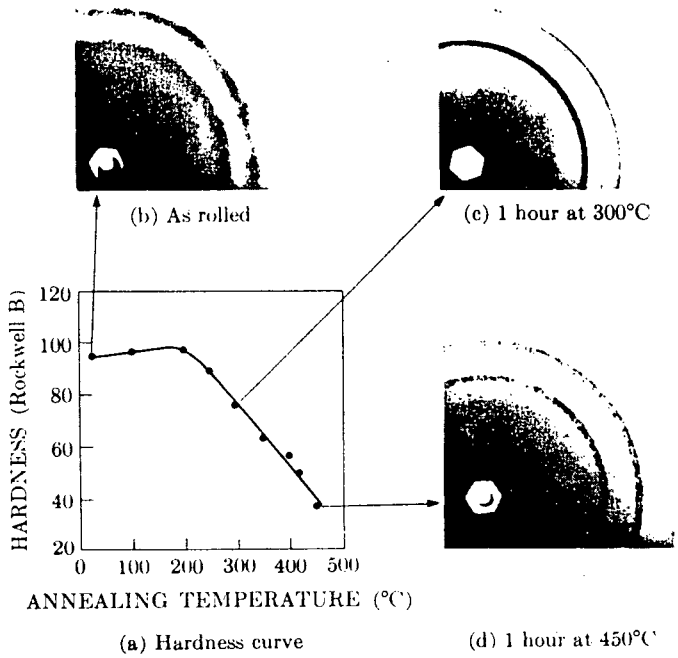

Fig. 2.15 Effect of recrystallization and grain growth on back reflection pinhole patterns of 70-30 brass specimens.(Ref.25)

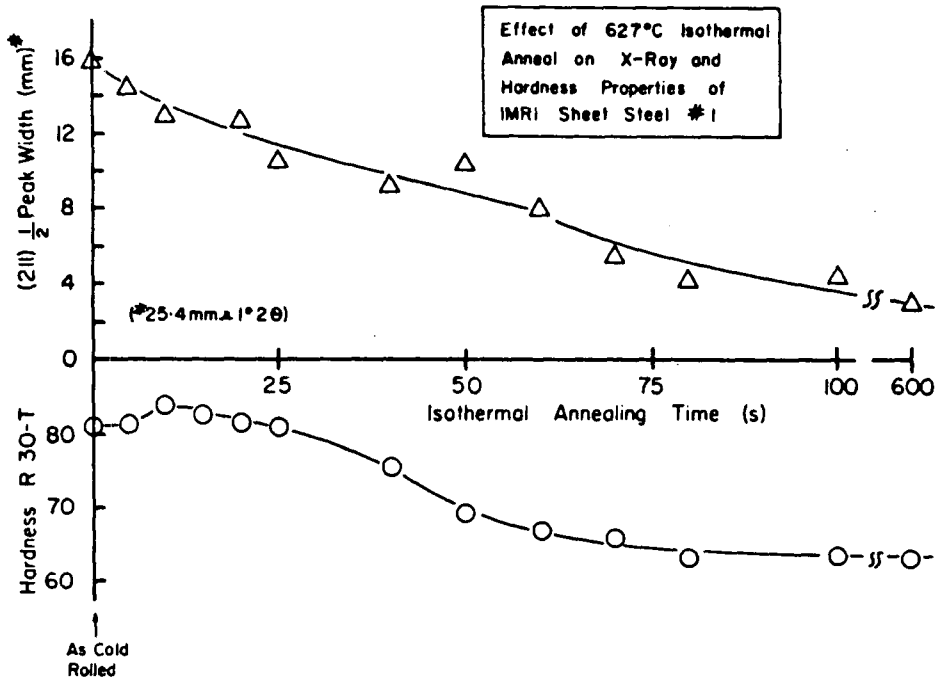

Fig. 2.16 {211} 1/2 peak width and R 30-T hardness versus time in annealed steel specimens.(Ref.26)

peak width readings do not display either the inflection point, or the sigmoidal shaped recrystallization curve.

Hawbolt[26] also examined the $K\alpha_2/K\alpha_1$ peak height ratio, which was correlated to hardness measurements and metallographic observations. Although a ratio change was noted during both recovery and recrystallization, it would appear that recovery affected the ratio to a greater extent than recrystallization, for the particular steel tested, Figure 2.17.

The main disadvantage of 1/2 peak width and $K\alpha_2/K\alpha_1$ peak ratio x-ray measurements appear to be the large counting interval required to obtain the required peak definition. This limits their usefulness during the high heating rates encountered during continuous annealing.

Hu and Goodman[28] examined the degree of recovery in low carbon steels of different manganese contents using a parameter called the "fractional residual line broadening", defined as:

$$(B_T-B_{rex}/(B_{cr}-B_{rex}) \qquad ...(2.32)$$

where B_T is the broadening parameter of the partially recovered (and recrystallized) specimen, B_{rex} and B_{cr} are the broadening parameters for a fully recrystallized and cold rolled specimen respectively. The variable B can be defined as:

$$B=(I_{min}-I_b)/(I_{max}-I_b) \qquad ...(2.33)$$

where I_{min} is the intensity minimum between the $K\alpha_1$ and $K\alpha_2$ peaks using Mo $K\alpha$ radiation, I_{max} is the intensity of the

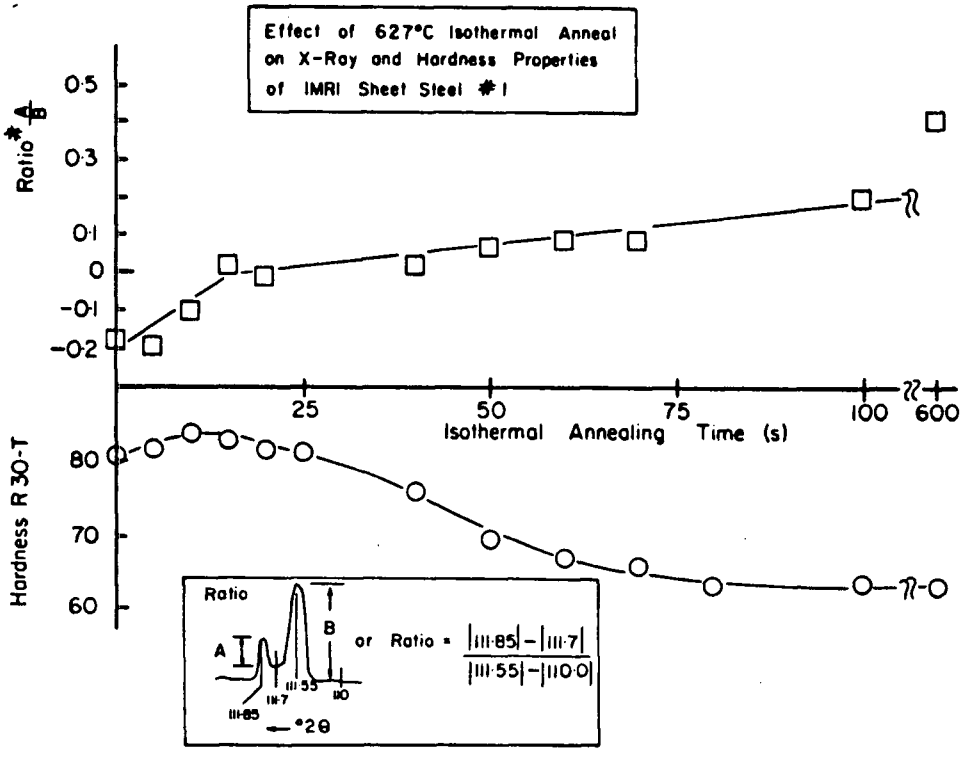

Fig.2.17 {211} x-ray peak ratio and R 30-T hardness versus time in annealed steel specimens.(Ref.26)

$K\alpha_1$ peak, and I_b is the background intensity.

The results obtained for {200}, {222} and {112} reflections, in addition to the actual percent recrystallized is shown in Figure 2.18. Once again, it appears that the parameter is affected to a greater extent by recovery than primary recrystallization. However, an inflection point appears to exist in each curve which roughly corresponds with the onset of recrystallization determined metallographically, Figure 2.18(c).

When a narrow beam of monochromatic x-rays are incident on a crystal, the intensity of the reflected beam will be greatest at the angle where the Bragg law, equation (2.31), is satisfied, known as the Bragg angle, θ_B. However, the intensity of the beam will be fairly large at angles which slightly deviate from θ_B. If all the diffracted beams are measured around θ_B, the total energy, termed the "integrated intensity" of the refracted beam is obtained.[25]

Ono et. al.[29] examined the recrystallization texture of cold rolled steel using the integrated intensity values of the {222}, {200} and {110} peaks. Their results are shown in Figure 2.19, where the changes in integrated intensities are compared with hardness changes during recrystallization and texture development. It is apparent that texture development reproduces the kinetics of the recrystallization process fairly well in some cases although the texture development is clearly dependent upon such factors as AlN precipitation.

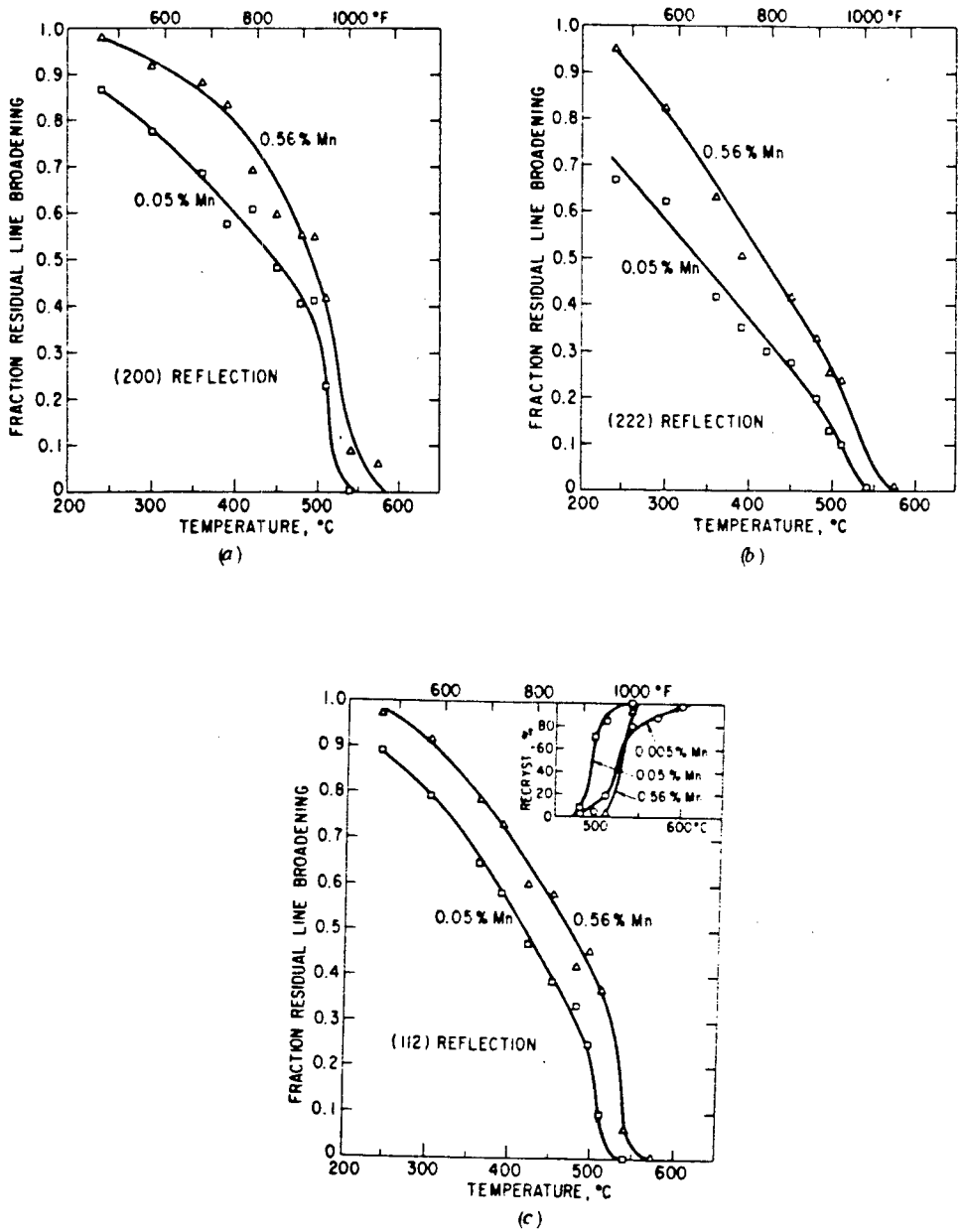

Fig. 2.18 X-ray line broadening and fraction recrystallized versus temperature in manganese steels.(Ref.29)

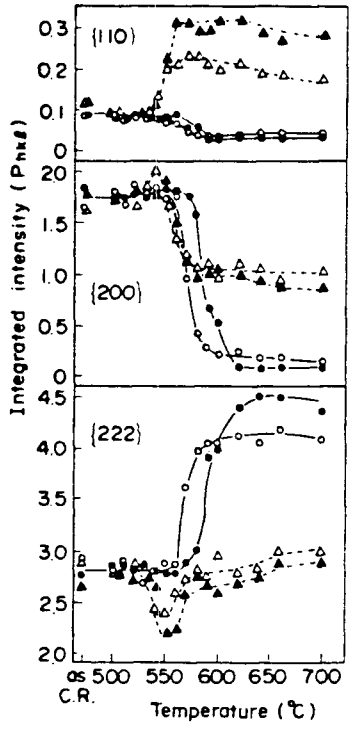

○, △: Steel 1 ●, ▲: Steel 4
△, ▲: Speciemens with AlN precipitation treatment in hot bands

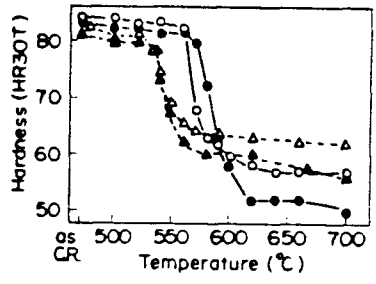

○, △: Steel 1 ●, ▲: Steel 4
△, ▲: Specimens with AlN precipitation treatment in hot bands

Fig. 2.19 Integrated x-ray peak intensities and hardness versus temperature in steels during continuous heating.(Ref.29)

2.4.3 MISCELLANEOUS TECHNIQUES

Abe and Suzuki[30] monitored the changes of a steel's electrical conductivity during annealing and correlated it to the various microstructural phenomena that occur. The resistivity changes in a cold rolled, low carbon steel during annealing are shown in Figure 2.20. For comparison purposes, the hardness changes and the fraction recrystallized are also plotted. Three distinct stages were noticed during annealing. During the first stage, the recovery stage, a decrease in resistivity is observed as dislocations were annihilated prior to any visible recrystallization. The second and third stages exhibit an increase in resistivity due to other factors unrelated to the various annealing phenomena.

DiCello and Cullity[27] noted that cold worked metals show a decrease in their magnetic permeability compared to annealed metals. Figure 2.21 illustrates the property changes exhibited by a low carbon steel sheet during annealing, comparing magnetic, hardness and {211} x-ray 1/2 peak line width values. Obviously annealing causes substantial changes in all properties, however both magnetic permeability and x-ray peak width display substantial change during the recovery process. In the case of magnetic permeability, the temperature at which recrystallization initiates is not clearly evident.

Hawbolt[26] also examined the use of magnetic permeability for measuring primary recrystallization of an

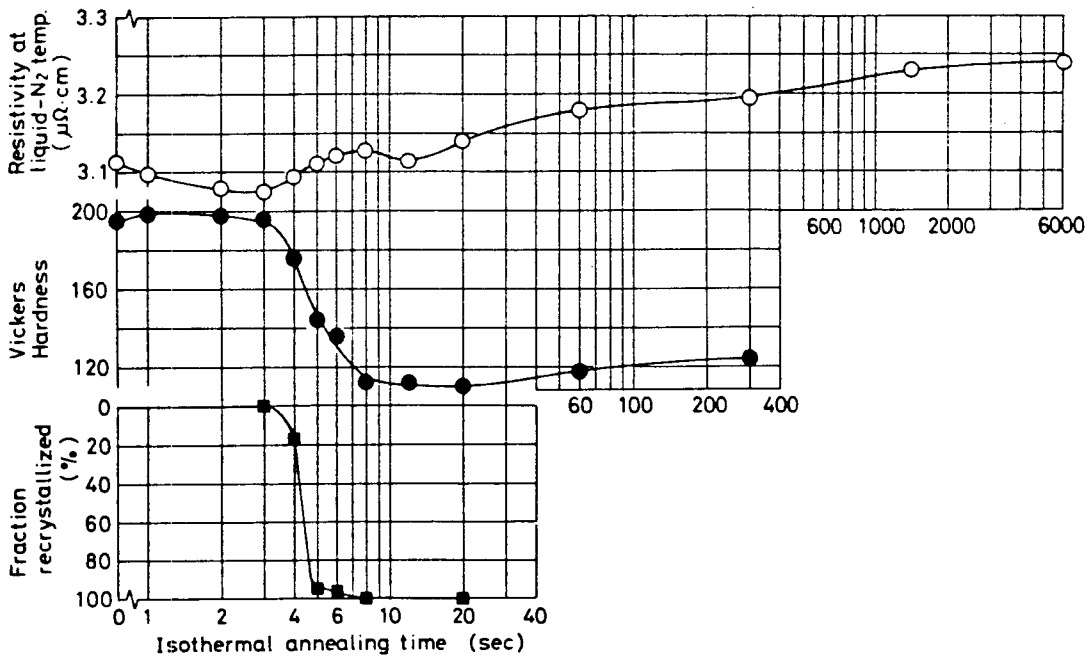

Fig. 2.20 Electrical resistivity, hardness and fraction recrystallized versus annealing time in low carbon steel. (Annealing temperature, 695°C.)(Ref.30)

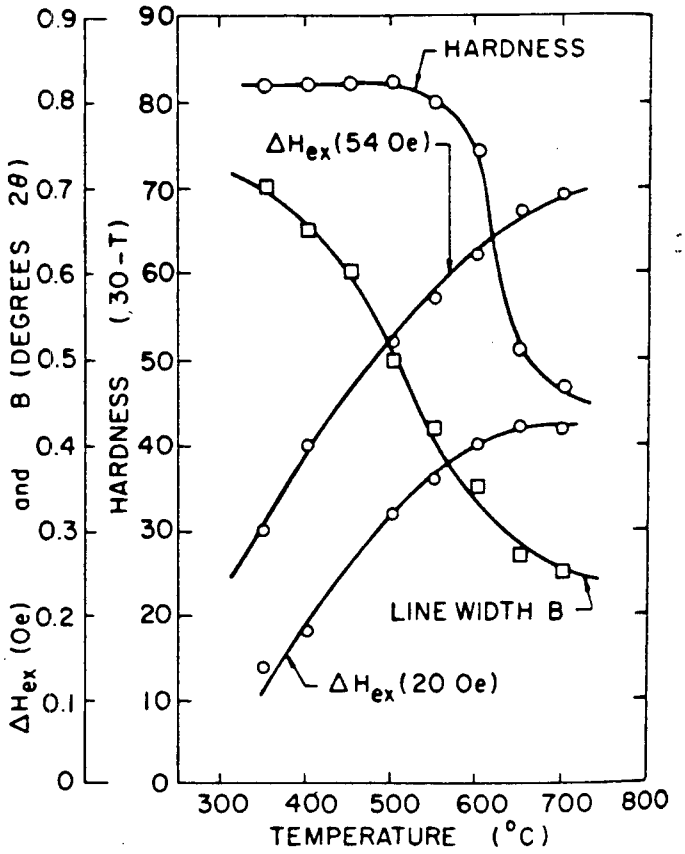

Fig. 2.21 Property changes in steel sheet annealed at various temperatures.(Ref.27)

80 percent cold worked steel using an experimental set-up similar to DiCello and Cullity. However, poor reproducibility resulted during the tests, and it was noted that specimen position with respect to the Hall effect device, as well as temperature gradients in the specimen gave rise to large errors.

Other methods that have been used to study the cold worked and annealed states have been summarized by Byrne[3]. These include mechanical properties such as yield strength, impact resistance, density, and changes in the elastic modulus. In addition, calorimetric measurements have been used to determine the total energy of cold work, and compare the energy released during recovery and recrystallization.

2.5 INDUSTRIAL ANNEALING PROCESSES

During the manufacture of cold rolled steel sheet, the plasticity of the material is exhausted, resulting in reduced formability, and increased hardness. If the sheet is to be used in subequent forming operations, the ductility must be restored through appropriate heat treatments which result in recrystallization and softening of the steel.

Two processes are currently employed by the steel industry for accomplishing this task, batch annealing (BA) and continuous annealing (CA).

2.5.1 BATCH ANNEALING

Batch annealing involves heating tight-wound coils in a gas fired furnace containing a recirculating atmosphere of inert gas. A schematic diagram of such a furnace is given in Figure 2.22.[31] The coils are stacked on convector plates which enable circulation of the inert gas over the coil edges. The whole stack is placed on an annealing base, and then covered by a protective cover of heat resistant material which confines the inert gas atmosphere, and protects the coils from the furnace gases. A furnace is then placed over the protective cover, and firing is accomplished by burners. A fan in the annealing base provides the means for recirculation of the inert atmosphere.

The tight-wound coils result in a large thermal mass, making heating and cooling rates relatively slow. A typical representation of the annealing cycle experienced during batch annealing is shown in Figure 2.23(A).[32] Heating rates are usually in the order of 20-100°C/h. The entire process generally takes several days to complete.

The maximum temperature obtained during the soak cycle is limited to approximately 700-730°C. At higher temperatures, coarse carbides will form, which are detrimental to formability during subsequent manufacturing operations. During the slow cooling cycle, nearly all the carbon will precipitate by the time ambient temperature is reached, thereby eliminating quench and strain aging from occuring.

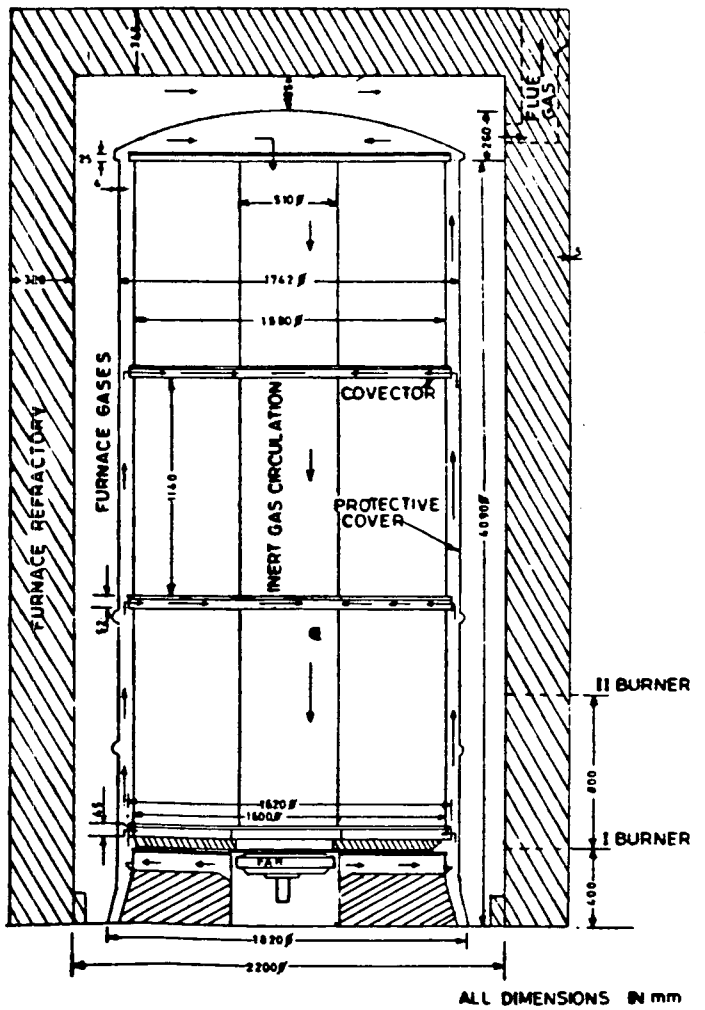

Fig. 2.22 Schematic drawing of a batch annealing furnace.(Ref.31)

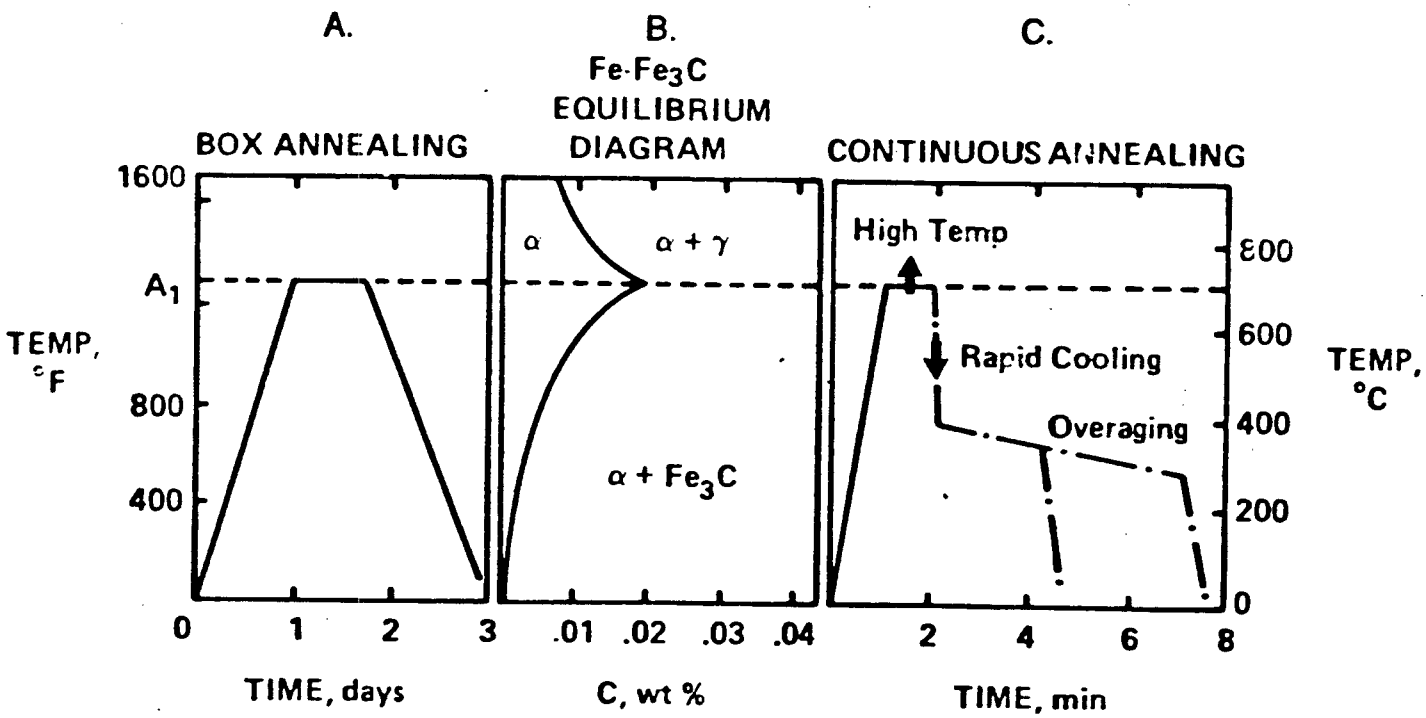

Fig. 2.23 Comparison of batch and continuous annealing cycles with the iron-carbon phase diagram.(Ref.32)

2.5.2 CONTINUOUS ANNEALING

Typical CA lines combine several different processes including electrolytic cleaning, annealing, overaging and sometimes temper rolling. Descriptions of CA lines are available in the literature.[33,34] A schematic drawing of a typical CA installation (at Inland Steel, Chicago) is shown in Figure 2.24. A more detailed schematic drawing of the annealing and aging furnaces is shown in Figure 2.25.

The annealing furnace consists of four sections, preheat, heat, soak and gas jet cool sections. The preheat section improves the efficiency of the heat section by using exhaust gases from the heat section to raise the strip temperature prior to heating. Both the heat and soak sections use multipass radiant tubes fired by natural gas to heat and maintain the steel to the required annealing temperature. Heating rates of 8-12°C/s are common. Cooling is then accomplished by gas jets, followed by water quenching using quench nozzles.

The aging furnace consists of the reheat, overage and fast cool zones. Reheating is accomplished by multipass radiant tubes, after which the strip passes into the overage section where recirculating fans provide convective cooling to bring the strip down to the required overaging temperature. Gas jets are then employed in the fast cool zone to cool the strip.

The main area where CA processes differ are in the cooling media used during cooling from the annealing

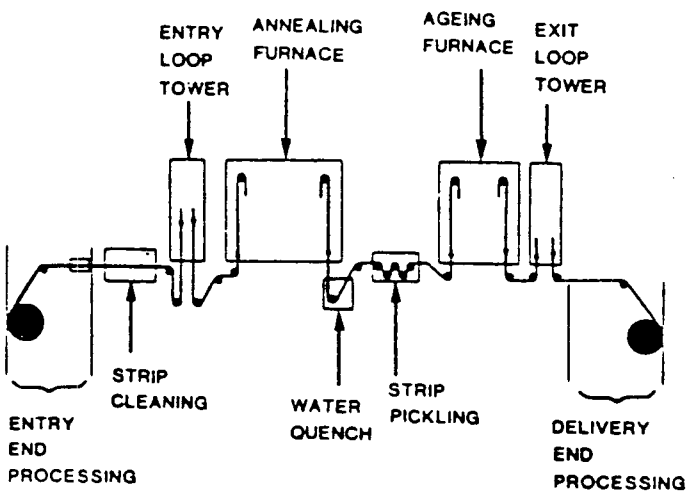

Fig. 2.24 Major components of a continuous annealing line.(Ref.34)

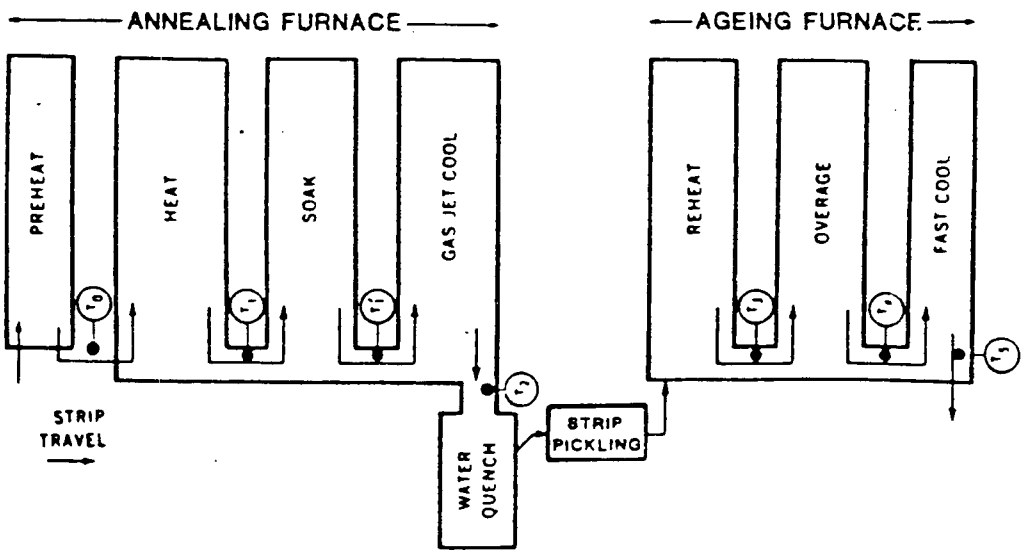

Fig. 2.25 Furnace sections of a continuous annealing line.(Ref.34)

temperature. Gas jet cooling employs a nitrogen/hydrogen gas mixture which passes through jets which impinge on the steel sheet. Using this method, cooling rates of about 5-30°C/s can be obtained. Gas/water cooling is used to obtain cooling rates in the order of 80-300°C/s during the manufacture of high strength steels.[35] Water quenching provides cooling rates in excess of 1000°C/s.

The selection of cooling media will affect the heating procedure in the aging furnace. Gas jet cooling enables the cooling to be arrested at the overaging temperature, eliminating subsequent reheating prior to aging that is necessary when water quenching is used.

The exact processing procedure used will vary depending on the steel composition and its application. Therefore, annealing processes will vary from company to company depending on their product line.

In the CA process, the time at maximum temperature is short, giving little time for carbide coarsening to occur. Therefore, temperatures which are considerably above the A_1 temperature, Figure 2.23(B), can be used to allow for faster recrystallization and grain growth, Figure 2.23(C). The fast cooling rate from maximum temperature does not allow for complete carbide precipitation from ferrite, making overaging necessary. The resultant carbides in CA products are finer which aids in formability of deep drawn parts.

The shorter processing times due to the higher heating rates and annealing temperatures, as well as the fast

cooling rates enables processing of the steel strip to occur in a matter of minutes (usually 4-8 min), resulting in improved yield over BA processes. CA is also more versatile in that a wide range of steel grades can be manufactured due to the wide range of temperatures and cooling rates available.

3. EXPERIMENTAL PROCEDURES

All experimentation was performed on 88.8 percent cold rolled, rimmed, low carbon steel sheet of gauge thickness 0.213 mm (0.0084"). The steel chemistry is listed in Table 3.1. A rimmed steel was choosen to avoid recrystallization problems related to AlN precipitation typical of aluminum killed steels.[16-18] Although some acid soluble aluminum is present, this is below the level required to cause delayed kinetic response. A typical microstructure of the cold rolled sheet is shown in Figure 3.1.

The experiments were divided into three distinct areas:

1. the determination of the test steel's isothermal recrystallization kinetics over an appropriate range of temperatures,
2. the determination of the steel's recrystallization kinetics during selected continuous heating cycles, and
3. a check on the applicability of the additivity principle for predicting the continuous heating recrystallization kinetics using the experimentally determined isothermal data.

3.1 ISOTHERMAL RECRYSTALLIZATION KINETIC MEASUREMENTS

Molten salt annealing was used to subject the test steel to the required isothermal temperatures. Draw Temp 430, a commercially available tempering salt, manufactured by Houghton, was used for this purpose.

Table 3.1 Steel Composition.

Element	Weight Percent
C	0.071
Mn	0.350
P	0.005
S	0.018
Si	0.002
Cu	0.011
Ni	0.010
Cr	0.032
Mo	0.002
V	0.002
Cb	0.002
Al	0.011 (0.002)*

* acid soluble aluminum

Fig. 3.1 Typical microstructure of the as received, 88.8 percent cold reduced, rimmed steel.(X353 mag.)

Specimens approximately 20 mm square were cut out of the steel strip using sheet metal shears. All specimens were then cleaned in denatured 90 percent ethanol to eliminate oil and other foreign substances from their surfaces.

Upon stabilization of the salt bath temperature, specimens were immersed for the required time interval. No more than four specimens were immersed in the salt bath at once. The salt bath temperature was found to deviate from it's setpoint by ±3°C for all temperatures investigated. Upon removal of the specimen, cooling was performed by water quenching to avoid further recrystallization on cooling.

The annealed specimens were fixed to a flat plastic mount using two sided tape. Metallographic preparation followed using 320, 400 and 600 grit grinding paper, and 5μ and 1μ alumina powder. The microstructures of the polished specimens were revealed using 2 percent nital etchant.

The determination of volume fraction recrystallized in each specimen was accomplished by microscopic examination, and by diamond pyramid microhardness testing (DPH) using a Tukon microhardness tester, and a 100g load.

The number of indentations necessary to give a statistically significant result was determined using statistical hypothesis testing.[38] Two specimens were annealed at 600°C for 5 and 9 seconds respectively, and subjected to 24 indentations each. For each specimen, the microhardness values were divided into random groups of 4, 6, 8 and 12. For each group, the mean and standard deviation

was calculated, and compared with that for all 24 indentations. This comparison yielded a "P value" for each group, which can be defined as the smallest significance level at which the hypothesis that the two group means are equal, can be rejected. Therefore, as P gets higher, the less evidence there is to reject the hypothesis.[38]

Values of P greater than 0.2 are typically considered to be acceptable. As can be seen in Table 3.2, only 4 indentations result in P values less than 0.20. Therefore, 6, 8 and 12 indentations would all appear to yield statistically significant results. Twelve indentations resulted in the best P values, with the smallest variability, however, the time involved in making this number of indentations was considered to be excessive. Eight indentations was finally choosen as being an acceptable compromise.

The isothermal recrystallization kinetic data obtained from hardness evaluation was converted to fraction recrystallized by determining the hardnesses at the start and finish of the recrystallization process and assuming it to be constant regardless of the isothermal temperature used. The sigmoidal shape of the hardness versus time curve was analyzed using equation (2.22). Assuming a linear relationship exists between fraction recrystallized, X, and hardness variation,[14-16,24] X was determined using the relationship:

$$X=(DPH_0-DPH_t)/(DPH_0-DPH_{100}) \qquad ...(3.1)$$

Table 3.2 Hypothesis Testing Results for the Determination of an Acceptable Number of Microhardness Indentations.

# Indentations/Group	P Value	
	Mean	Range
4	0.54	0.04-0.98
6	0.42	0.26-0.84
8	0.61	0.30-0.97
12	0.73	0.62-0.84

where DPH_0 and DPH_{100} are the hardnesses of the steel at the start and completion of the isothermal recrystallization event, and DPH_t is the hardness at time t, during recrystallization.

The recrystallization start time, t_{av} , for each isothermal temperature, was initially determined by visually estimating the times, t_{est} , at which recrystallization initiates through use of metallographic examination, and visual examination of the hardness data. The sigmoidal shape of the hardness versus time curve was analyzed using equation (2.22). Using least squares analysis, the best fit line was determined for a plot of ln ln(1/1-X) versus ln $(t-t_{est})$, and it's correlation coefficient recorded. The estimated start time was then varied by a small time increment, Δt, and the best fit line determined once again. The procedure was repeated until the maximum correlation coefficient was determined; this start time was taken as t_{av} .

The Avrami parameters b and k, equation (2.22), were then determined by taking the intercept of the $\ln(t-t_{av})$ vs ln ln(1/1-X) plot at $(t-t_{av})=1s$, and the line slope respectively.

The experimental isothermal recrystallization kinetics for a range of temperatures were then described by mathematical expressions describing the temperature dependence of the kinetic parameters b and k.

3.2 CONTINUOUS HEATING RECRYSTALLIZATION KINETIC MEASUREMENTS

Two methods were used to determine the recrystallization kinetics of the test steel during continuous heating conditions. The method employed was determined by the heating rate.

For heating rates meant to simulate batch annealing conditions (70.7°C/h and 65.5°C/h), recrystallization was monitored insitu using a controlled temperature hot x-ray camera. Strip specimens shown in Figure 3.2, were resistance heated in the inert, helium atmosphere at the required heating rate. The temperature was controlled and monitored by means of a chromel-alumel thermocouple spot welded to the bottom surface, directly beneath the x-ray examination position. The temperature variation with position in the specimen was determined experimentally. The results are contained in Appendix 3. The resistance heated hot x-ray camera and sample are shown in Figure 3.3.

Recrystallization was monitored insitu by recording the shape of the {211} peak using FeKα radiation. The scan rate was set at 1/2°(2θ)/min, with a count interval of 1 or 2 seconds. The time required to scan from the Kα_1 peak through the valley between the Kα_1 and Kα_2 peaks was approximately 12 seconds, which is equivalent to 0.23°C at a heating rate of 70°C/hr, making each scan essentially isothermal.

The method of analysis used to determine the volume fraction recrystallized was based on the resolution of the

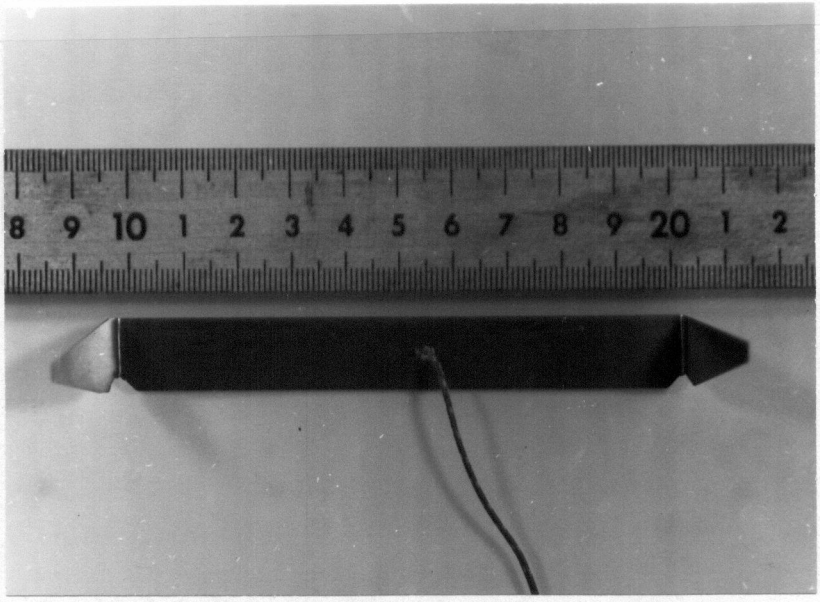

Fig. 3.2 Continuous heating strip specimen with thermocouple attached at centre of bottom surface.

(a)

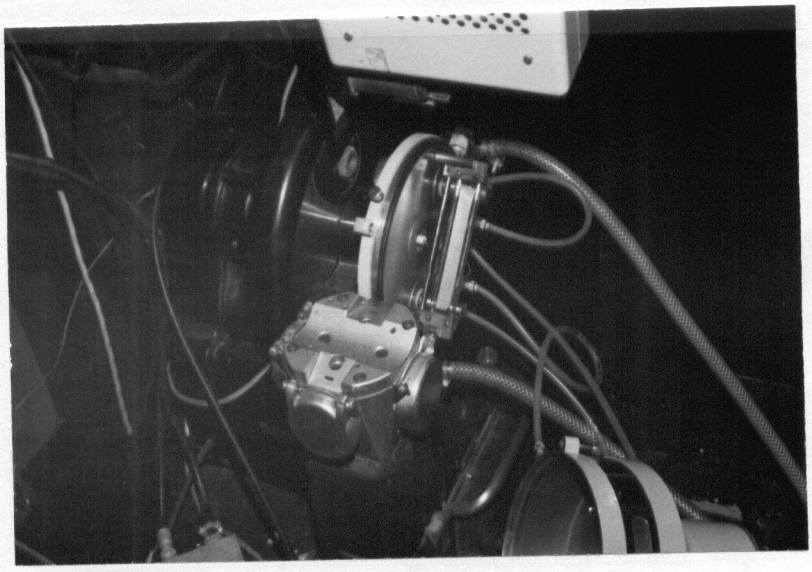

(b)

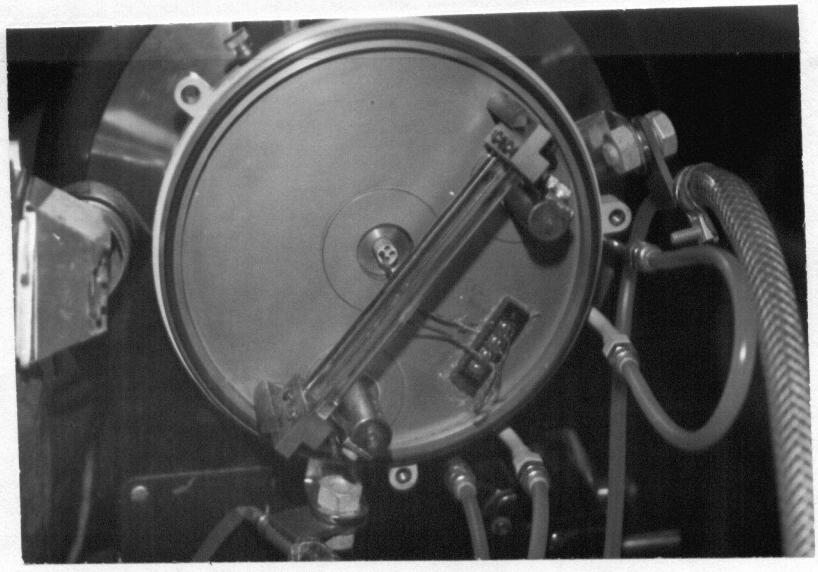

Fig. 3.3 (a) Experimental apparatus for continuous heating trials, (b) closeup of mounted specimen in open hot x-ray camera.

valley in the Kα doublet peak, as shown in Figure 3.4.[25,26] The parameter which was found to monitor recrystallization most effectively is given by the equation:

$$R_I=(I_{K\alpha_1}-I_{min})/(I_{K\alpha_1}-I_b) \qquad ...(3.2)$$

where $I_{K\alpha_1}$ is the intensity of the {211}, $K\alpha_1$ peak, I_{min} the intensity of the valley in the Kα doublet of the {211} peak, and I_b the background intensity.*

For heating rates greater than those encountered in batch annealing, the available x-ray scan rates were found to be too slow to enable use of the insitu method of recrystallization monitoring. This is because non-isothermal scans would result from the high heating rates. Therefore, an interrupted heating-quenching method was devised where successive specimens were heated up at the required rate to progressively higher temperatures, followed by cooling to room temperature. Heating rates used were 686°C/min, which is typical of CA conditions, and 43.8°C/min which is between BA and CA conditions. Cooling was accomplished by shutting off the power and air cooling the specimen in the furnace atmosphere; the cooling rate was enhanced by the water cooled grips used for resistance heating of the specimen. Cooling rates of approximately 63°C/s were realized using this procedure.

After the specimens were cooled to room temperature, a series of four x-ray scans were performed and analyzed for Kα valley resolution as described by equation (3.2) above. A

---

* Cullity suggested use of the ratio $I_{min}/I_{K\alpha_1}$ for describing fraction recrystallized.[25]

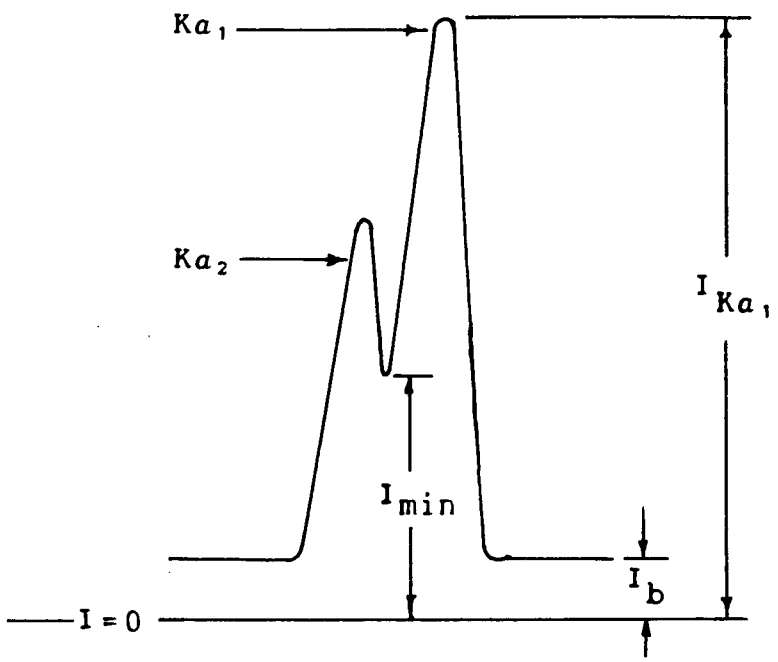

$$R_I = (I_{K\alpha_1} - I_{min})/(I_{K\alpha_1} - I_b)$$

Fig. 3.4 Method of analysis of {211} Kα x-ray peak using equation (3.2).

small section was removed from the centre portion of each specimen, mounted, polished, etched and microscopically examined for recrystallization. Eight microhardness indentations were made in each polished specimen immediately adjacent to the thermocouple position.

The interrupted heating-quenching method was also used to determine hardness on specimens subjected to the BA heating rate of 70.7°C/h.

The start times and temperatures of recrystallization during continuous heating were determined by visually examining the shape of the continuous heating kinetic curves obtained by x-ray and microhardness testing.

The effect of a prior recovery heat treatment on recrystallization kinetics was also investigated. Here, a specimen was subjected to a recovery heat treatment of 440°C for 14,000 seconds, and then allowed to cool to room temperature. During the recovery heat treatment, oscillating scans of the {211} Kα peak were performed to monitor the progress of recovery. The specimen was then heated at a rate of 65.5°C/h, the recrystallization being monitored using the insitu x-ray method described above.

The effect of continuous heating on pre-recystallization recovery response, and the subsequent recrystallization kinetics was examined by heating a strip specimen, at a rate of 2.58°C/s, to 480°C, where it was recrystallized isothermally. The progress of recrystallization was monitored insitu by using oscillating

x-ray scans of the {211} Fe Kα doublet peak. The Avrami kinetic parameters were then calculated by determining the best fit Avrami line using least squares analysis.

3.3 CONTINUOUS HEATING RECRYSTALLIZATION KINETIC PREDICTIONS

The recrystallization kinetics obtained during continuous heating were predicted utilizing the experimentally determined start times, t_s , the isothermal recrystallization kinetic data, and the principle of additivity. A computer program was written to perform the calculations; the program is listed in Appendix 1.

The procedure used for predicting the recrystallization kinetics on continuous heating can be explained with the aid of Figure 3.5. The continuous heating cycle employed can be described by assuming it to be made up of a series of isothermal steps, Figure 3.5(a). At each step after recrystallization has started, i.e. after t_s , the fraction recrystallized was calculated based on the isothermal recrystallization kinetics at the temperature of the particular isothermal step, and the fraction of recrystallized material already present, ie., assuming that recrystallization is an additive structure change.[21] This is illustrated schematically in Figure 3.5(b). If the temperature at which transformation starts is T_1, then during the time interval $\Delta t/2$, the volume fraction transforming, ΔXT_1, is determined using the isothermal kinetic equation at T_1. At T_2 the virtual time required to

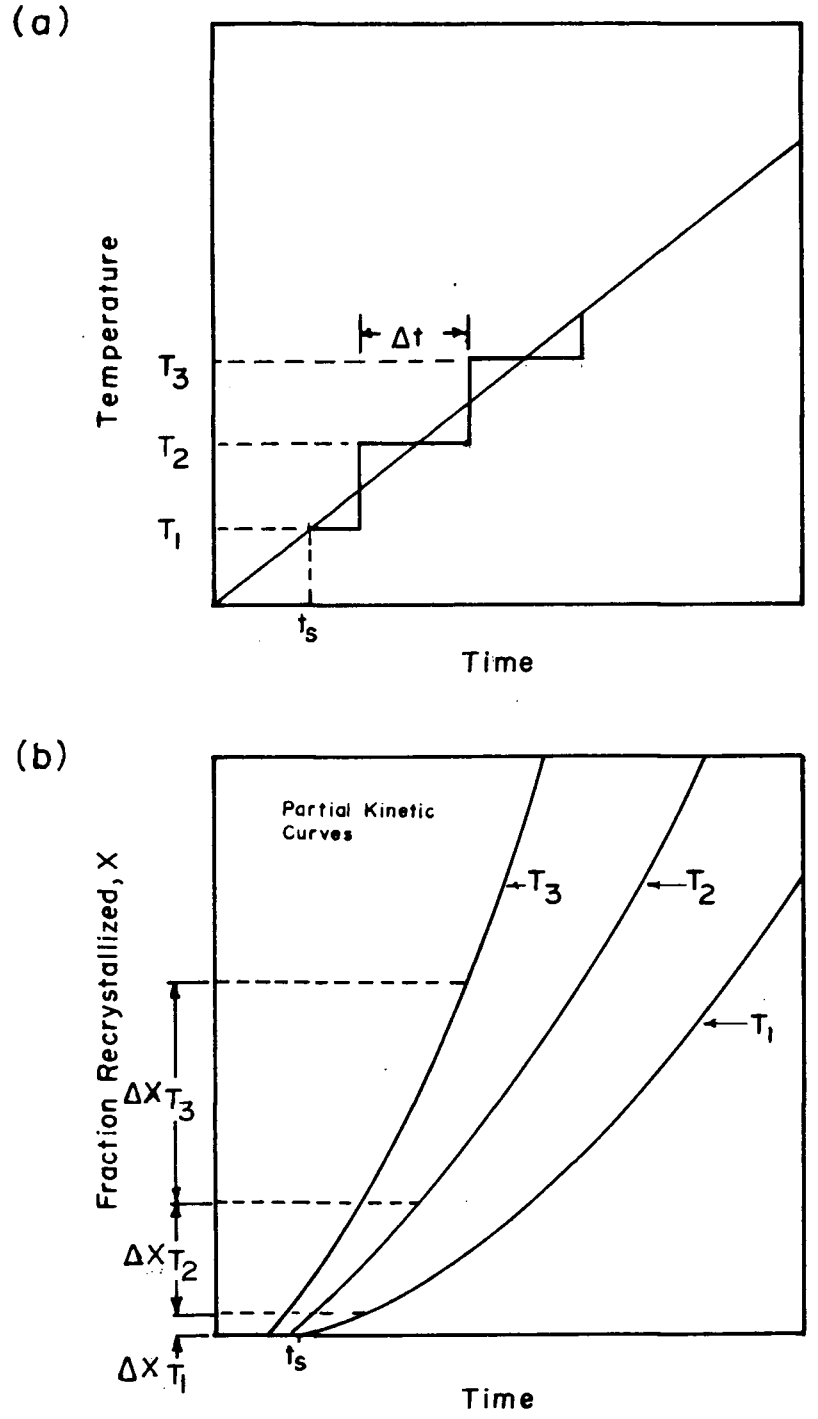

Fig. 3.5 Procedure for predicting continuous heating recrystallization kinetics using isothermal kinetic data.

produce ΔXT_1 at T_2 is calculated. To this time, Δt is added, and a new fraction is calculated for T_2 based on the isothermal kinetic equation. This process is continued until all the cold worked matrix has been consumed, and the volume fraction recrystallized equals one.

4. EXPERIMENTAL RESULTS AND DISCUSSION

4.1 ISOTHERMAL RECRYSTALLIZATION KINETIC RESULTS

Isothermal recrystallization kinetic results of microhardness versus time, for the temperature range of 440-560°C, are shown in Figures 4.1 to 4.8. Each point on the curve is the average of 8 indentations, the two error bars represent the maximum and minimum standard deviations observed during evaluation of the specimens. The hardness of the 88.8 percent cold rolled, as-received steel sheet based on 16 indentations was determined to be DPH 250.0±16.9. The hardness immediately prior to the onset of recrystallization was determined to be 252.2±4.2, based on 25 indentations. After recrystallization was complete, the hardness decreased to 127.3±2.3, based on 14 indentations. As a first approximation, the hardness prior to the initiation, and after the completion of recrystallization was assumed to be independent of the isothermal annealing temperature.

Three regions were typical of the isothermal recrystallization curves. Recovery occurred in the initial, relatively flat portion. As already mentioned, hardnesses in this region generally increased over that of the as received product, due to the return of short range order associated with the formation of subgrain boundaries.[3] In some instances, for instance at 500°C, shown in Figure 4.5, hardnesses as high as DPH 268 were encountered, followed by softening to a hardness typical of the recovered structure.

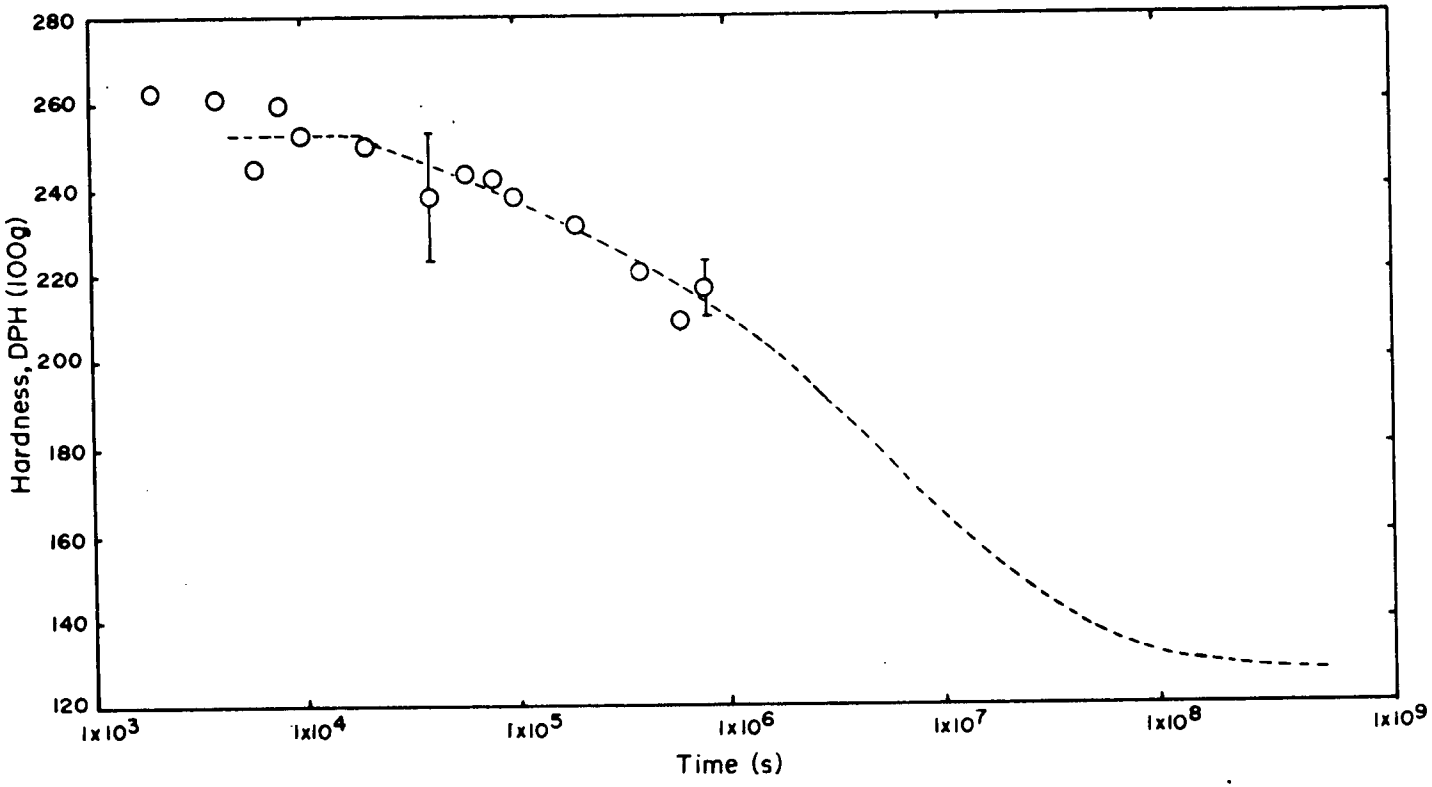

Fig. 4.1 Isothermal recrystallization kinetics, T=440°C.

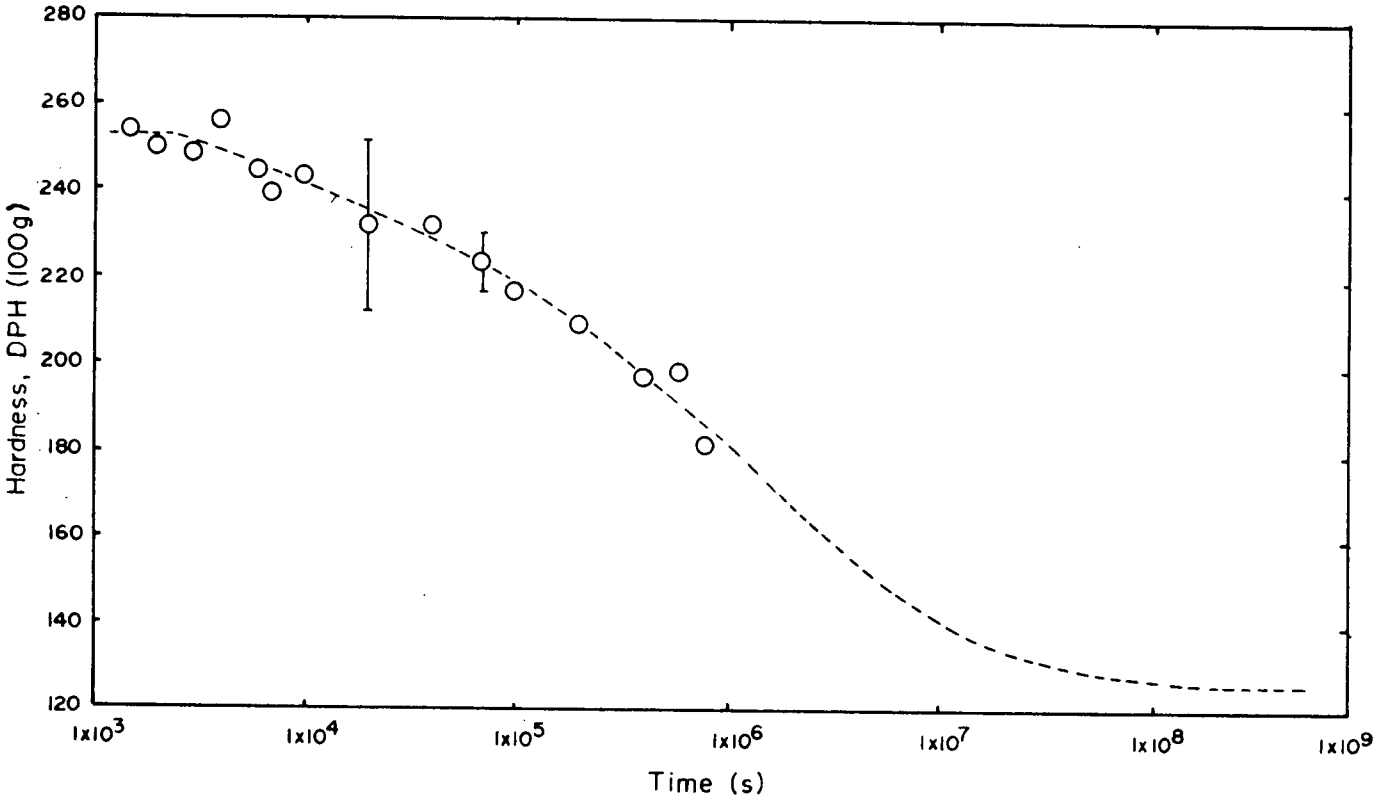

Fig. 4.2 Isothermal recrystallization kinetics, T=460°C.

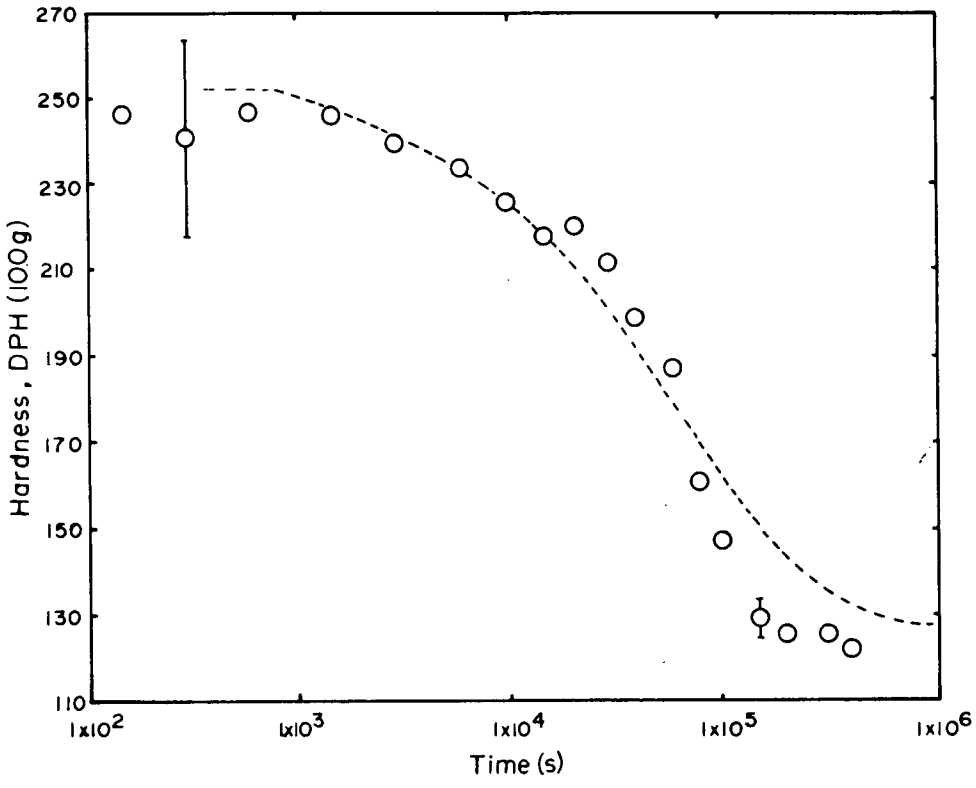

Fig. 4.3 Isothermal recrystallization kinetics, T=480°C.

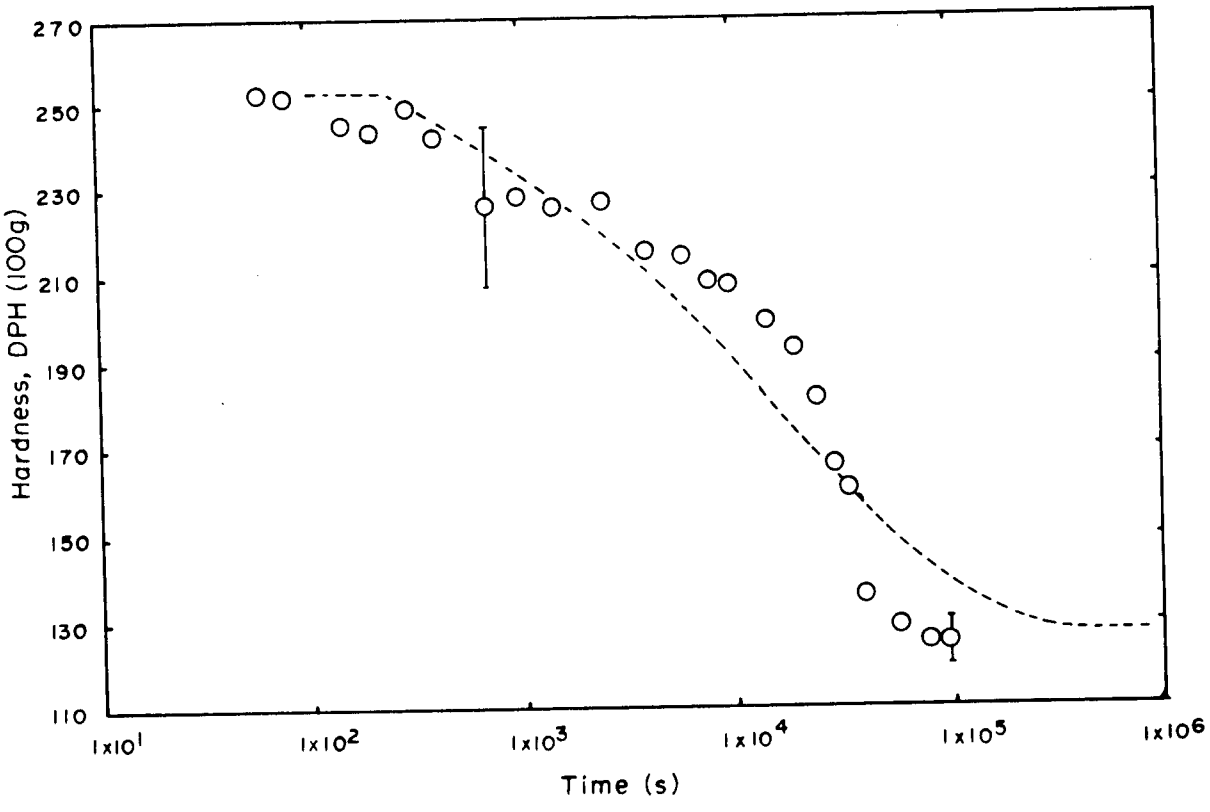

Fig. 4.4 Isothermal recrystallization kinetics, T=490°C.

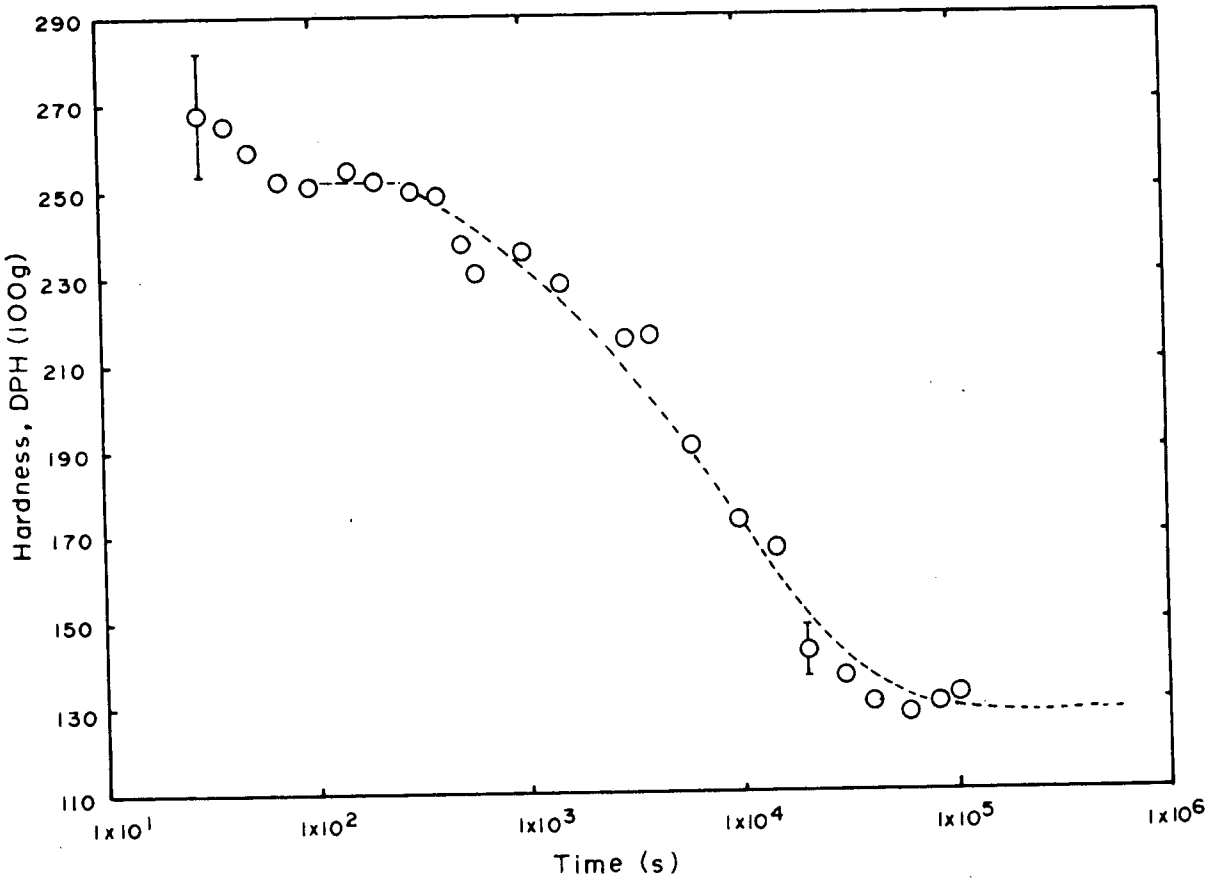

Fig. 4.5 Isothermal recrystallization kinetics, T=500°C.

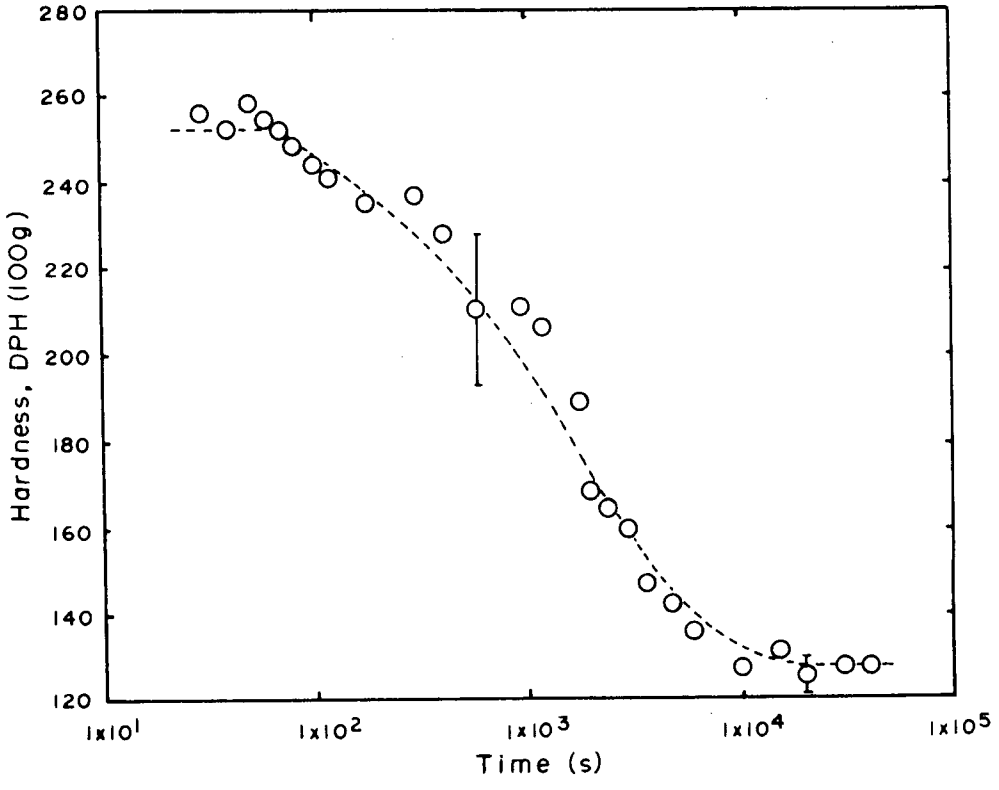

Fig. 4.6 Isothermal recrystallization kinetics, T=520°C.

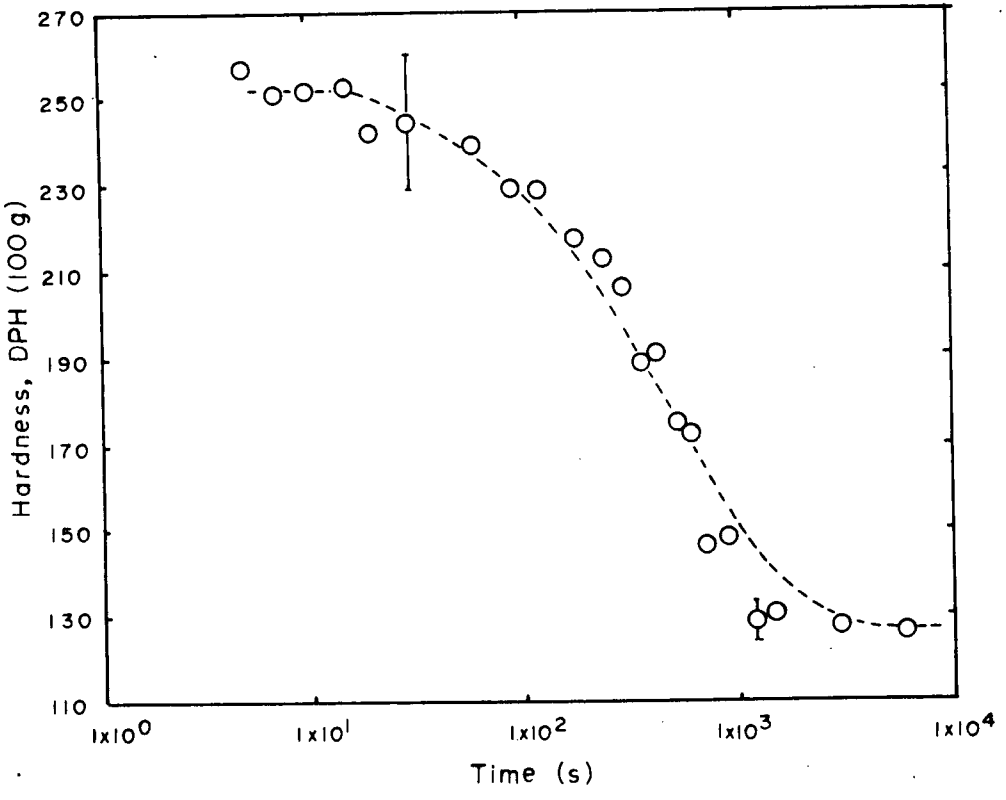

Fig. 4.7 Isothermal recrystallization kinetics, T=540°C.

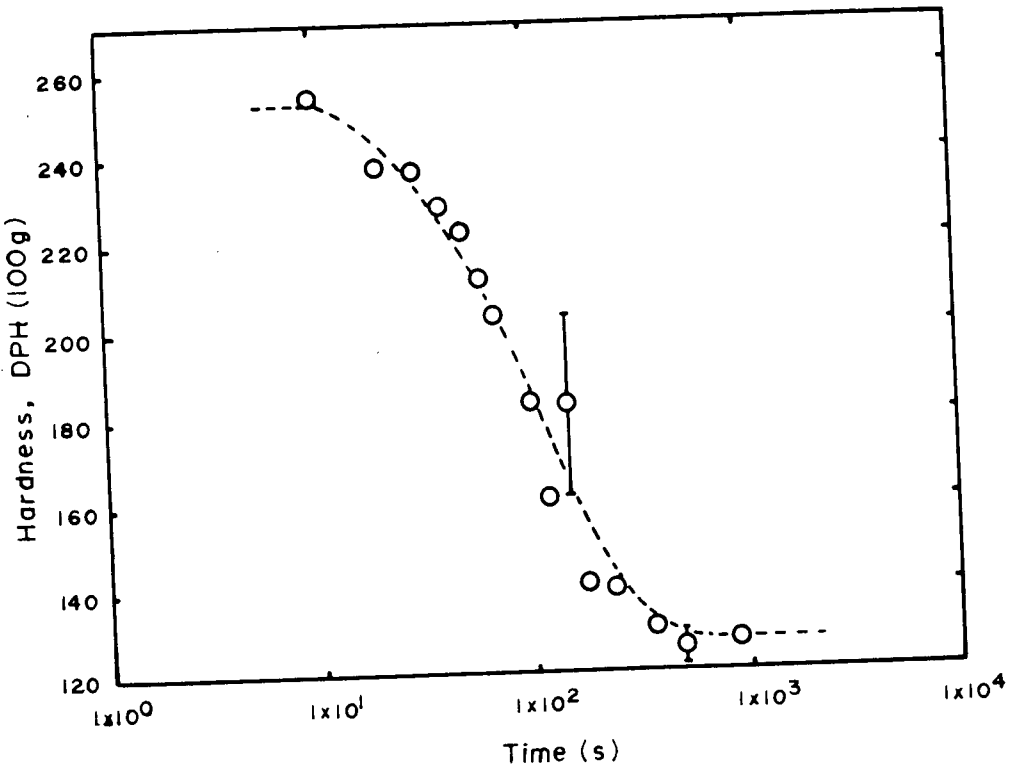

Fig. 4.8 Isothermal recrystallization kinetics, T=560°C.

This large hardness increase prior to recrystallization has been observed by other researchers, and attributed to the occurance of strain aging.[39] Any dissociated carbon present in the cold rolled steel may cause dislocation pinning, resulting in the return of the yield point, higher strength, and higher hardness. Once the carbon precipitates, it will no longer be in the form capable of causing strain aging, and the hardness values will return to those more typical of the recovered structure. Therefore, the slight hardness increase of DPH 2-5 can be attributed to recovery processes, while the more substantial hardness increase of approximately DPH 18 can be attributed to strain aging.

The second stage typical of the isothermal recrystallization curves displayed a sigmoidal hardness drop typical of recrystallization. In this region, the dislocation density is reduced due to the consumption of the cold rolled matrix by the high angle boundaries of the growing recrystallized grains.

The third region, representing grain growth displayed stabilization of the hardness resulting in a leveling off of the curve. Very little hardness variation was found to exist during isothermal grain growth at the temperatures investigated.

Using the procedures described earlier, the recrystallization kinetics have been described in terms of the isothermal start times, t_{av} , the associated Avrami constants k and b, and the correlation coefficients; the

results are shown in Table 4.1. For all curves, the correlation coefficients were found to be fairly good. The experimentally determined recrystallization completion times, t_{end} are also listed and compared with the 99 percent recrystallization times, t_{99} , based on the best fit Avrami equations. In all cases, the predicted times for completion are greater than those actually observed. It was found to be quite difficult, if not impossible to detect the end of recrystallization metallographically.

The TTR (time-temperature-recrystallization) diagram for the isothermal recrystallization of the test steel is shown in Figure 4.9. The "start time" is based on the best fit t_{av} values, while the "end time" is based on the visually estimated recrystallization completion times. The dashed lines represent the time necessary at each temperature for the formation of the specified percent of recrystallized structure. These times were based on the best fit t_{av}, b and k values. The discrepancy that exists between the observed and predicted completion times could be caused by the difficulty in pinpointing the exact time at which recrystallization is complete using metallographic procedures.

The TTR diagram was constructed on the assumption that the specimens exposed to the molten salt reached the required temperature immediately upon immersion. Obviously, this assumption is false. To determine the amount of error introduced by this assumption, a chromel-alumel thermocouple

Table 4.1 Isothermal Recrystallization Kinetic Results.

Temp. (C)	Avrami Parameters		t_{av}(s)	Corr. Coeff.	t_{end}(s)	t_{99}(s)
	k	b				
440	.463	6.88×10^{-4}	1.9×10^{4}	0.957	-	1.83×10^{8}
460	.432	2.12×10^{-3}	2600	0.985	-	5.30×10^{7}
480	.690	4.47×10^{-4}	700	0.982	3×10^{5}	6.55×10^{5}
490	.540	4.70×10^{-3}	280	0.943	8×10^{4}	3.46×10^{5}
500	.690	1.78×10^{-3}	270	0.975	4×10^{4}	8.86×10^{4}
520	.736	3.78×10^{-3}	69	0.977	9×10^{3}	1.56×10^{4}
540	.830	5.31×10^{-3}	16	0.980	1200	3480
560	1.030	7.4×10^{-3}	11	0.944	360	527

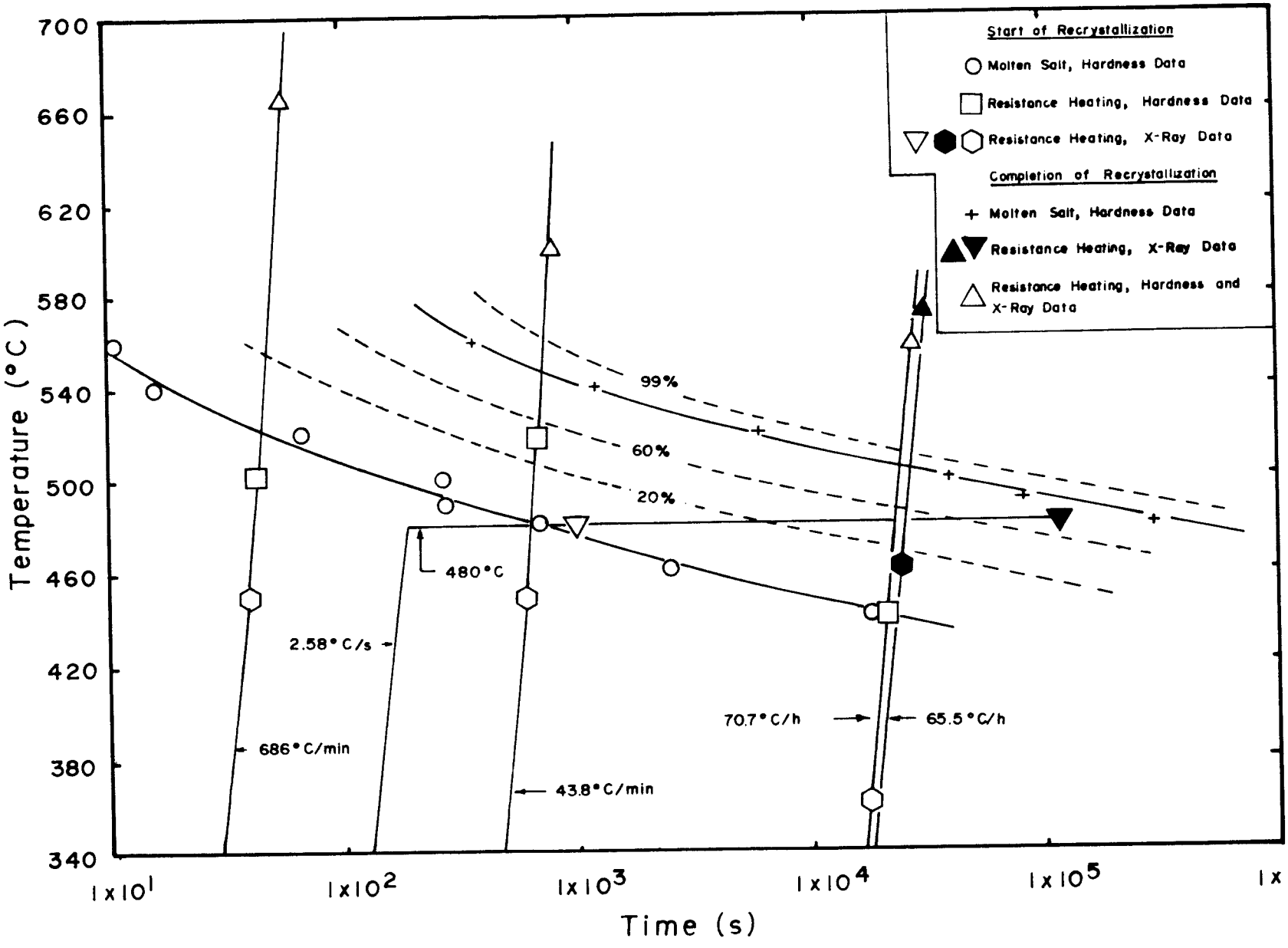

Fig. 4.9 TTR diagram with superimposed annealing cycles, showing start and end times for recrystallization.

was spot welded to a standard size salt bath specimen, which was immersed in the molten salt at different isothermal temperatures. The temperature response with time was recorded, the results being listed in Table 4.2. The time necessary to raise the specimen to the required temperature ranged from 3.8s to 5.6s. The specimens reach 95 percent of the required temperature in only 2.0s to 2.2 s.

The assumption of an instantaneous temperature response is a poor one only at higher temperatures, where the incubation period prior to recrystallization is short. For example, a 4s time delay results in approximately 0.6 percent, 6 percent and 36 percent errors in the predicted t_{av} values at 480°C, 520°C and 560°C respectively. Thus due to the experimental difficulties associated with attaining and measuring accurate recrystallization times at high temperatures, the recrystallization kinetics were not determined above 560°C. Instead, the values of k and b at temperatures outside the experimental range were determined by extrapolation.

It should also be noted that the Avrami constants obtained for the recrystallization at 460°C and 440°C were based on partial recrystallization data, since annealing times in excess of one million seconds were necessary for complete recrystallization to occur, resulting in unreasonably long experimental times.

The temperature dependence of the Avrami parameters b and k are shown in Figures 4.10 and 4.11. The constant k was

Table 4.2 Temperature Response During Immersion of the Steel Specimen into the Molten Salt.

Saltbath Temp. (C)	Specimen Temp. (C)	% of Max. Temp.	Time to Temp. (s)
432	412	95.0	2.2
	432	100.0	5.6
484	462	95.2	2.0
	484	100.0	3.8
517	490	94.5	2.0
	517	100.0	4.2
553	527	95.0	2.2
	553	100.0	5.4

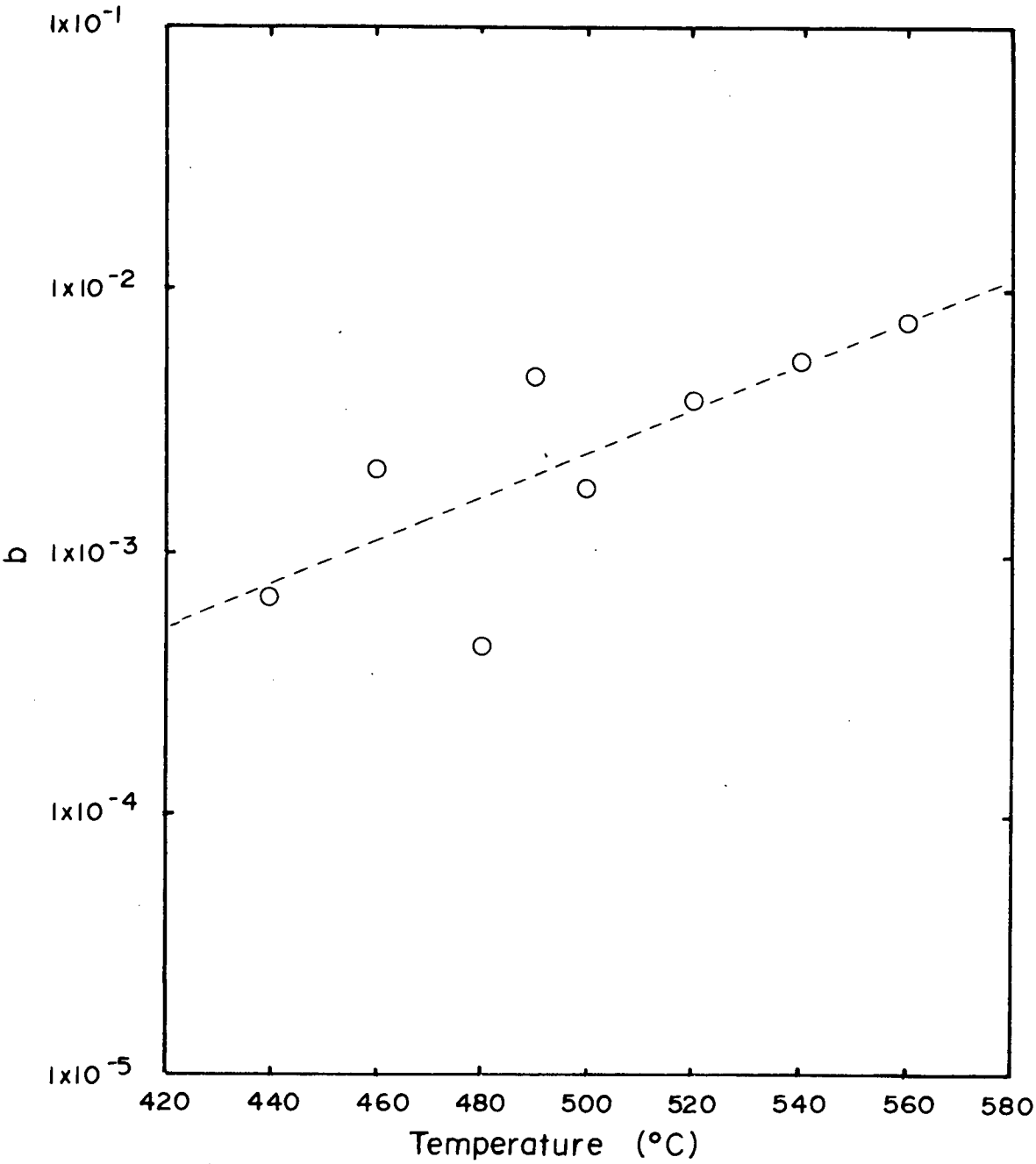

Fig. 4.10 Temperature dependence of Avrami parameter b.

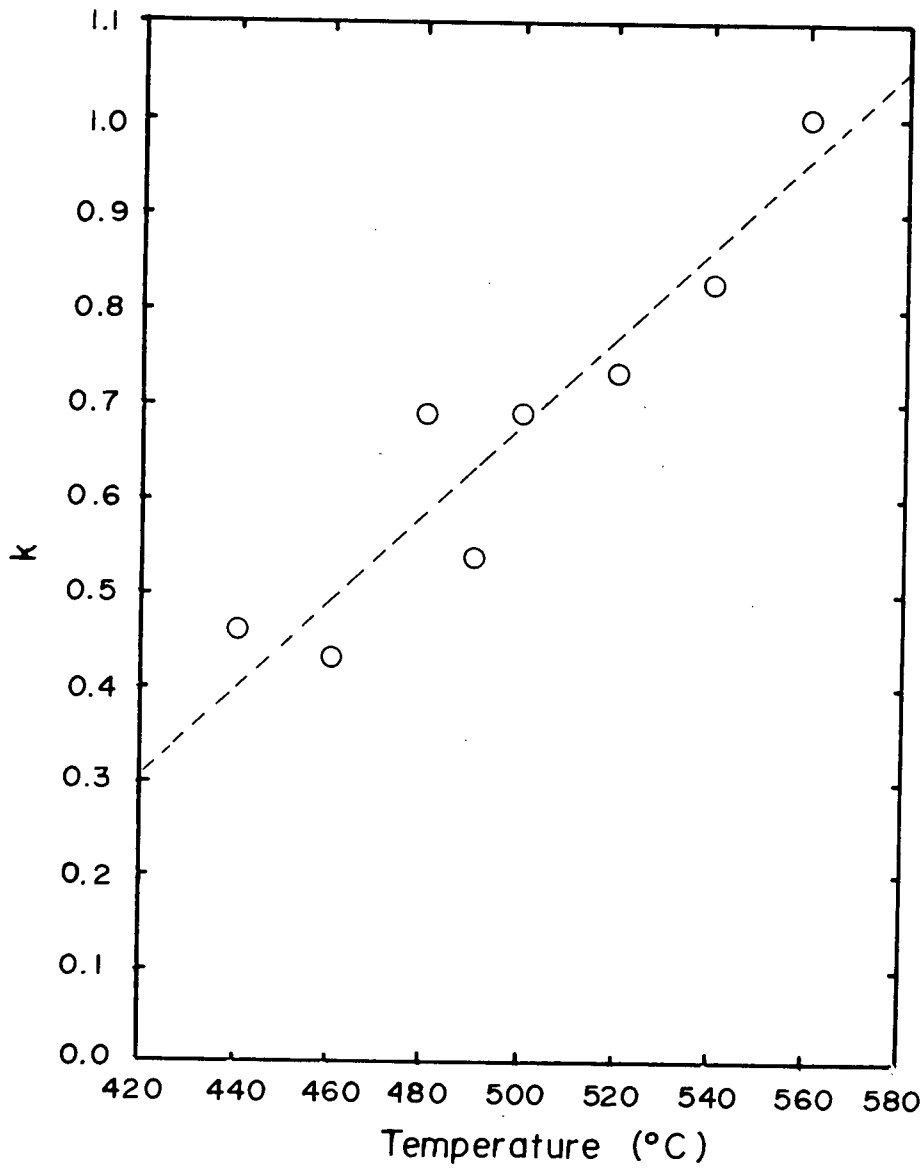

Fig. 4.11 Temperature dependence of Avrami parameter k.

found to fit the linear relationship:

$$k=-1.63+4.63\times10^{-3}\ T \qquad ...(4.1)$$

while b was found to vary with temperature according to:

$$\ln b=-15.56+1.90\times10^{-2}\ T \qquad ...(4.2)$$

where T is the temperature in °C.

The variation of k with temperature was previously examined by Rosen et. al.[9] They said that k will vary depending on the progress of recovery processes prior to the onset of recrystallization. According to Avrami[20] the nucleation rate varies with time according to equation (2.18), or:

$$N=\bar{N}\nu\exp(-\nu\tau) \qquad ...(2.18)$$

When recovery occurs extensively prior to recrystallization, so that early site saturation occurs, the probability that a potential site is occupied by a nuclei is large, therefore $\nu\tau$ is large and equation (2.18) becomes equal to zero for all times after the formation of all the nuclei. Therefore, in the case of early site saturation the mathematical expression relating fraction recrystallized to time is given by equation (2.19):

$$X=1-\exp(-fG^3\bar{N}t^3) \qquad ...(2.19)$$

When no recovery occurs prior to recrystallization, the probability that a site is occupied by a nuclei is small, therefore $\nu\tau$ is small, and the equation describing nucleation will become:

$$N=\bar{N}\nu \qquad ...(2.21)$$

and the corresponding recrystallization equation will be

$$X=1-\exp(-fG^3\bar{N}\nu t^4/4) \qquad ...(2.20)$$

Therefore, the value of k can vary depending on the degree of recovery that occurs prior to recrystallization.

In this study, the value of k was found to vary between 0.43 at 460°C and 1.03 at 560°C. Therefore, it appears that at higher isothermal annealing temperatures less recovery is able to occur prior to the onset of recrystallization.

The value of the exponent k will also be affected by factors such as the growth shape of the recrystallized nuclei (ie. one, two or three dimensional growth), and how the growth rate changes with time.[21] In the development of the Avrami and Johnson-Mehl equations, the growth rate is considered to be constant.

4.2 CONTINUOUS HEATING RECRYSTALLIZATION KINETIC RESULTS

The experimental x-ray and hardness results of the continuous heating annealing experiments performed without prior recovery heat treatments, are shown in Figures 4.12 to 4.14.

The results of the run conducted at the simulated batch annealing rate of 70.7 °C/h are shown in Figure 4.12. This x-ray run was performed insitu with oscillating scans of the {211} Kα peak. The dashed lines indicate the range over which the individual scans were found to vary during the course of the annealing cycle. The hardness results were obtained on specimens subjected to the interrupted heating-cooling procedure described previously.

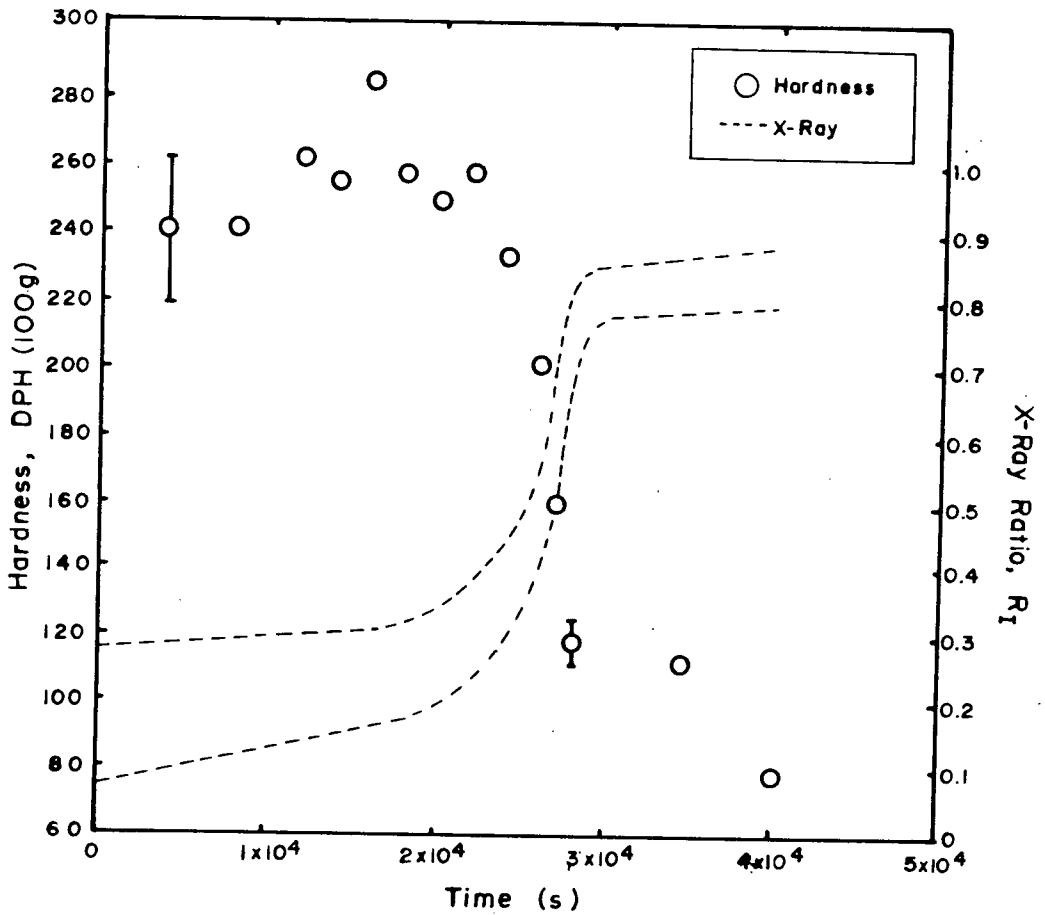

Fig. 4.12 Experimental continuous heating hardness and x-ray results, heating rate=70.7°C/h.

The x-ray results differentiate between the three stages of annealing. For approximately the first 18000s, the x-ray ratio increases in a relatively linear fashion, indicating some $K\alpha$ doublet peak resolution to be occuring due to stress relief during recovery.

At approximately 18000s, (345°C), the x-ray ratio begins to increase more rapidly with time, first slowly, and then at a greater rate. This region appears to indicate the onset of recrystallization, where large scale, rapid dissipation of residual strain energy occurs.

At approximately 28000s, (557°C), the x-ray ratio levels off once more and becomes linear with time. This stage apparently corresponds with grain growth after the completion of recrystallization. Very little change in the x-ray ratio occurs during this time period, indicating negligble strain relief to be occuring.

The equivalent hardness results show a marked increase in hardness at approximately 16000s. Since x-ray analysis indicate no substantial increase in the rate at which strain relief occurs until approximately 18000s, strain aging is probably responsible for this hardness increase. The hardness was then found to level off at a value of approximately DPH 254 during the time interval of 18000s to 22000s.

Based on the shape of the hardness curve, recrystallization would appear to start somewhere in the region of 18000s (345°C) to 22000s (440°C). These times are

approximately the same, or slightly longer than that predicted by x-rays. Once recrystallization initiates, a rapid decrease is noted until it begins leveling off at a value of DPH 117.5 at 28000s. Continued heating results in a further hardness reduction to DPH 76.8 caused by grain growth.

The kinetics of recrystallization at the two higher heating rates, 43.8°C/min, and 686°C/min, employed the interrupted heating procedure in which strip specimens were rapidly cooled to room temperature. X-ray and hardness tests were conducted at room temperature.

Figure 4.13 shows the results of the continuous heating run conducted at 43.8°C/min. Comparing the x-ray results with those obtained using hardness, a discrepency once again exists in the apparent start time of recrystallization. X-rays show a ratio increase at approximately 605s, (449°C), while the first appreciable hardness decrease occurs after 701s, (449°C). Both techniques predicted recrystallization to be complete at 866s, (640°C). This was verified using microscopic examination.

Figure 4.14 shows the results of the continuous heating trial conducted at 686°C/min. Once again, x-rays suggest an apparent recrystallization start time of approximately 38s, (450°C), compared with 43s, (500°C), obtained using hardness evaluation. In both cases recrystallization appears to be complete at approximately 57s, (660°C), which was varified metallographically.

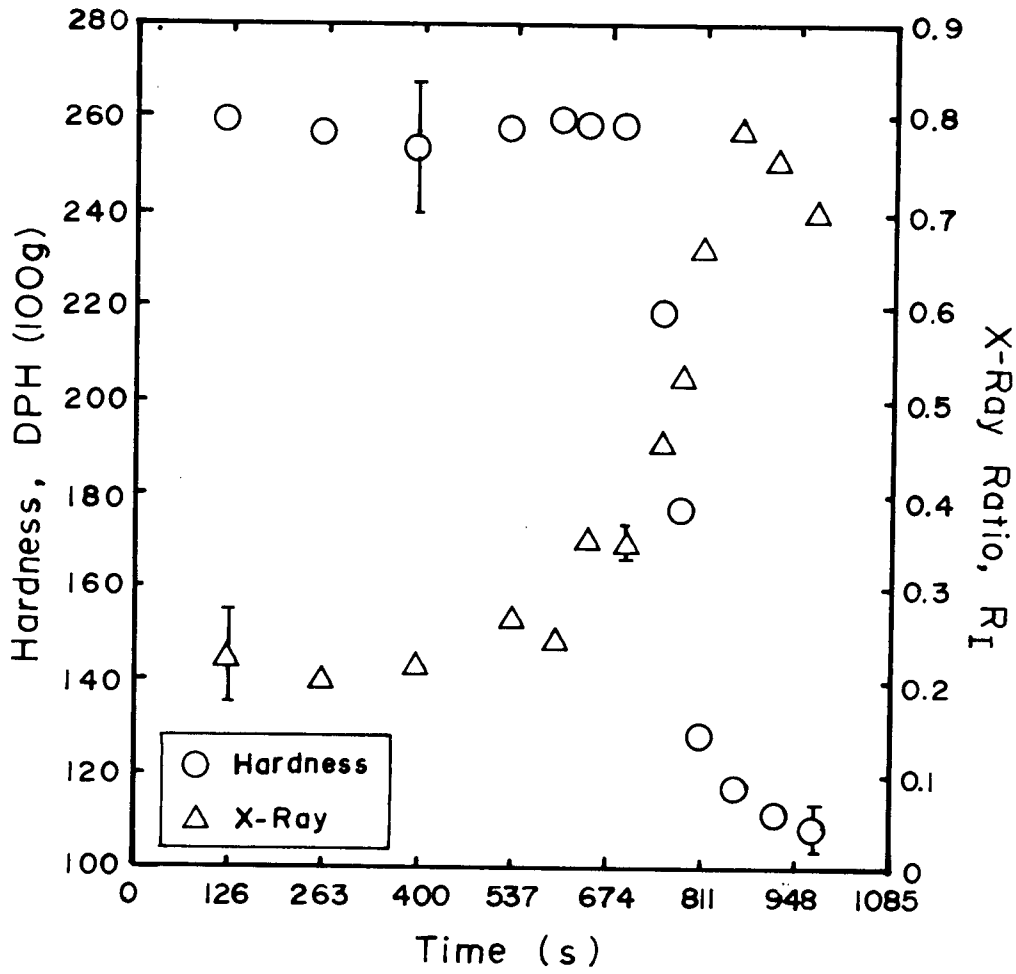

Fig. 4.13 Experimental continuous heating hardness and x-ray results, heating rate=43.8°C/min.

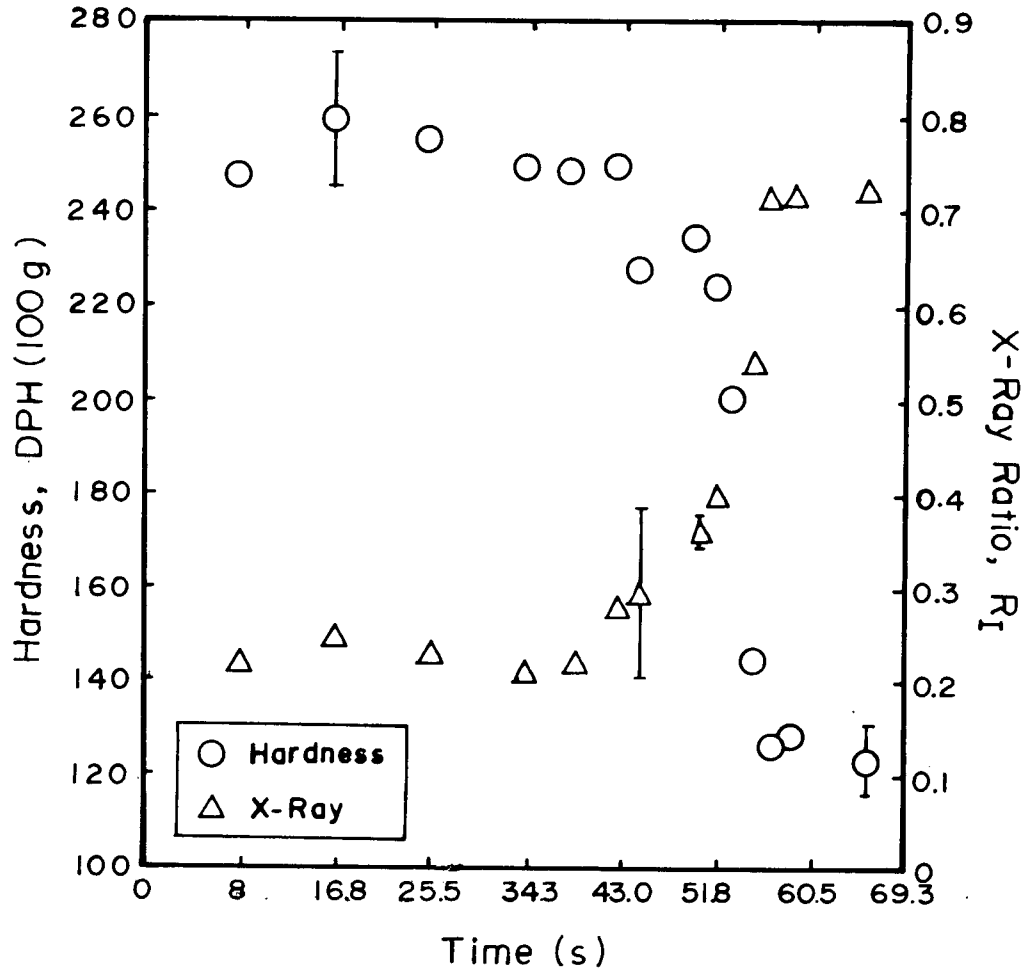

Fig. 4.14 Experimental continuous heating hardness and x-ray results, heating rate=686°C/min.

At all heating rates employed, the x-ray technique predicted recrystallization to initiate well before that predicted by microhardness evaluation. Metallographic examination failed to yield any concrete evidence to support the findings of the x-ray results, although in some instances extremely small recrystallized grains appeared to be present at the cold worked grain boundaries of specimens which were predicted to contain no recrystallized material, based on hardness predictions. These grains were very difficult to discern due to their extremely small size, and the poor image obtained at the high magnifications used during the examination.

It is possible that the microhardness indentations will fail to see these isolated, small patches of recrystallized material since each indentation covers only a very small area of each specimen. The x-ray beam analyzes a much larger area, and will include the small recrystallized grains in each scan.

However, since the amount of recystallized material required to cause the observed initial increases in the x-ray ratio will be much larger than that actually observed metallographically, it seems more likely that the initial increase in the x-ray ratio is due predominantly to strain relief by recovery effects. As discussed earlier, recovery involves the rearrangement of various lattice defects. At higher temperatures, large scale dislocation movement that occurs during the formation of strain free nuclei capable of

growth, can take place.[3] Since the continuous heating cycle involves a gradual increase in temperature, these nucleation processes will only be able to occur later in the annealing cycle, when the temperature reaches the required level. Once this temperature is reached, nuclei begin to form, and a reduction in lattice strain occurs. This mechanism is consistent with metallographic observations and microhardness results. In addition, other researchers have noted similar effects of recovery on the various x-ray parameters used to monitor recrystallization.[26-28]

The experimental heating rates, as well as the times for the initiation and completion of recrystallization, as determined by hardness and x-ray analysis are plotted on the TTR diagram in Figure 4.9. For all heating rates, the x-ray technique predicts recrystallization to start at shorter times than predicted by the intersection of the continuous heating curves with the TTR curve. The hardness results indicate a shift to shorter times only for specimens heated at 686°C/min. A heating rate of 70.7°C/h resulted in recrystallization initiation somewhere between 18000s and 22000s which is slightly before or roughly at the intersection of the TTR curve and the continuous heating curve. A heating rate of 43.8°C/min resulted in a shift to longer times past the point of intersection of the TTR and continuous heating curves.

The observed shift of the initiation time for recrystallization during continuous heating, obtained from

x-ray examination is opposite to that which occurs during austenite decomposition during continuous cooling transformation (CCT), as shown in Figure 4.15.[40] In this case, a shift to longer transformation start times occurs on continuous cooling because the sample spends longer times at higher temperatures where the incubation period is longer. Thus using Scheil's[22] suggested consumption of fractional incubation time as a criterion for the onset of transformation, the transformation start time would be shifted to longer times than those shown in the isothermal transformation diagram (TTT).

If a similar argument is applied for recrystallization under continuous heating conditions, one might expect a shift to longer times during the recrystallization of cold reduced material. However, the recovery processes which precede recrystallization are thermally activated, and therefore much less effective at lower temperatures as realized during continuous heating. Thus, on continuous heating to a specific temperature, a larger fraction of the original strain energy is retained, the driving force for recrystallization is higher, and therefore less thermal energy is required to initiate recrystallization. Therefore, recrystallized nuclei are able to grow at lower temperatures during continuous heating.

The expected peak shift to longer times on continuous heating, with respect to the TTR curve, was only observed in the microhardness results of the continuous heating rate of

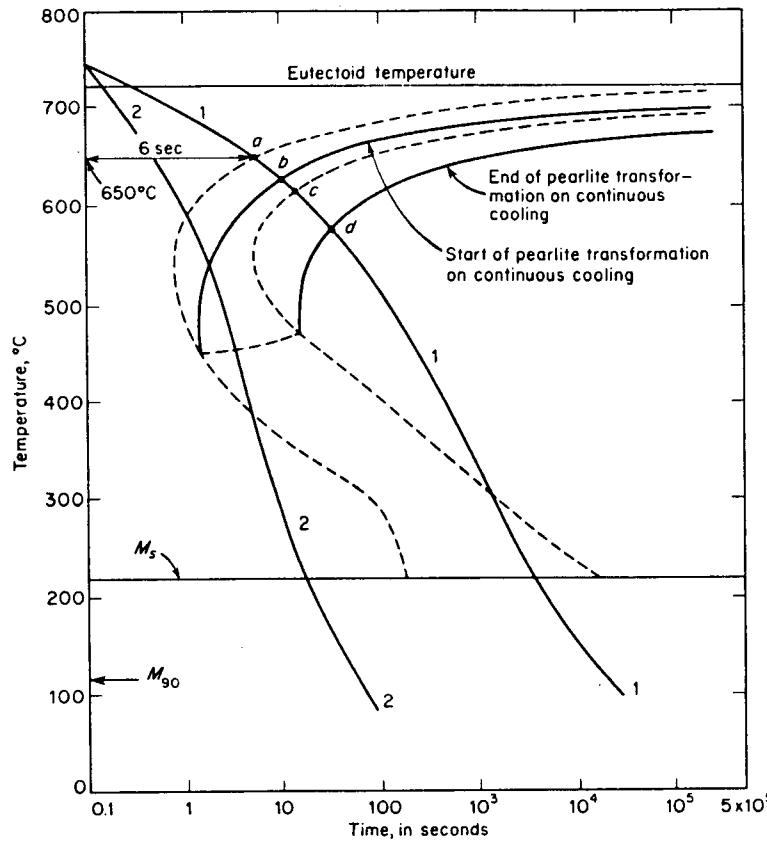

Fig. 4.15 Relationship of the continuous cooling and isothermal diagrams for a eutectoid steel.(Ref.40)

43.8°C/min. To further varify the effect of recovery on the shift of the start time, a strip specimen was subjected to a recovery anneal of 440°C for 14000s, and then recrystallized at a heating rate of 65.5°C/h. The recovery treatment was designed to make the microstructural conditions in the continuously heated specimen similar to those existing in the isothermally annealed specimen prior to the onset of recrystallization. The x-ray results of the {211} Kα peak during the recovery and recrystallization heat treatments are shown in Figures 4.16 and 4.17, respectively. The recovery anneal displayed a typical exponential decay pattern with time, as is typical of recovery kinetics.[3] The x-ray ratio during the continuous heating cycle shows very little change prior to the onset of recrystallization. Recrystallization was found to initiate considerably above the isothermal start line, and to display much quicker kinetic response, due to the high thermal driving force present at these temperatures.

The heating rate of the recovery annealed specimen with its corresponding start and completion times for recrystallization are plotted on the TTR diagram in Figure 4.9. The start of recrystallization was found to have shifted to approximately 25100s (465°C), with the completion occuring at roughly 31000s (570°C).

This shift can be explained by considering that the incubation period during an isothermal anneal at 440°C lasts for roughly 19000s. Annealing for 14000s does not allow time

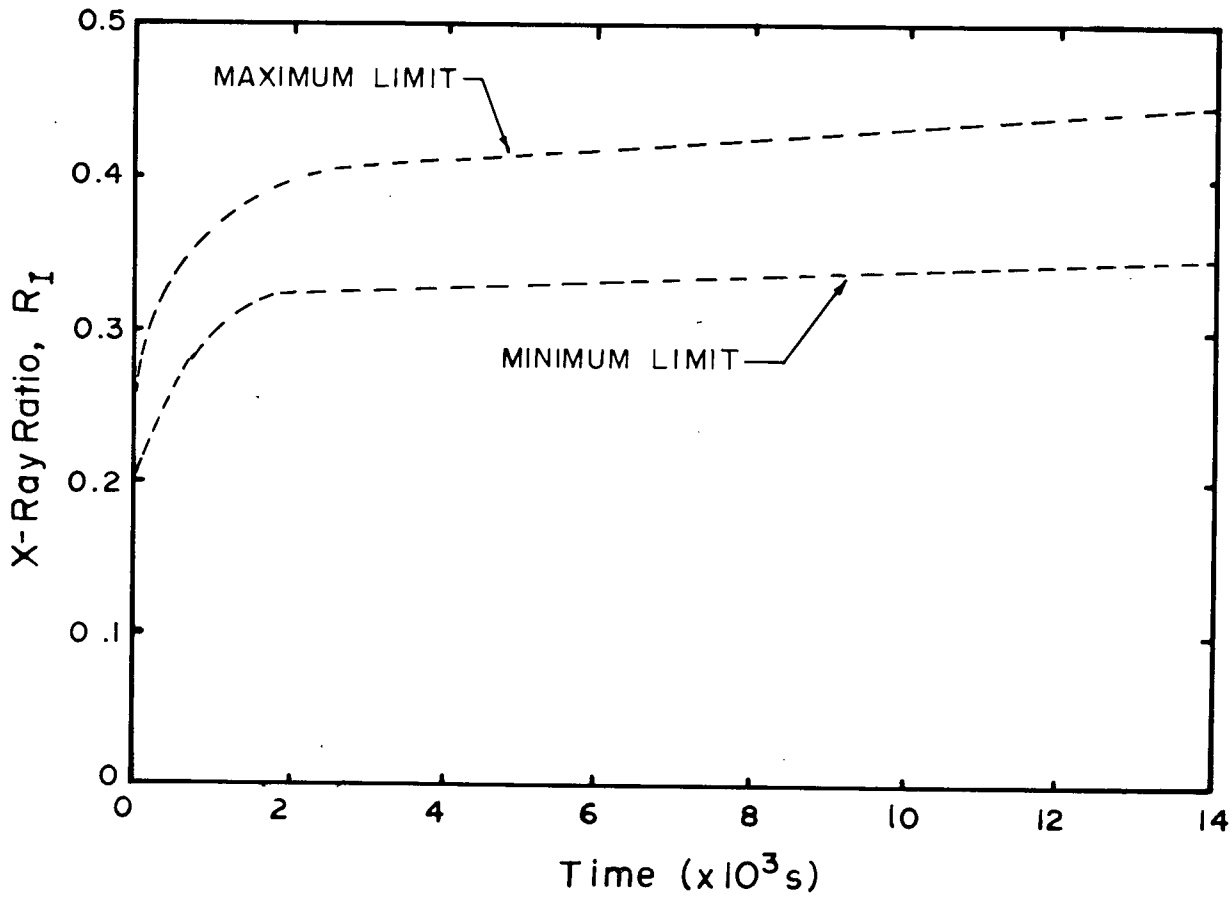

Fig. 4.16 X-ray results from the recovery anneal conducted at 440°C, for 14000s.

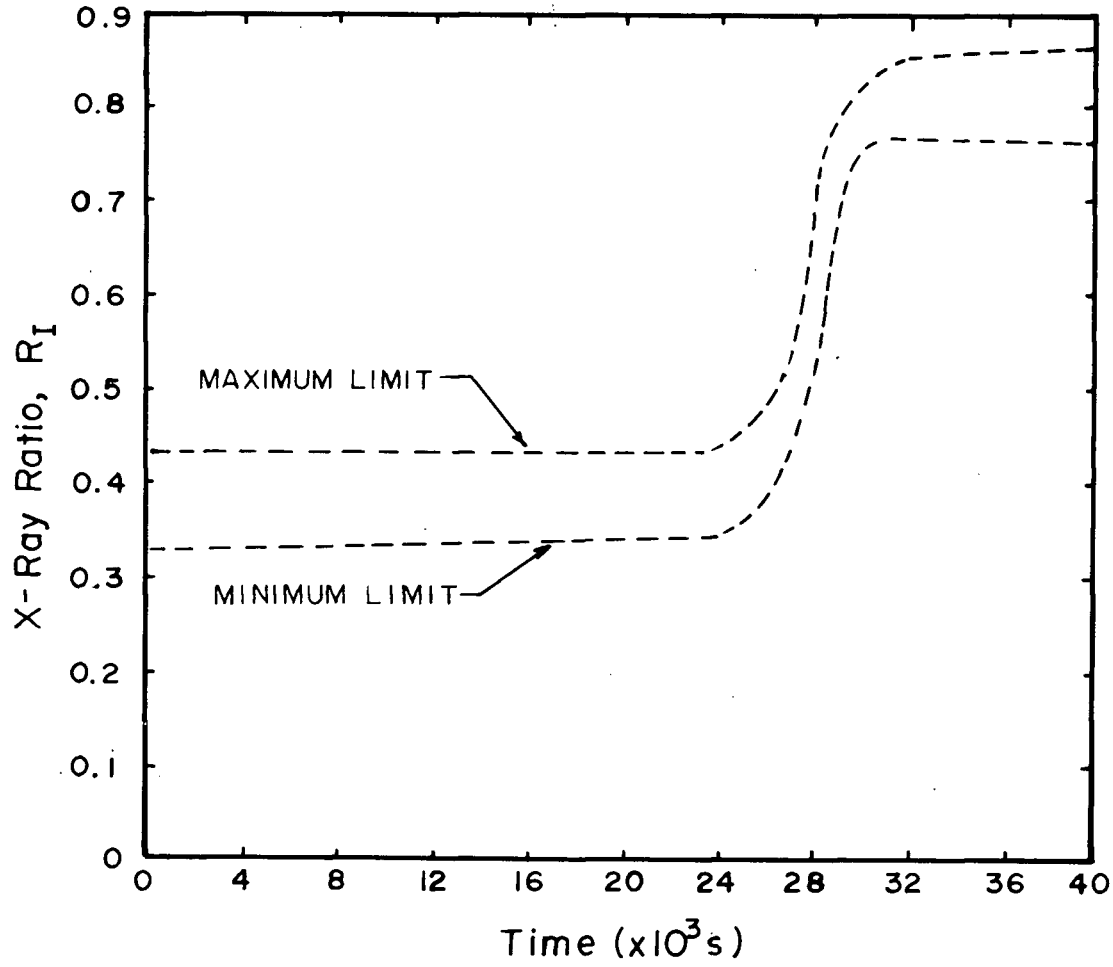

Fig. 4.17 X-ray results from the continuous heating annealing cycle conducted at a heating rate of 65.5°C/h, after annealing at 440°C for 14000s.

for the required microstructural modifications necessary for recrystallization to occur at this temperature. Therefore, on subsequent continuous heating, more recovery will be required, very little of which will occur until the temperature reaches 440°C. The additional time necessary for the remaining recovery to occur isothermally at 440°C would be 5000s. During continuous heating, less additional recovery time will be required since higher temperatures will be reached once 440°C is exceeded. Experimentally, it was found that an additional 1400s was required during continuous heating, once the temperature exceeded 440°C, for the additional recovery to occur, and for recrystallization to initiate.

Further evidence that continuous heating affects the amount of recovery prior to recrystallization, and also the subsequent recrystallization kinetic response, is shown in the experimental results of the specimen that was continuously heated at 2.58°C/s to a temperature of 480°C, at which point it was isothermally recrystallized. The results of the insitu x-ray analysis performed on the specimen are shown in Figure 4.18.

Least squares analysis of the data yielded a best fit start time, and the corresponding Avrami parameters listed in Table 4.3. For comparison purposes, the Avrami parameters of the specimen isothermally recrystallized in molten salt are shown in the table. The k parameter was found to be increased by the continuous heating treatment, indicating

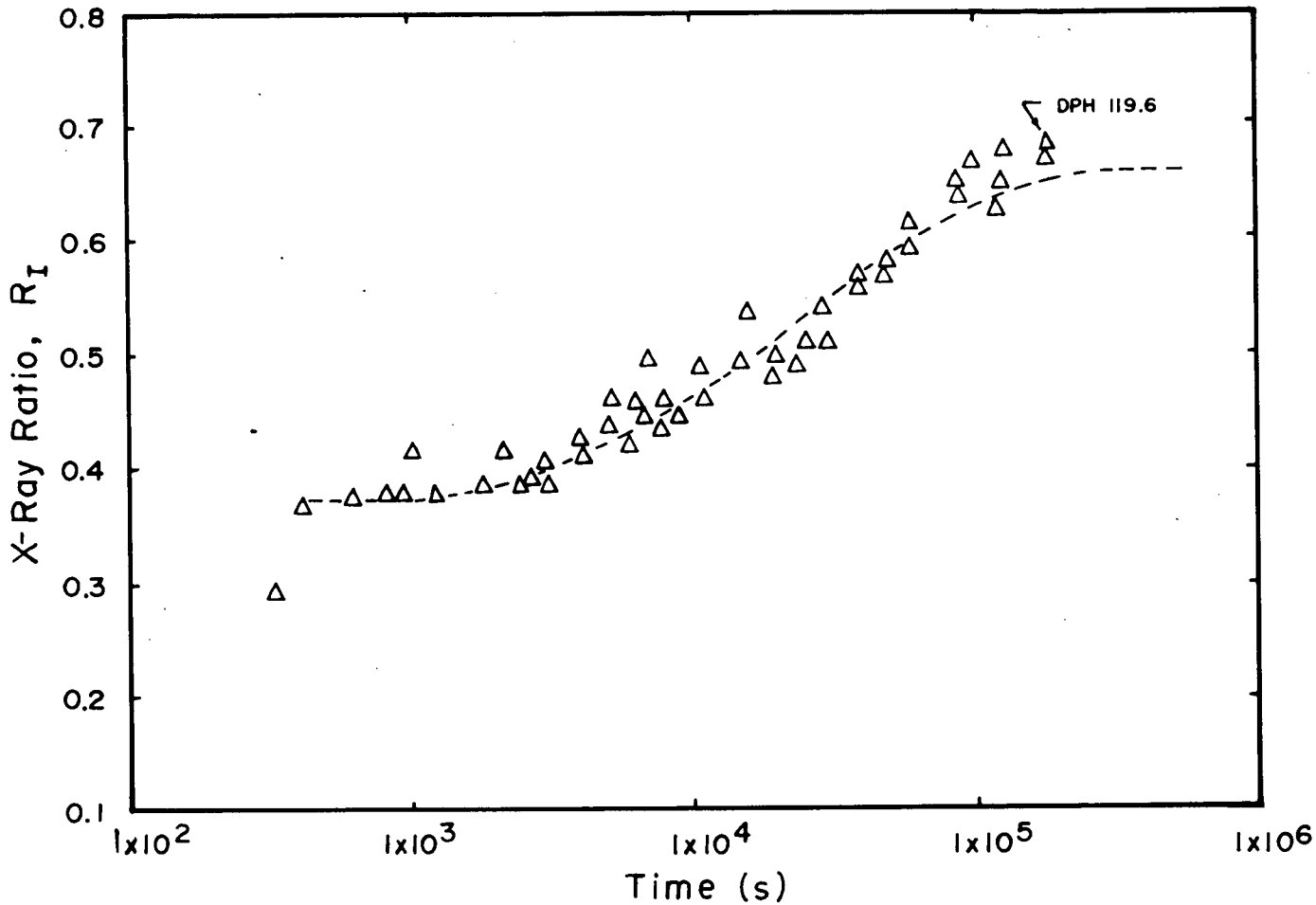

Fig. 4.18 Experimental x-ray results of the strip specimen continuously heated at 2.58°C/s, and isothermally recrystallized at 480°C.

Table 4.3 Avrami Parameters Obtained from the Isothermal Anneals Conducted at 480°C, Using Two Different Heating Methods.

Heating Method	Avrami Parameters		Corr. Coeff.
	k	b	
Continuous heating at 2.58 C/s	0.791	2.74×10^{-4}	0.933
Molten salt anneal	0.690	4.47×10^{-4}	0.982

that recovery occurs to a lesser extent due to the smaller thermal driving force at the low temperatures encountered during continuous heating. The total time neccesary for the recrystallization process to be completed was found to be substantially reduced by the continuous heating cycle, as shown in the TTR diagram, Figure 4.9. This can be attributed to the higher residual strain energy resulting from the reduced amount of recovery during continuous heating.

4.3 CONTINUOUS HEATING RECRYSTALLIZATION KINETIC PREDICTIONS

The computer predicted recrystallization kinetic curves for all continuous heating runs, performed without prior recovery heat treatments, are shown in Figure 4.19 to 4.21. Each figure also contains the experimentally observed kinetic x-ray analysis techniques.

Figure 4.19 shows the predicted and experimental curves for the continuous heating rate of 70.7°C/h. The isothermal time increment on which the computer predictions were based was 10s. The assumed start time for recrystallization during continuous heating was set at 18000s or 22000s, which were the outer limits of the range in which recrystallization was considered to start, based on hardness and x-ray predictions. The predicted kinetic curves based on those two start times show very little difference.

The observed insensitivity of the predicted kinetics to the assumed start time can be explained by the slow isothermal kinetic response in the temperature range

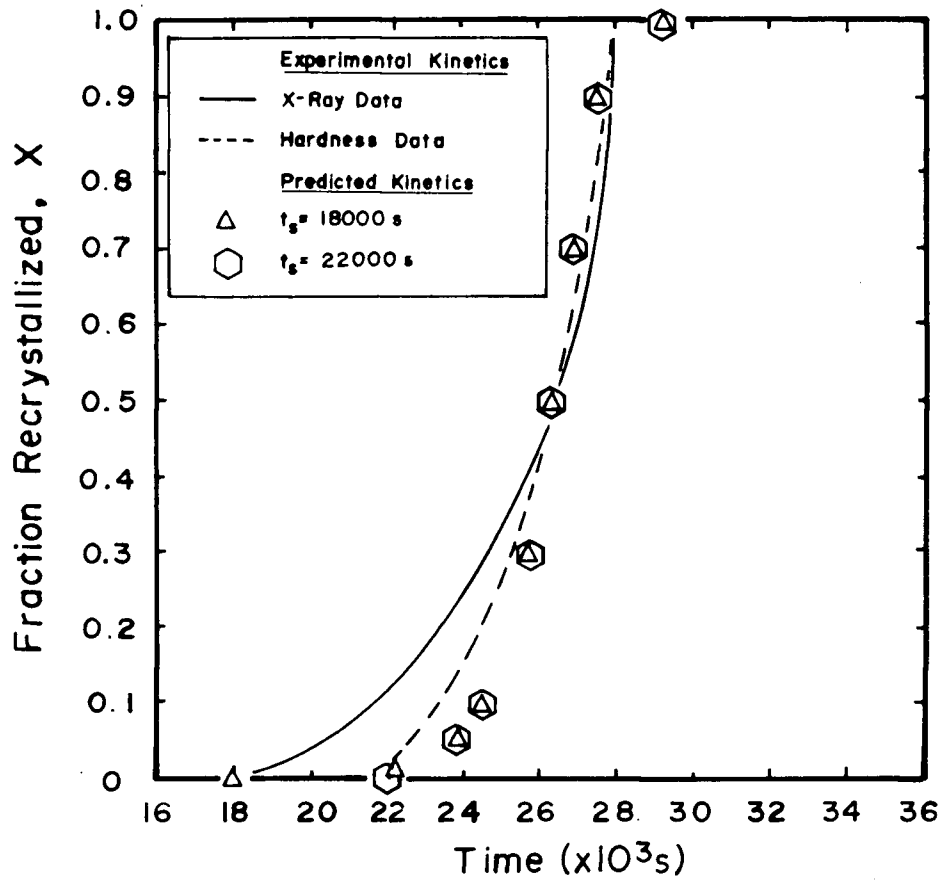

Fig. 4.19 Predicted and experimental continuous heating recrystallization kinetic curves, heating rate=70.7°C/h.

associated with the time interval 18,000s to 22,000s. Therefore, very little recrystallization is predicted to occur during this time interval if the start time is considered to be 18000s. Therefore, based on either start time, the initial microstructual conditions are essentially the same at 22,000s, and the fraction recrystallizing during subsequent isothermal time increments will be virtually the same, enabling the two kinetic curves to combine after approximately 22,000s.

Good correlation was found to exist between the kinetic curve obtained using hardness, and the computer predicted recrystallization kinetic curve. Less correlation exists between the x-ray results and the computer predictions.

The experimental and computer predicted recrystallization kinetic curves for the continuous heating rate of 43.8°C/min are shown in Figure 4.20. The isothermal time increment used for computer predictions was 0.2s. Once again, the computer predictions were based on a start time of either 605s (based on x-ray analysis) or 701s (based on hardness data). The two predicted curves were found to be the same after the volume fraction of recrystallized material present was roughly 0.10 to 0.15. Once again, the best correlation existed between the hardness data and the computer predictions based on hardness start time.

Figure 4.21 shows the results obtained for the recrystallization treatment carried out at 686°C/min, using a isothermal time increment of 0.015s for computer

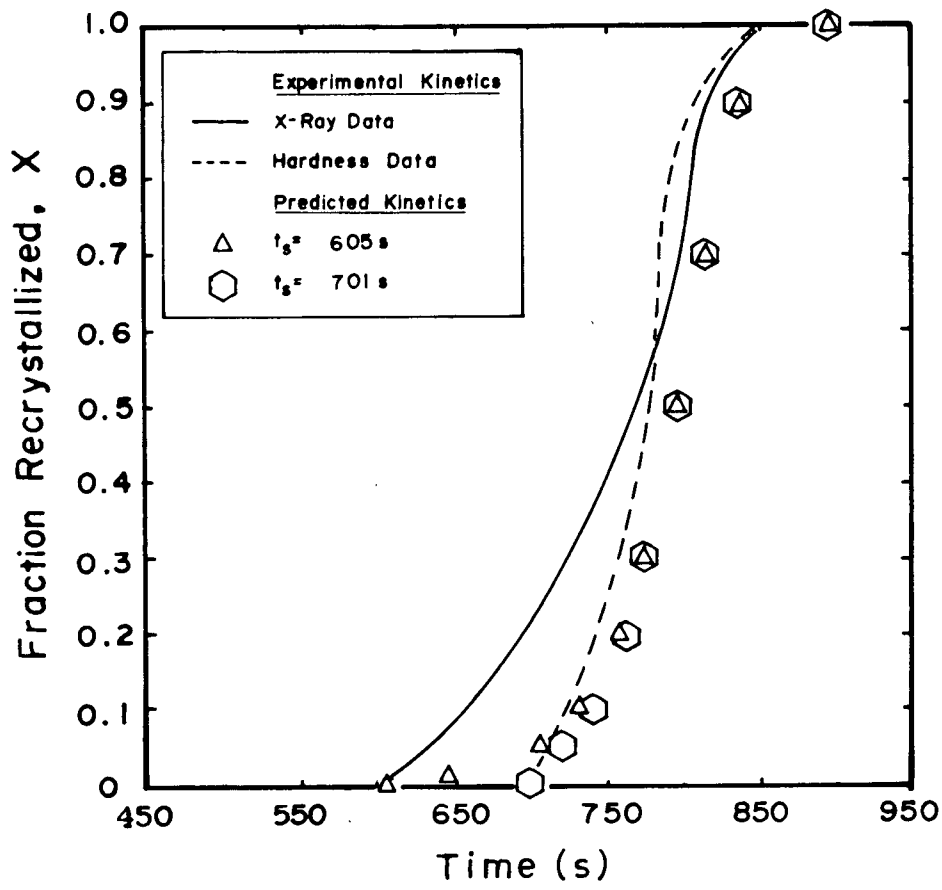

Fig. 4.20 Predicted and experimental continuous heating recrystallization kinetic curves, heating rate=43.8°C/min.

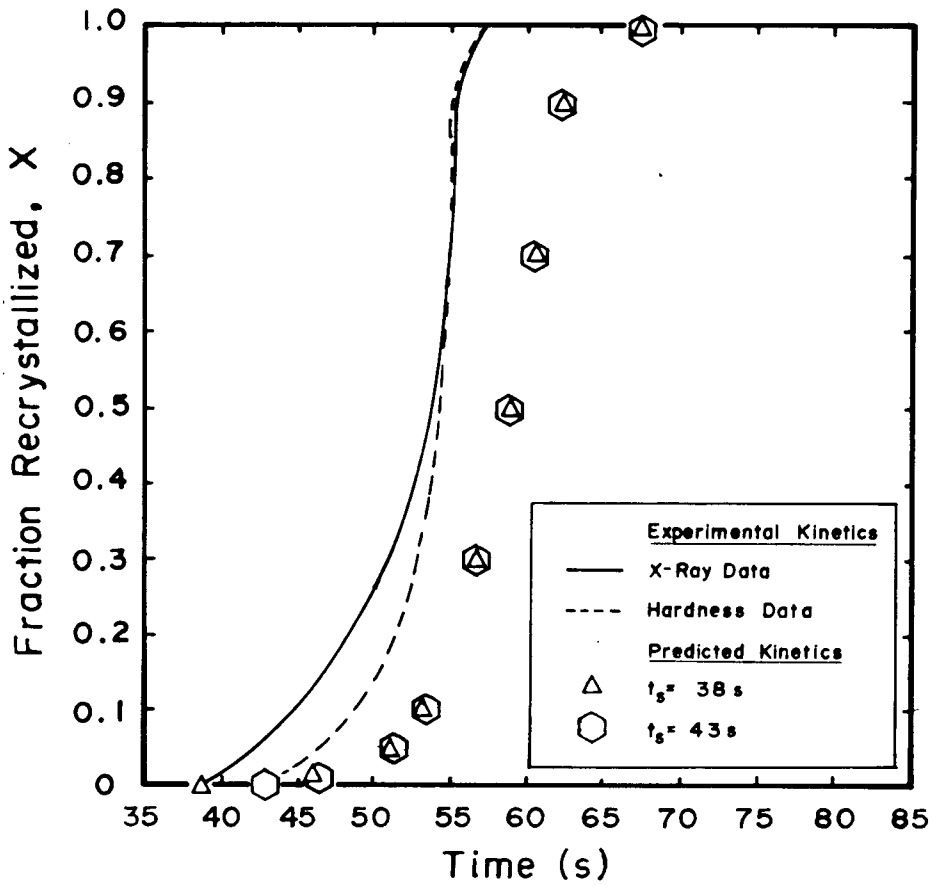

Fig. 4.21 Predicted and experimental continuous heating recrystallization kinetic curves, heating rate=686°C/min.

predictions. Varying the start time from 38s to 43s had little effect on the predicted recrystallization kinetic response. Considerable variation existed between the predicted and experimental kinetic curves, with respect to the time necessary for the formation of a given volume fraction of recrystallized structure. However, the shape of the predicted experimental curves are similar once approximately 0.10 volume fraction of recrystallized structure is present.

The similar kinetic response of the two curves is surprising, since one might expect a faster kinetic response at the higher temperatures present in the computer predictions, since the thermal driving force is greater. The rapid kinetic response observed experimentally can be explained in terms of additional strain energy being present in the lattice due to the occurrance of less recovery during continuous heating, prior to the onset of recrystallization. The fact that recrystallization appears to initiate at a shorter time than predicted by the TTR curve also suggests recovery to be hindered by continuous heating. The computer predicted kinetics, on the other hand, are based on isothermal data, which experiences more recovery during the incubation period, resulting in less strain energy and slower predicted kinetics. A higher annealing temperature during continuous heating will therefore be necessary to result in similar kinetics, as was actually observed during experimentation.

It was thought that some of the error that exists between the experimental and predicted kinetic curves at the continuous heating rate of 686°C/min could be attributed to further recrystallization during cooling from temperature, during the interrupted heating - cooling tests. Based on the experimental results, cooling rates of approximately 63°C/s were common, depending on the maximum temperature obtained. Making the assumption that all specimens subjected to the interrupted heating - cooling tests cooled at this rate, and calculating the additional fraction recrystallized on cooling, only a slight shift of the predicted curve in the direction of the experimental curve was noted, as shown in Figure 4.22. Therefore, although some of the error can be accounted for by further recrystallization during cooling from the required temperature, clearly the recovery effect has the dominating influence on the experimental recrystallization kinetics.

Therefore, it appears that the process of recovery can affect the accuracy with which recrystallization kinetics can be predicted using isothermal data. If the amount of recovery prior to recrystallization during continuous heating can be made to more closely simulate that present during isothermal annealing, the kinetics should be able to be predicted more accurately.

This in fact was what was found to occur in specimens subjected to the recovery anneal of 440°C for 14,000s, followed by continuous heating annealing of 65.5°C/h, as

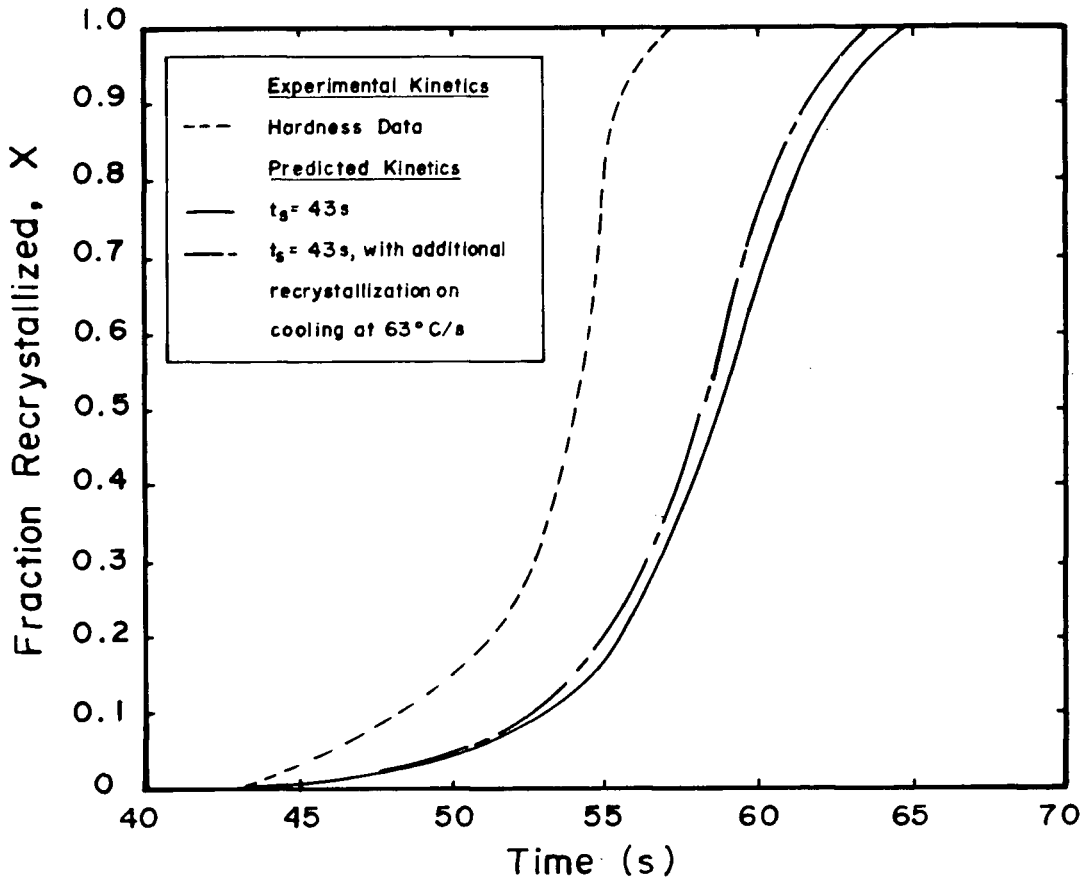

Fig. 4.22 Additional recrystallization occuring on cooling from temperature during continuous heating annealing. Heating rate=686°C/min, cooling rate=63°C/s.

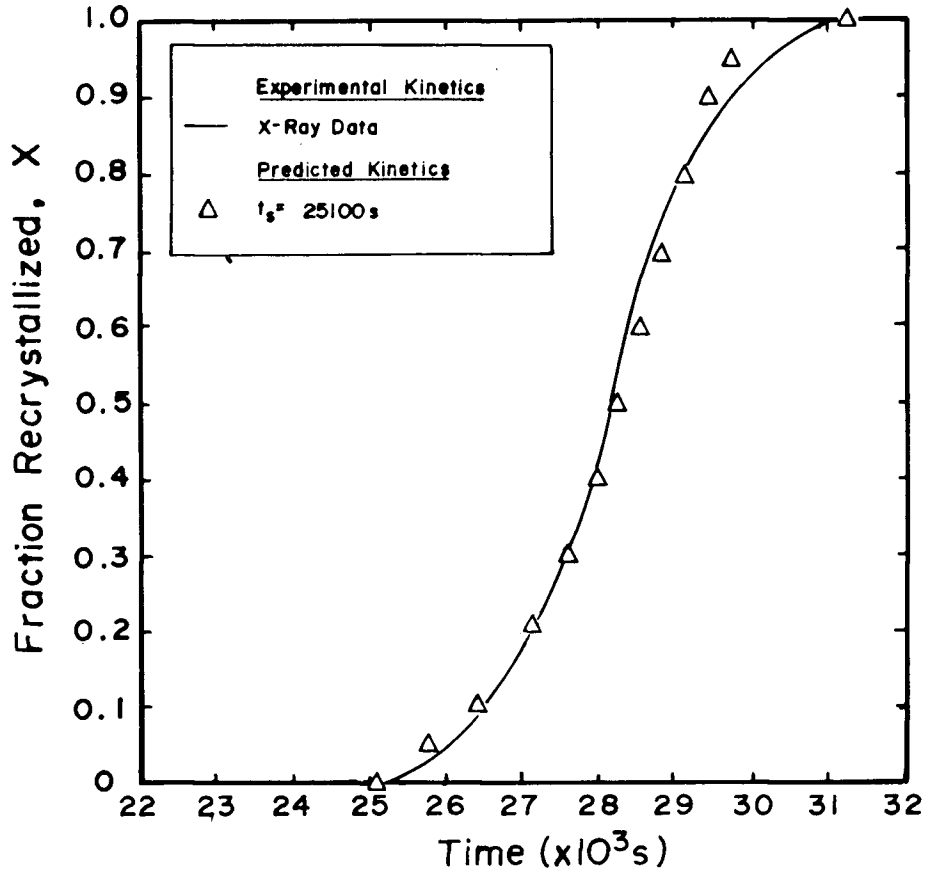

Fig. 4.23 Predicted and experimental continuous heating recrystallization kinetic curves after a recovery anneal of 440°C for 14000s. Heating rate=65.5°C/h.

shown in Figure 4.23. Excellent correlation was found to exist between the computer predicted and experimental results. The recovery anneal resulted in the occurrence of essentially the same amount of recovery prior to recrystallization in specimens annealed isothermally, or by continuous heating methods. Once the pre-recrystallization recovery conditions are duplicated, much better recrystallization predictions can be made using isothermal data, and recrystallization can be considered to be additive.

4.4 DISCUSSION

The following observations were attributed to the variability in the extent of recovery occurring prior to recrystallization during annealing:

1. The increase in the Avrami constant k with increase in isothermal annealing temperature.
2. The apparent lowering of the required temperature to initiate recrystallization during continuous heating in comparison to isothermal annealing.
3. The slow computer predicted recrystallization kinetics observed immediately preceeding the start of recrystallization during continuous heating.
4. The faster kinetic response observed in isothermally recrystallized specimens brought to temperature by employing continuous heating methods.

The idea of recovery having a marked effect on recrystallization is not a new one. Other investigators have noticed that recovery can markedly affect the recrystallization of iron alloys. Stanley and Mehl[42] noted that the length of time at which a cold worked silicon ferrite specimen was left at room temperature prior to annealing had a significant affect on subsequent nucleation. They noted that when recrystallization was performed immediately after cold working, four times more nuclei were present per unit area than if the material was recrystallized thirty days after cold working. This was attributed to recovery processes taking place during this time interval.

Hu[43] noted that the growth of recrystallized grains in a silicon iron crystal depended on the degree to which the cold worked matrix had recovered into a polygonized structure. In specimens with a well-defined polygonized structure, recrystallized nuclei that were present did not experience any growth, even at high annealing temperatures. If a poorly developed polygonized structure was present, due to less recovery, growth of the recrystallized nuclei was found to proceed fairly rapidly.

These observations were attributed to the fact that recovery reduces the driving force available for subsequent nuclei growth by lowering the stored strain energy.

In very pure iron, recovery can occur to such a large extent, that softening can be completed without

recrystallization occuring. This is due to the high stacking fault energy of iron. However, both substitutional and interstitial impurities reduce the ease by which recovery can proceed, due to impurity drag effects.[12-15] Therefore, it would appear that recovery processes are responsible for the various experimental observations listed above. Further proof of this argument is provided by the results of the specimen recrystallized after being subjected to a recovery anneal designed to reduce recovery effects. Once the pre-recrystallized, microstructual conditions (ie. degree of recovery) were made to more closely duplicate those obtained during isothermal annealing, the recrystallization kinetics during the continuous heating cycle was predicted very accurately using isothermal kinetic data. Therefore, additivity can be applied to the process of recrystallization.

5. SUMMARY

5.1 CONCLUSIONS

The following conclusions summarize the results obtained from the experiments carried out to determine the applicability of the additivity principle for predicting continuous heating recrystallization kinetics of cold rolled, low carbon steel sheet. In addition, the results of the work to determine an effective x-ray parameter to monitor recrystallization are summarized.

1. Diamond pyramid microhardness (DPH), using 100g loads effectively monitored isothermal recrystallization in steel specimens annealed in molten salt. However, various microstructural phenomena such as grain growth after recrystallization affect hardness significantly.
2. The Avrami equation:

$$X=1-\exp(-bt^{k})$$

was found to satisfactorily fit the isothermal hardness data describing the recrystallization event. Least squares analysis was performed on the recrystallization kinetic data at each isothermal temperature to determine the transformation start time t_{av}, as well as the constants b and k.

3. The Aurami constant k was found to vary with temperature according to:

$$k=-1.63+4.63\times10^{-3}\,T$$

for the experimental temperature range 440°C to 560°C.

The increase in k with higher isothermal annealing temperature indicates that less recovery occurs prior to the onset of recrystallization at these higher temperatures.

4. The Avrami constant b was found to vary with temperature according to the equation:

$$\ln b = -15.56 + 1.90 \times 10^{-2}\ T$$

for the experimental temperature range 440°C to 560°C.

5. A time-temperature-recrystallization (TTR) curve was constructed using the best fit t_{av} values, and the microscopically determined times for recrystallization completion, t_{end}, at each temperature. The t_{end} values, and the completion times predicted by the best fit Avrami lines are in reasonable agreement although the predicted 99 percent recrystallization time, t_{99}, always exceeds the microscopically determined completion of recrystallization.

6. The x-ray parameter, R_I, was found to be a fairly effective measure of the progress of recrystallization during continuous heating. It was found to be affected by grain growth and other microstructural processes such as strain aging to a small degree. However, generally recrystallization was found experimentally to start at shorter times, and lower temperatures than those predicted by microhardness and metallographic observations.

7. The insitu method of monitoring the state of

recrystallization by recording the shape of the {211} Kα x-ray peak was found to be effective only at low heating rates typical of batch annealing. At these heating rates, recrystallization kinetics are relatively slow, and in addition, essentially isothermal scans were obtained. At higher heating rates, an interrupted heating-quenching method was used where successive specimens were heated to temperature, cooled, and then scanned at room temperature. This method was more time consuming and far less accurate due to fewer number of data points obtained.

8. The continuous heating recrystallization kinetic curves predicted using isothermal kinetic data resulted in fairly good correlation with the experimentally observed kinetics, particularly at the heating rates simulating batch annealing, 70.7°C/h, and intermediate to batch and continuous annealing, 43.8°C/min. At heating rates simulating continuous annealing, 686°C/min, the predicted and experimental kinetic results show less correlation.
9. The predicted continuous heating recrystallization kinetic curves are affected very little by the time and temperature at which recrystallization is assumed to start.
10. If a prior recovery anneal is given to the steel specimen prior to the continuous heating recrystallization anneal, the predicted and experimental

recrystallization kinetics are very similar. Therefore, once the initial microstructural conditions prior to the onset of recrystallization, during continuous heating, are made to be similar to those obtained isothermally, recrystallization seems to be additive.

11. The test steel's isothermal recrystallization kinetics are affected by the heating rate used to bring the specimen to the required temperature. Continuously heating a specimen to temperature results in less recovery, more retained strain energy in the lattice, and subsequently faster kinetic response.

5.2 RECOMMENDATIONS FOR FUTURE WORK

1. In order to improve the ability to predict recrystallization kinetics on continuous heating, the extent of prior recovery, and it's effect on recrystallization kinetic response must be determined. This might be accomplished by correlating x-ray ratio change during recovery, to the amount of recovery, and examining the effect of different amounts of recovery on the time and temperature of recrystallization initiation, and the resultant transformation kinetics. A more fundamental approach might involve calorimetric examination of energy released during recovery, and comparing this to recrystallization kinetics.
2. An improved method of instantaneously collecting the {211} Kα peak intensity values during annealing must be

determined to make the x-ray ratio R_I , viable for the higher heating rates encountered during CA processes. In addition, the process must be made more fully automated to follow the shift of the {211} peak with temperature during continuous annealing. High energy x-rays should be employed to reduce the time necessary for collecting peak intensity data.

3. The use of integrated intensities for recrystallization monitoring, either directly (for texture formation), or as a ratio with I_{min} or $I_{K\alpha}$, should be investigated.
4. The x-ray and microhardness techniques should be more closely calibrated to the actual volume fraction of recrystallized material using metallographic techniques. An effort should be made to pinpoint the start times of recrystallization during continuous or isothermal annealing by using electron microscopic techniques.

BIBLIOGRAPHY

1. P.K. Agarwal and J.K. Brimacombe: Met. Trans. B, 1981, vol.12b., pp.121-33.

2. M.B. Kuban, R. Jayaraman, E.B. Hawbolt, and J.K. Brimacombe: Accepted for publication in Met. Trans. A, Dec. 1985.

3. J.G. Byrne: Recovery, Recrystallization and Grain Growth, The Macmillan Company, 1965.

4. H. Hu: Trans. Met. Soc. AIME, 1962, vol.224, pp.75-83.

5. R.W. Cahn: Proc. Phys. Soc., A63, 1950, vol.323, pp.121-143.

6. R.H. Goodenow: Trans. ASM, 1966, vol.59, pp.804-823.

7. J.E. Burke and D. Turnbull: Prog. Met. Phys., 1952, vol.3, pp.220-292.

8. P. Cotterill and P.R. Mould: Recrystallization and Grain Growth in Metals, Surrey University Press, 1976.

9. A. Rosen, M.S. Burton and G.V. Smith: Trans. Met. Soc. AIME, 1964, vol.230, pp.205-215.

10. F.J. Humphreys: Met. Sci., 1979, vol.13, pp.136-145.

11. D.T. Gawne and G.T. Higgins: J. Mater. Sci., 1971, vol.6, pp.403-412.

12. G. Venturello, C. Antonione and F. Bonaccorso: Trans. Met. Soc. AIME, 1963, vol.227, pp.1433-1439.

13. C. Antonione, G. Della-Gatta and G. Venturello: Trans. Met. Soc. AIME, 1964, vol.230, pp.700-706.

14. W.C. Leslie, E.J. Plecity and J.T. Michalak: Trans. Met. Soc. AIME, 1961, vol.221, pp.691-700.

15. W.C. Leslie, F.J. Plecity and F.W. Aul: Trans. Met. Soc. AIME, 1961, vol.221, pp.982-989.

16. R.L. Rickett, S.H. Kalin and J.T. Mackenzie: Trans. Met. Soc. AIME, 1949, vol.185, pp.721-726.

17. R.L. Solter and C.W. Beattie: Trans. Met. Soc. AIME, 1951, vol.191, pp.721-726.

18. W.C. Leslie, R.L. Rickett, C.L. Dotson and C.S. Walton: Trans. ASM, 1954, vol.46, pp.1470-1499.

19. W.A. Johnson and R.F. Mehl: Trans. Met. Soc. AIME, 1939, vol.135, pp.416-442.

20. M. Avrami: J. Chem. Phys., 1939, vol.7, pp.103-112; 1940, vol.8, pp.212-224; 1941. vol.9, pp.177-184.

21. J.W. Christian: The Theory of Transformations in Metals and Alloys, Pergamon Press, 1965.

22. E. Scheil: Archiv. fur Eisenhuttenwesen, 1935, vol.12, pp.565-567.

23. J.W. Cahn: Trans. Met. Soc. AIME, 1957, vol.209, pp.140-144.

24. J.D. Dankoff, R.W. Lindsay and J.K. Magor: Iron and Steel, 1967, vol.40, pp.2-6.

25. B.D. Cullity: Elements of X-ray Diffraction, Addison-Wesley Publishing Co. Inc., 1956.

26. E.B. Hawbolt: In Situ Measurement of Recrystallization Kinetics and Application of the Data to Recrystallization During Continuous Heating, Report for N.R.C. of Canada, Dept. Met. Eng., U.B.C.

27. J.A. DiCello and B.D. Cullity: Met. Trans., 1972, vol.3, pp.2703-2704

28. H. Hu and S.R. Goodman: Met. Trans., 1970, vol.1, pp.3057-3064.

29. S. Ono, T. Shimomura, K. Osawa and K. Matsudo: Trans. ISIJ, 1982, vol.22, pp.732-738.

30. H. Abe and T. Suzuki: Trans. ISIJ, 1979, vol.19, pp.689-693.

31. K.V.V. Iyer, N.Ramachandran, P. Mohanty, S. Kumar, S.M. Aeron and Y. Jaluria: Steel India, 1984, vol.7, pp.43-53.

32. P.R. Mould: J. Metals, 1982, vol.34, pp.18-28.

33. F. Weber, R.Edzer and H. Knoche: Met. Plant and Tech., 1985, vol.3, pp.68-77.

34. K.M. Gaskey, V.R. Hoffman and D.T. Crosby: Iron and Steel Eng., 1985, vol. 62, pp.15-20.

35. T. Ohara, H. IIda, M. Iwaki, H. Horiuchi and N. Nagira: Trans. ISIJ, 1985, vol.25, pp.1156-1162.

36. G.E. Dieter: Mechanical Metallurgy, McGraw-Hill, 1961.

37. P. Gordon: Trans. AIME, 1955, vol.203, pp.1043-1052.

38. S.C. Choi: Introductory Applied Statistics in Science, Prentice-Hall, Inc., 1978.

39. H.J. Eckstein and H.L. Steyer: Met. Odlew., 1980, vol.6, pp.85-105.

40. R.E. Reed-Hill: Physical Metallurgy Principles, D. Van Nostrand Co., 1973.

41. Metals Handbook, 9th ed., vol.1: Properties and Selection, Irons and Steels, ASM, 1978.

42. J.K. Stanley and R.F. Mehl: Trans. Met. Soc. AIME, 1942, vol.150, pp.260-271.

43. H. Hu: Trans. AIME, 1959, vol.215, pp.320-326.

APPENDIX 1

APPENDIX 1: COMPUTER PROGRAM FOR PREDICTING CONTINUOUS HEATING RECRYSTALLIZATION KINETICS

```
C        THE FUNCTION OF THIS PROGRAM IS TO
C        PREDICT THE RECRYSTALLIZATION KINETICS
C        OF A LOW CARBON, COLD ROLLED STEEL SHEET DURING
C        A CONTINUOUS HEATING ANNEALING CYCLE, USING THE
C        PRINCIPLE OF ADDITIVITY, AND EXPERIMENTALLY DETERMINED
C        ISOTHERMAL RECRYSTALLIZATION KINETIC DATA.
C        ISOTHERMAL KINETIC DATA
C        IS DESCRIBED BY THE AVRAMI EQUATION,
C        X=1-EXP(-B*T**K).
      REAL TINCR,HR,XINCR(5000),XPRE,XNEW,B,Z,G,
     Q TEMP(5000),X(5000),N,K,Q
      INTEGER LIST(1)/'*'/
C        ENTER THE DESIRED ISOTHERMAL TIME INCREMENT.
      TINCR=10.
C        ENTER THE PARAMETERS WHICH DESCRIBE HOW THE AVRAMI
C        CONSTANTS (K AND B) VARY WITH TEMPERATURE.
      N=-1.63
      Q=0.00463
      G=0.019
      Z=1.747E-7
      DO 99 I=1,5000
      X(I)=0.0
      XINCR(I)=0.
99    TEMP(I)=0.
      I=1
C        THE TEMPERATURE AT WHICH RECRYSTALLIZATION IS ASSUMED
C        TO INITIATE IS USED TO CALCULATE THE AVRAMI KINETIC
C        CONSTANTS, AND THE SUBSEQUENT VOLUME FRACTION OF
C        RECRYSTALLIZED MATERIAL FORMED DURING THE INITIAL
C        TIME INCREMENT.
      TEMP(I)=465.0
      HR=.0182
      K=N+Q*TEMP(I)
      B=Z*EXP(G*TEMP(I))
      XINCR(I)=1.-EXP(-B*(0.5*TINCR)**K)
      X(I)=XINCR(I)
      XPRE=X(I)
      I=I+1
      J=I-1
C        CALCULATE THE TEMPERATURE AT THE NEXT ISOTHERMAL TIME
C        INCREMENT.
44    TEMP(I)=(HR*TINCR)+TEMP(J)
      B=Z*EXP(G*TEMP(I))
      K=N+Q*TEMP(I)
C        FIND THE VIRTUAL TIME REQUIRED AT THE NEW TEMPERATURE
C        TO HAVE FORMED THE FRACTION ALREADY RECRYSTALLIZED.
      TEQ=(ALOG(1.-XPRE)/(-B))**(1/K)
      TNEW=TEQ+TINCR
      XNEW=1.-EXP(-B*(TNEW)**K)
C        FRACTION TRANSFORMED DURING NEW TIME INCREMENT.
      XINCR(I)=XNEW-XPRE
C        TOTAL FRACTION TRANSFORMED UP TO THIS POINT.
      X(I)=XNEW
C        CHECK TO SEE WHETHER THE STEEL HAS TOTALLY
C        RECRYSTALLIZED.
      IF(X(I).GE.1.0)GO TO 7
      XPRE=X(I)
      I=I+1
      J=I-1
      GO TO 44
C        PRINT OUT RESULTS OF TEMP VS FRACTION TRANS.
7      WRITE(5,1900)
1900  FORMAT(' ','TEMP',9X,'XINCR',9X,'XTOTAL')
      DO 456 I=1,5000
      WRITE(5,700) TEMP(I),XINCR(I),X(I)
700    FORMAT(' ',F9.4,4X,F8.6,6X,F8.6)
456   CONTINUE
      STOP
      END
```

APPENDIX 2

APPENDIX 2: EVALUATION OF X-RAY PROCEDURE

The effectiveness of the x-ray procedure used in this study for monitoring recrystallization can be determined by considering the following factors.

1. The relative amount by which the x-ray ratio, R_I, is affected by microstructural processes, other than recrystallization, that occur during annealing.
2. The ability of the x-ray ratio to determine the start and completion of recrystallization.
3. The applicability of the x-ray method to different heating rates.

Examination of the experimental kinetic results obtained for a heating rate of 70.7°C/h, Figure 4.12, shows that the hardness increase prior to recrystallization (attributed to strain aging), does not result in any effect upon the x-ray ratio. In addition, grain growth after recrystallization was found to affect the x-ray ratio to a very small extent, while microhardness is affected much more. For instance, the specimen annealed for 28,000s was found to have totally recrystallized, with a resulting grain size of ASTM No. 11, Figure A2.1. The microhardness value was found to be DPH 117.5. The specimen annealed for 40,000s displayed an increase in grain size to ASTM No. 8, Figure A2.2, with a microhardness value of DPH 76.8. Examination of the x-ray data reveals very little change in the ratio during this time interval. Therefore, the x-ray ratio employed during this study seems to be affected to a

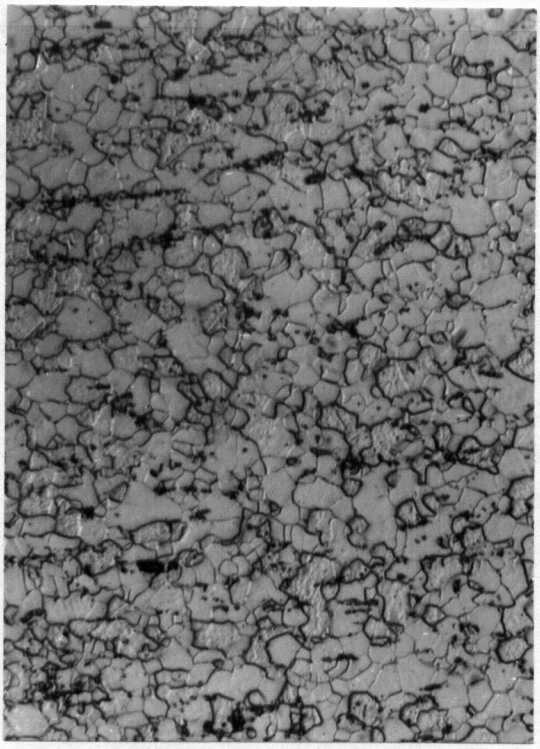

Fig. A2.1 Microstructure in the specimen continuously annealed at 70.7°C/h for 28000s. ASTM grain size no. 11.(X353 mag.)

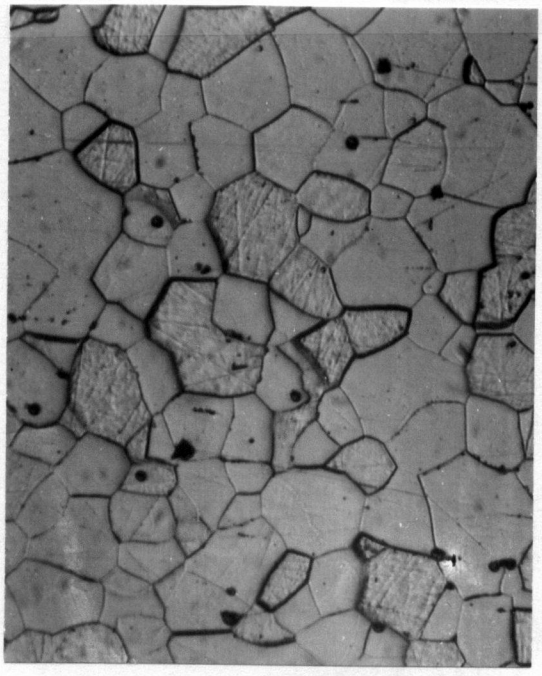

Fig. A2.2 Microstructure in the specimen continuously annealed at 70.7°C/h for 40000s. ASTM grain size no. 8.(X353 mag.)

lesser extent by various metallurgical processes that affect microhardness measurements. *

Based on the experimental results of this study, the x-ray procedure does not accurately determine the time at which recrystallization starts during continuous heating. At all heating rates employed (without the application of a prior recovery heat treatment), x-ray analysis predicted quicker start times and lower start temperatures for recrystallization, as compared to those predicted by microhardness evaluation. However, the completion times for recrystallization was predicted accurately by x-ray analysis, and good agreement existed with the completion times obtained from microhardness and metallographic evaluation.

The applicability of the insitu x-ray method involving oscillating scans is limited to slow heating rates, due to the long time interval necessary to scan the $K\alpha$ doublet peak, and achieve the desired peak resolution. A very high energy x-ray source with a more rapid scan rate capability would be required for insitu monitoring of continuous annealing.

Another problem that complicates the use of x-ray data for the monitoring of recrystallization during continuous heating is the x-ray peak shift with temperature change. According to Bragg's law, given in equation (2.31), the

---

*Back reflection Laue tests indicated that the {211} diffraction lines had remained continuous for all grain sizes encountered in this work.

position of the diffracted x-ray peak is dependent upon the spacing of the crystal planes of interest, d_o. Based on linear thermal expansion coefficients of an AISI-SAE 1008 steel,[41] the position of the {211} FeKα x-ray peak, 2θ, in degrees is related to the temperature, T in °C, by:

$$(2\theta)°=111.72-0.00249T \qquad ...(A2.1)$$

Experimentally, it was determined that the equation describing the peak shift with temperature increase was:

$$(2\theta)°=109.30-0.00264T \qquad ...(A2.2)$$

Although the experimentally determined peak position is considerably different than the theoretical value (probably caused by improper positioning of the specimen), the peak shifts for a given temperature change (ie. slope of the lines) are fairly similar.

During continuous heating using the insitu method of monitoring recrystallization, the peak shift was compensated for by manually adjusting the limit switches which control the angular range of the 2θ scan. If an improved method of continuously monitoring the peak and valley intensities is devised, then the temperature dependence of the peak position will have to be accounted for.

APPENDIX 3

APPENDIX 3: EVALUATION OF THE STRIP SPECIMEN THERMAL GRADIENT

To determine the temperature variation with position in the resistance heated strip specimens, four thermocouples were welded onto a typical specimen, at the positions indicated in Figure A3.1. The specimen was then held isothermally at temperatures over a range of 200°C to 600°C. The difference between the setpoint temperature maintained at the centreline of the specimen by the control thermocouple, and that of the three measuring thermocouples, was then determined.

The results are shown in Table A3.1 The largest deviation from the setpoint temperature was found to occur at position B, located 5mm from the centreline across the width of the specimen. Here a temperature difference of up to 29°C could exist. This large difference can be attributed to the presence of the glass specimen holders immediately adjacent to this position. The glass holders appear to act as heat sinks, thereby lowering the temperature of the adjacent metal.

Smaller thermal gradients were found to exist at positions A and C. The difference from the temperature maintained at the centreline was generally found to be no more than 6°C. Only at 600°C did the temperature at postion A differ substantially from that of the control thermocouple temperature. In addition, the temperature gradient across the width of the specimen was found to be greater than that

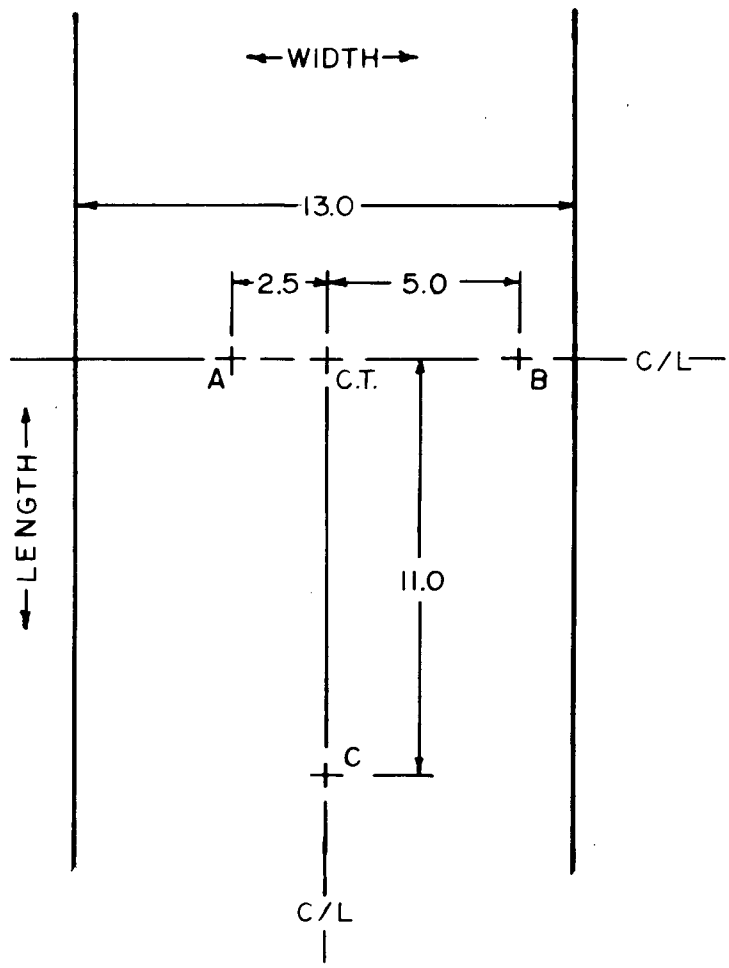

ALL DIMENSIONS IN mm
C.T. = CONTROL THERMOCOUPLE
C/L = CENTRELINE

Fig. A3.1 Strip specimen thermocouple positions for determining the thermal gradient.

Table A3.1 Strip Specimen Thermal Gradient.

Temperature at Control Thermocouple (°C)	Temperature at Measuring Thermocouple (°C)		
	A	B	C
200	197	198	199
300	295	289	300
400	394	385	398
500	497	477	495
600	586	571	596

experienced along the length.

Of the three positions monitored, only position A fell within the area covered by the x-ray beam during analysis for volume fraction of recrystallized material. Although the thermal gradient existing in this area appears to be relatively small, reduction of the area covered by the beam will further reduce any error introduced by the thermal gradient. This reduced area can be obtained by using a high energy x-ray source, thereby enabling the use of a smaller x-ray slit size.